DISCOVERY AND CHARACTERIZATION OF THE FIRST HUMAN MONOCLONAL ANTIBODIES TO SOSUGA VIRUS

By

Helen M. Parrington

Dissertation

Submitted to the Faculty of the

Graduate School of Vanderbilt University

in partial fulfillment of the requirements

for the degree of

DOCTOR OF PHILOSOPHY

in

Microbe-Host Interactions

May 12, 2023

Nashville, Tennessee

Approved:

Kristen Ogden, Ph.D. (Chair)

Borden Lacy, Ph.D.

Kelli Boyd, D.V.M., Ph.D.

Lars Plate, Ph.D.

Scott Smith, M.D., Ph.D.

James E. Crowe, Jr., M.D. (Advisor)

To my parents, Mark and Linda, and my siblings, Sharon, and Edward:
Thank you for your love and support throughout this endeavor.

AND

in loving memory of Eunice Parrington

ACKNOWLEDGEMENTS

Thank you to my thesis advisor, Dr. James E. Crowe, Jr., for allowing me to train in your laboratory and to work on such an exciting and interesting project. I am grateful for the advice you gave me, both professionally and personally, and the support you provided me over 5 years. One of the most meaningful discussions for me was when you were able to see the benefit of what you described as my “prophetic voice”—my talent in finding flaws and inefficiencies. You were the first person who recognized this ability as a skill, but cautioned that I needed to be careful when I use it to not be seen as an overly negative person. I don’t recall which of the many management and/or leadership books you’ve read that this particular idea came from, but I do remember the summary in how it relates to me (in my words):

> prophetic voices are incredibly powerful at transforming environments, systems, institutions, workplaces, etc. when there is a king (the boss or leader) who listens.
>
> Also, things start to go really bad when the king ignores the prophet.

This is something I think about a lot while looking into post-doctoral positions or dreaming of my future career. I also appreciate your insight into how I am a “rule breaker”—someone who recognizes major structural problems and challenges the system to change (as you described). I hope I will be able to continue pushing to change science, academia, the world, etc. for the better. I also want to thank you for allowing to get more animal work since that was one of my goals with grad school by teaching me how to do challenge studies with RSV in cotton rats—including coming in to the ABSL-2 lab and showing us how to do the inoculations yourself. I really learned a lot from you directly and from being in your lab, and I appreciate all the skills I have acquired since joining and the mentorship that you provided.

Thank you to all of our collaborators during this project, particularly Punya Shrivastava-Ranjan, Shilpi Jain, and César G. Albariño for doing the BSL-3 neutralization assays and Guillaume B.E. Stewart-Jones for the SOSV F constructs and guidance on protein purifications. Also thank you to Paul Rothlauf and Sean Whelan for the tremendous effort put into trying to make a recombinant VSV-SOSV virus for me.

Thank you to my dissertation committee, Drs. Kristen Ogden, Borden Lacy, Kelli Boyd, Lars Plate, and Scott Smith, for all your feedback, support, and encouragement over the years. I particularly want to thank my committee chair, Kristen, for being such an amazing mentor. I really enjoyed my rotation with you and learned so much, I often referred back to some of the protocols/techniques we did in the RVB FAST-protein paper during my Sosuga research. Thank you all so much for everything you’ve done for me over the past 5 years.

Also, thank you to the many lab members who assisted me with various assays and work. I learned a lot from all of you and am grateful that many of you I can also call friends. I appreciate all of the protein expressions, DNA purifications, antibody QC, and glycerol stock duplications done by the current and previous members of iCore: James Martinez, Laura Handal, Chris Gainza, Summer Monroig, Erica Armstrong, Jessica

Rodriguez, Rachel Sutton, Rachel Nargi, and Mattie Jensen. I would like to thank all of the past and present members of Robocore for their work in DNA sequencing of constructs and hybridomas: Joe Reidy, Andrew Trivette, Robin Bombardi, and Christian Haliburton. Thank you for all of the instruction I received from Stephanie Cronin, Nurgun Kose, and Drs. Lauren Williamson, Kristen Reeder, Laura Powell, Elad Binshtein, Iuliia Gilchuk, Pavlo Gilchuk, Fatima Nawaz, Jinhui Dong, Seth Zost, Cameron Buchman, Silvia Rivera, and Thomas Voss. Also thank you to Luke Myers and Ross Troseth for all of your technical support with laptops, Zoom, iQue computers, software licenses, etc. I especially want to thank Luke for all the work he did on antibody sequence analysis.

I would like to personally thank Dr. Lauren Williamson for all of her help with many of the common techniques we use in the lab. Since you have done just about any technique imaginable, you were always one of my go-to people when I had an idea or interest in doing something like Octet, alanine scanning, VLP production, etc. I appreciate how helpful you were, and how much you taught me. Giving me the tools to develop an assay and having the patience to allow me to try and plan out my experiment and come back multiple times to ask questions or get further input. I also appreciate how much you looked out for me and had my back in a lab that is very large and at time overwhelming with all of the different sub-groups. I am grateful for our friendship and hope we will see each other in the future!

Dr. Laura Powell, you were the first grad student I met from the Crowe lab as I talked with you before rotating. I appreciate how kind, generous, and helpful you were to me especially when I first joined the lab. I am also glad that I was able to spend time with you outside of lab and that we could go SCUBA diving a few times! I am grateful that you were a coworker and remain a friend and diving buddy! If you ever end up in Australia in the next couple of years, I hope we can meet up!

To Stephanie Cronin: thank you for all of your help and advice over the past several years. I appreciate how much you have been there for me as a coworker and friend! I will never forget the massive deep dive we did in ELISA and neut data analysis on relative vs absolute EC_{50}/IC_{50} values. I also appreciate all of the advice you gave me and thank you so much for listening to me and helping me through the challenges of grad school. I will miss hearing all of your wild and/or hilarious stories about cats, Guinea pigs, camping, fisheries, etc. I hope you can come visit me in Australia!

To Erica Armstrong: thank you for being one of my first friends in the lab and for eating lunch with me! Despite being a large group, it can get very isolating and lonely, and I appreciate that you never shunned anyone for being in a different clique/group. I also want to thank you for all of your help in teaching me on how to use the 96-well plate barcode reader, 96-well minipreps, and for all of the glycerol stock duplications you did or helped me do so that I did not need to rely on someone from iCore to grow up all of my bacteria cultures from Twist plates. Teaching me those skills and assisting with stock duplications really saved me a lot of time since I no longer had to be dependent on members of the core. I also really appreciated how you too identified areas needing improvement and helped make our lab function better overall. While you

didn't officially hold a management position, it was clear you were a great leader, and I am glad I got to learn a bit about management myself from working with and watching you.

To Ryan Irving: thank you so much for everything you do around the lab. I have never had so much privilege in a lab before where we could just let a lab manager know about empty CO_2, LN_2, freezers down, items out of stock, broken equipment, etc. and that whatever needed changing, repairing, restocking, etc. would get addressed. I am also very grateful for how well organized and stocked you keep the lab consumables/reagents, it makes it so much easier to do experiments without having to worrying about if there will be enough pipet tips or plates. Also, thank you for being our in-lab biosafety officer who makes sure we don't hurt ourselves/others. I really appreciate how you help us address safety concerns while still finding a way to make the proposed experiments move forward. I also learned a lot from working with you for the cotton rat assays and I appreciate how much you helped me get used to sacrificing animals and took my concerns around ensuring animals had been humanly euthanized seriously. You do so much for this group and always address things with a sense of humour that makes it easy to acknowledge and take accountability for when we need reminding of the rules. I will miss having you as a lab manager and I hope we will stay in touch.

To Dr. Elad Binshtein, thank you for all of your patience and guidance with learning how to use the FPLC (or "AKTA" as it will always be known to me) for protein purifications and size-exclusion. It was a lot of fun to work with you and I will miss your humour, knowledge, and expertise. I also appreciate all of the EM work that you did for my project. There were a lot of parts of this project that were challenging or didn't go according to plan, and it was so exciting to see where some of my Fabs are binding to their antigens. There's still a lot that can (should) be done with Sosuga, but the 3D reconstruction data helped me feel a lot more complete with my role in studying the virus and I would not have gotten that without you. I am hoping that your hard work can be published outside of this dissertation in another SOSV paper!

To the SOSV-donor, thank you so much for being part of this project. I suspect every grad student thinks that their dissertation is the best project, but I think I objectively have the best donor. I am so grateful that I had the unique opportunity to meet the donor behind my project. You had so much interesting knowledge and insight about bats, viruses, and Sosuga. It means so much to me to know that you are behind me supporting this work. I hope you can be proud of the work I did and know that it couldn't have happened without you, not just for the blood donation but for all of the networking and connections you helped us make with collaborators to support this project. Thank you so much for everything!

Thank you to all of the friends I met since starting grad school. I'll never forget being part of the original "Kay Bob's Five" where I met Hillary Layden, James Held, and Tyler Hansen at an IGP meet-up at Kay Bob's a day or so before classes officially started. I really enjoyed our Tuesday night Kay Bob's happy hours, where I met Payam

Fathi and Logan Richards, and all the additional times we hung out where I got to meet Emili Hansen, Emily Colwell, and Dr. Carolina Vogel. It's been exciting to see our group grow with our newest and youngest members and I am so grateful that I got to meet Henry, Hattie, and Adelaide. I am so glad that I got to experience all of the happy hours, Super Bowl parties, Friendsgivings, weddings, birthday parties, celebrations, and now defenses with you. I really appreciate all of the friendship, support, help, advice, and joy that you have all given me over the years.

I also am glad and grateful for Kaitlyn Schaaf and Jacky Lu for all of their insight and help with qualifying exam preparation or dissertation questions. I enjoyed walking at Hidden Lake and participating in Pride (pre-COVID), the department happy hours or events, and doing the library science club together. I am so thankful for our friendship am looking forward to seeing what you two do next!

I also want to thank my Canadian friends, Melissa O'Donohoe, Michelle Peters, and Alicia Reid for their friendship and support. I hope that you can take pride in my accomplishments as a representation for homeschoolers. In particular I want to thank Melissa for being there for me even though we've been separated by a border and many, many miles for over a decade. I am so grateful that no matter how much distance or time comes between us that our friendship doesn't change. I am so happy for you and your amazing family and I hope I will get to start visiting more again in the next few years!

Thank you to the Guinea pigs of this dissertation: Tucker, Caboose, Grif, Donut, and Delta.

Finally, thank you so much to my parents (Mark and Linda) and siblings (Sharon and Edward) for all of your support and patience throughout this endeavor. Doing this Ph.D. was not easy and I am so glad I had your love and support to help me get through it. Sharon and Edward, thank you for all the shenanigans and hilarity you bring me, whether its watching movies, having "not-so-sneaky" conversations about what presents to buy the parents, funny cat pictures, or memes. I am so happy that I have you both in my life. Please take good care of my piggies for me while I am in Australia!

Mom, so much for talking with me on the phone when I was walking home at night, making sure I was OK, sending me care packages, and supporting me through the darkest parts of this degree. Also thank you for sacrificing your time and energy to homeschool me and help me get to this point. I am so fortunate to have such a caring and loving mother. Dad, thank you for being my first and most constant scientific mentor. I will always remember the day you took me to your laboratory at work and taught me PCR when I was a kid. It is so fun to talk about science with you and to bounce ideas off of you. I learn so much from our discussions and I am grateful for the advice on experiments, careers, and management. I look-up to you so much as a professional, a scientist, and a parent. You're also a great diving buddy and I can't wait to dive with whale sharks with you!

TABLE OF CONTENTS

LIST OF TABLES

LIST OF FIGURES

LIST OF ABBREVIATIONS

Ab/Abs	antibody/antibodies
AP	alkaline phosphatase
Ara-C	cytosine β-D-arabinofuranoside
BLOSUM	blocks substitution matrix
BSL	biosafety level
BSA	bovine serum albumin
CDC	Centers for Disease Control and Prevention
cDNA	complementary DNA
CDR3	complementarity determining region 3
CPE	cytopathic effect
DAPI	4,6-diamidino-2-phenylindole, dihydrochloride
DMEM	Dulbecco's Modified Eagle Medium
DENV	Dengue virus
D gene	immunoglobulin diversity gene
DMSO	dimethyl sulfoxide
DPBS	Dulbecco′s Phosphate Buffered Saline
EBV	Epstein-Barr virus
EC_{50}	half maximal effective concentration
Env (HIV-Env)	envelope protein
F	fusion protein
FBS	fetal bovine serum
FRNT	foci reduction neutralization test
FSC-A	forward scatter area
FSC-H	forward scatter height
G	glycoprotein (attachment protein; glycoprotein)
GFP	green fluorescent protein
HAT	hypoxanthine-aminopterin-thymidine
H	hemagglutinin (attachment protein)
HIV/HIV-1	human immunodeficiency virus/virus type 1
HN	hemagglutinin-neuraminidase (attachment protein)
HRP	horseradish peroxidase
IC_{50}	half maximal inhibitory concentration
ICTV	International Committee on Taxonomy of Viruses
IgG	immunoglobulin G
J gene	immunoglobulin joining gene
LCL/LCLs	lymphoblastoid cell lines
mAb/mAbs	monoclonal antibody/antibodies
MEM	Minimal Essential Medium
MenV	Menangle virus
MFI	median fluorescent intensity
MMR	measles, mumps, and rubella (vaccine)
MuV	Mumps virus

NS-EM	negative-stain electron microscopy/micrograph
p (prefix)	plasmid (*e.g.*, pTwist-CMV)
PBS-T	phosphate buffered saline tween 20
PCR	polymerase chain reaction
PFA	paraformaldehyde
PIV1	human parainfluenza virus 1/respirovirus 1
PIV2	human parainfluenza virus 2/orthorubulavirus 2
PIV3	human parainfluenza virus 3/respirovirus 3
PIV4	human parainfluenza virus 4/orthorubulavirus 4
PIV5	parainfluenza virus 5/mammalian orthorubulavirus 5
r (prefix)	recombinant (*e.g.*, rmAb means recombinant mAb)
RACE	Rapid amplification of cDNA ends
RdRP	RNA-dependent RNA polymerase
RFU	relative fluorescent units
SOSV	Sosuga virus
SFM	serum-free media
SSC-A	side scatter area
SSC-H	side scatter height
ssRNA	single-stranded RNA
TuV3	Tuhoko virus 3
UCA	unmutated common ancestor
V gene	immunoglobulin variable gene
VSV	vesicular stomatitis virus
VSV-G	vesicular stomatitis virus G (glycoprotein) protein
VSV-N	vesicular stomatitis virus N (nucleocapsid) protein
VRC	Vaccine Research Center
WT	wildtype

CHAPTER I

Introduction to Sosuga virus

Disclaimer: part of the data and information presented in this chapter were adapted from the following:

Parrington HM, Kose N, Armstrong E, Handal LS, Diaz S, Reidy J, Dong J, Stewart-Jones GBE, Shrivastava-Ranjan P, Jain S, Albariño CG, Carnahan RH, Crowe JE. 2023. Potently neutralizing human monoclonal antibodies against the zoonotic pararubulavirus Sosuga virus. JCI Insight https://doi.org/10.1172/jci.insight.166811.

Overview of dissertation

This thesis represents the work I performed during my doctoral studies under Dr. James E. Crowe, Jr. at Vanderbilt University from 2018-2023. During this time, I received support from many members of the Crowe Laboratory, as well as collaborations with colleagues at the Center for Disease Control and Prevention, the Vaccine Research Center of the National Institute for Allergy and Infectious Diseases, Colorado State University, the Washington University in St. Louis, and Vanderbilt University Medical Center. In Chapter I, I provide an introduction to paramyxoviruses, specifically Sosuga virus (SOSV) which is the main subject of this work and some background information on the humoral immune response as it relates to this work. Chapter II describes the discovery of the first human monoclonal antibodies (mAbs) to Sosuga virus and the methodology used. Chapter III begins the characterization of the

isolated monoclonal antibodies such as the conformational or domain specificity to their target antigens. Chapter IV expands on Chapter III by characterizing the neutralizing response of the mAbs to live SOSV. Chapter IV also discusses the attempts to produce SOSV pseudoviruses for use in neutralization assays and the possibilities for why pseudotyping was not successful. Chapter V provides the summary and conclusion of this work as well as future directions for this project, including preliminary data that were not able to be further worked on during my time as a graduate student. It is my hope that those in the field of emerging or zoonotic viruses will find this work insightful, and that the antibodies discovered and characterized will be useful in future research.

Introduction to paramyxoviruses

Family *Paramyxoviridae*

Members of the family *Paramyxoviridae*, or paramyxoviruses, are all enveloped, single-stranded, negative-sense, non-segmented RNA viruses (1–3). Paramyxoviruses are globally dispersed and found in a broad range of vertebrate hosts, including various mammals such as ruminants, rodents, and bats as well as birds, fish, and reptiles (1–4). The genome size of paramyxoviruses ranges from 13 kB to just under 22 kB, containing 6-8 genes (1, 5). Shared genes and proteins between all members include: nucleocapsid (N), matrix (M), fusion (F), attachment (G, H, or HN), and large (L) (1, 5). Apart from a single subfamily, all paramyxoviruses also carry the phosphoprotein (P) gene, which encodes at least two proteins, between the N and M genes (**Figure 1.1A**) (1). Variation in proteins produced by the phosphoprotein gene and other additional

genes varies across the subfamilies or even individual viruses (1). All paramyxoviruses have the fusion (F) and attachment protein on the viral surface, the attachment protein is named glycoprotein (G), hemagglutinin (H), or hemagglutinin-neuraminidase (HN) (1, 5, 6). Attachment proteins that cause hemagglutination of erythrocytes are H proteins, and attachment proteins that cause hemagglutination and have neuraminidase activity on sialic acid are HN proteins, while attachment proteins that do neither of these activities are simply G proteins (1, 5, 6). Paramyxovirus fusion occurs at physiological pH and replication takes place in the cytoplasm (**Figure 1.1B**) (1, 5–7). As a negative-strand virus, paramyxoviruses encode and package an RNA-dependent RNA polymerase (RdRP), which a complex of at least the L and P proteins (1, 5). The viral RdRP is essential for making positive-sense viral mRNAs for protein production and antigenomes that serve as the template for replication—which is again performed by the RdRP (1, 5).

Both attachment (G/H/HN) and fusion proteins (F) are necessary for viral replication as they facilitate the binding and fusing of virion and plasma membranes. F is a type I transmembrane protein that forms homotrimers, while the G/H/HN is a type II transmembrane protein that forms a tetramer (1). The F protein requires cleavage by the a host-cell protease in order to expose the end of the fusion peptide-which is inserted into the host-cell membrane during fusion (**Figure 1.2**) (1, 5, 8, 9). The attachment protein contains the receptor binding domain (RBD); the receptor for paramyxoviruses is variable with some using proteins as receptors and others molecules such as sialic acid (1, 5). Both the F and G/H/HN proteins can have variations in their conformational state with the F protein in particular having a dramatic

change between the prefusion and postfusion conformations (**Figure 1.2**) (1, 5, 10, 11) while the G/H/HN proteins can vary the orientation of the globular head domains from pointing down to up (1, 12). Currently there are two models for paramyxovirus membrane fusion depending on if the receptor is a protein or a carbohydrate, both rely on the interactions of the F protein with the HN-stalk domain but differ in whether there is association with the HN protein prior to attachment or not respectively (1). The size and morphology of paramyxoviruses is variable, with some being over 1 μm in diameter (13) though the typical size is considered around 150-350 nm (1, 14–16). Particles may also be spherical or filamentous (1, 13, 17–19) (**Figure 1.3**).

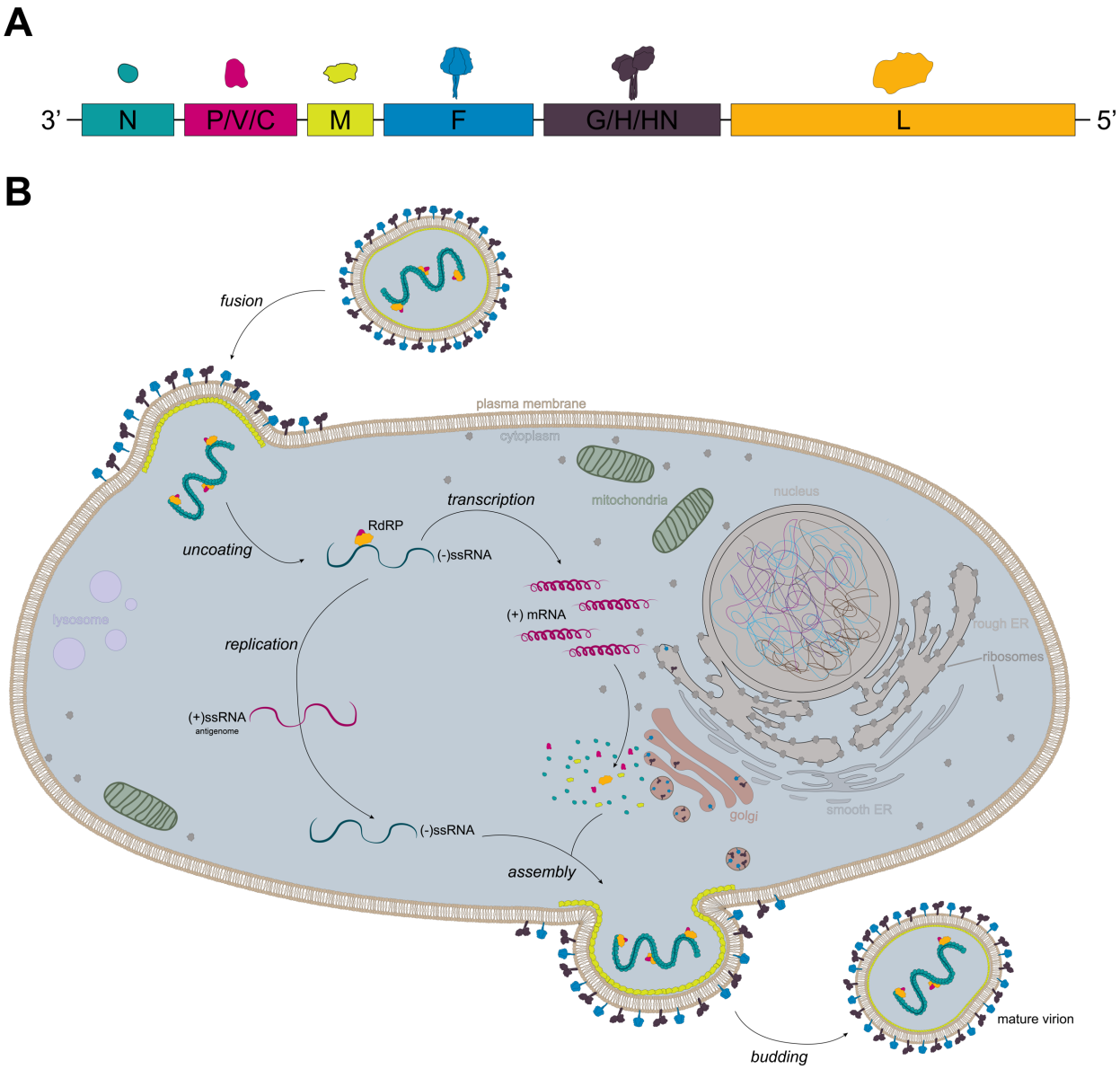

Figure 1.1. Paramyxovirus genome organization and replication cycle. **(A)** Genome organization of a typical paramyxovirus showing commonly shared genes including P. **(B)** Replication cycle of paramyxoviruses. Virions fuse to plasma membrane of host cell where the genome is uncoated and transcribed to make positive-sense viral mRNA or a positive-sense antigenome. The viral mRNAs are translated by host ribosomes, the positive-sense antigenome is used as a template for the negative-sense genome which is then packaged and assembled into a virion at the plasma membrane where it buds out to form a mature virus. Adapted from Shahriari et al. (2016) (20) and Plemper and Lamb (2021) (1).

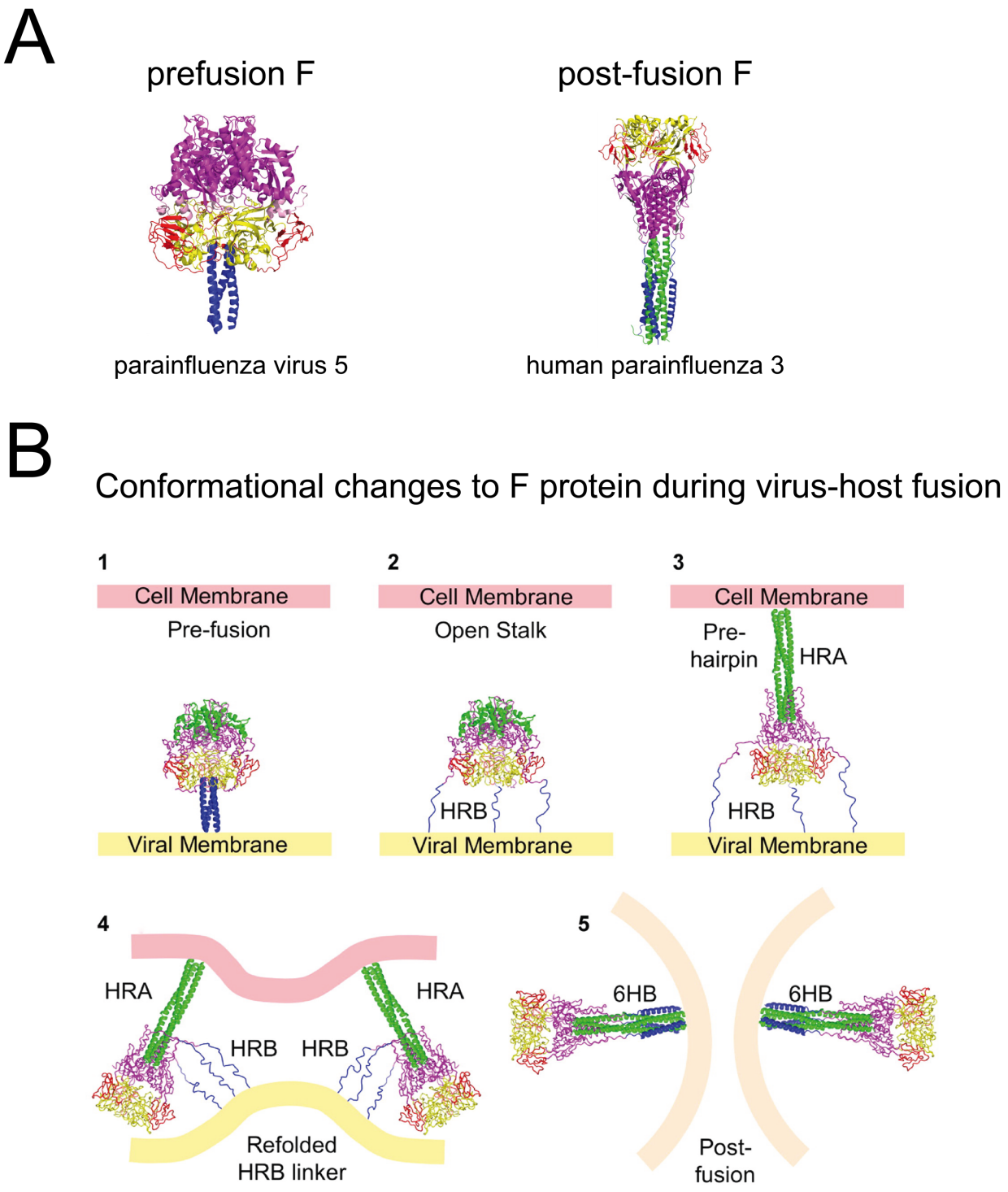

Figure 1.2. Conformations of paramyxovirus and pneumovirus F proteins. **(A)** Crystal structures of parainfluenza virus (PIV) 5 and 3 in the prefusion (PPIV5) and postfusion (PIV3) states. **(B)** Changes in conformation of the F protein during viral fusion process. From Bose S, Jardetzky TS, Lamb RA. 2015. Timing is everything: fine-tuned molecular machines orchestrate paramyxovirus entry. *Virology* 479–480:518–531. *Copyright © 2015 Elsevier Inc. All rights reserved*. Used and modified with permission under Rightslink license ID 5473191122741.

Introduction to rubulaviruses

Current taxonomy guidelines divide *Paramyxoviridae* into four subfamilies: *Avulavirinae*, *Rubulavirinae*, *Orthoparamyxovirinae*, and *Metaparamyxovirinae* (2, 21). From a human disease standpoint, *Rubulavirinae* and *Orthoparamyxovirinae* are perhaps the more significant of these subfamilies as they include many of the paramyxoviruses known to cause disease in humans. *Orthoparamyxovirinae* contains the notable human pathogens: human parainfluenza viruses 1 and 3 (genus *Respirovirus*), measles virus (genus *Morbillivirus*), and Hendra virus and Nipah virus (genus *Henipavirus*) (21, 2, 3, 15, 6). *Rubulavirinae* contains only two genera: *Orthoarubulavirus* which include human pathogens human parainfluenza viruses 2 and 4 and mumps virus, while genus *Pararubulavirus* includes Menangle virus and Sosuga virus which have both caused disease in humans (21, 2, 15, 22, 17). While some pararubulaviruses have crossed into humans or domestic livestock, so far all of the discovered ones have originated in bats (4, 22–29). It is entirely possible that bats are the ancestral host for the entire *Pararubulavirus* genus. Orthorubulaviruses can be found in several animal species including pigs, dogs, humans, and bats (3, 15, 30–36).

Members of *Rubulavirinae* have a genome of about 15 kB and have 6-7 genes encoding 7-8 proteins (**Figure 1.3**). The glycoprotein system used is F and an HN protein, though some rubulaviruses such as mumps and PIV5 also have a 3rd envelope protein called the small-hydrophobic protein (SH) (5, 37, 38) (**Figure 1.3**). The function and role of SH is not well understood and non-essential for viral replication (5, 14, 37, 38). The rubulaviruses create a bit of a challenge for paramyxovirus conventions. The orthorubulaviruses all have a true HN protein capable of hemagglutination and

neuraminidase activities and bind to sialic acid. The pararubulavirus HN protein is very similar to the orthorubulavirus HN, however, they lack the ability to bind to sialic acid and neither cause hemagglutination nor neuraminidase. Canonically, these proteins should be considered as, and named, G proteins like the nomenclature for Nipah and Hendra viruses, however currently these proteins are still referred to as HN in the literature and GenBank deposits. The major difference in HN enzymatic abilities between the ortho- and pararubulaviruses raises questions of the evolutionary origins of this subfamily and the two genera within it. Considering that the HN protein of pararubulaviruses retain some of the residues necessary for sialic acid binding, I think it is more likely that the pararubulavirus genus was formed from the loss of sialic acid binding rather than the orthorubulaviruses transitioning from a proteinaceous receptor to sialic acid. Other subfamilies or genera within *Paramyxoviridae* also contain sialic acid-binding paramyxoviruses, such as avulaviruses or respiroviruses, making it possible that the ancestral paramyxovirus bound to salic acid, and over time various viruses diverged to recognizing and binding proteins. As it stands, the receptor for pararubulaviruses remains unknown, and more work is needed to understand the evolutionary origin of the genera with in *Rubulavrinae*.

Many of the pararubulaviruses have been discovered in the past 30 years while studies of orthorubulaviruses go back into the mid 1900s when the vaccine for mumps was developed. However, mumps has been causing disease in humans since ancient Greece (39, 40) and thus there has been a long evolutionary relationship between virus and host. Mumps is one of the two paramyxoviruses for which vaccines have been made, the other being measles virus (*Orthoparamyxovirinae*, genus *Morbillivirus*). While

the mumps vaccine has been highly effective from an epidemiologic and public health standpoint (41, 42), from a vaccinology standpoint the vaccine could be improved. For instance, the vast majority of the humoral immune response induced by the vaccine is directed against the N protein which is a non-neutralizing target (43–45). This is not surprising given the abundance of N produced during viral replication and the fact that the vaccine uses live-attenuated virus (46–48). Additionally, recent outbreaks of mumps virus among vaccinated individuals has suggested waning immunity (41, 42, 49–51). While the predominant circulating genotype of mumps virus has changed from the vaccine strain immune escape has not been achieved (52). Additionally, despite the existence of a mumps vaccine for over 50 years, not much characterization of the immune response to the virus beyond the key protein targets has been done (43, 53, 54) nor is there a known correlate of protection (49, 51, 54, 55). Additionally, recent discovery of a bat mumps virus (56–58)—that was so similar to human mumps that it was removed as its own species by the ICTV (59)—suggests that the mumps virus may also have originated in bats (29). In conclusion, the *Rubulavirinae* subfamily is relatively understudied but appears to have deep evolutionary ties to bats, making this subfamily a concern for zoonotic spillover.

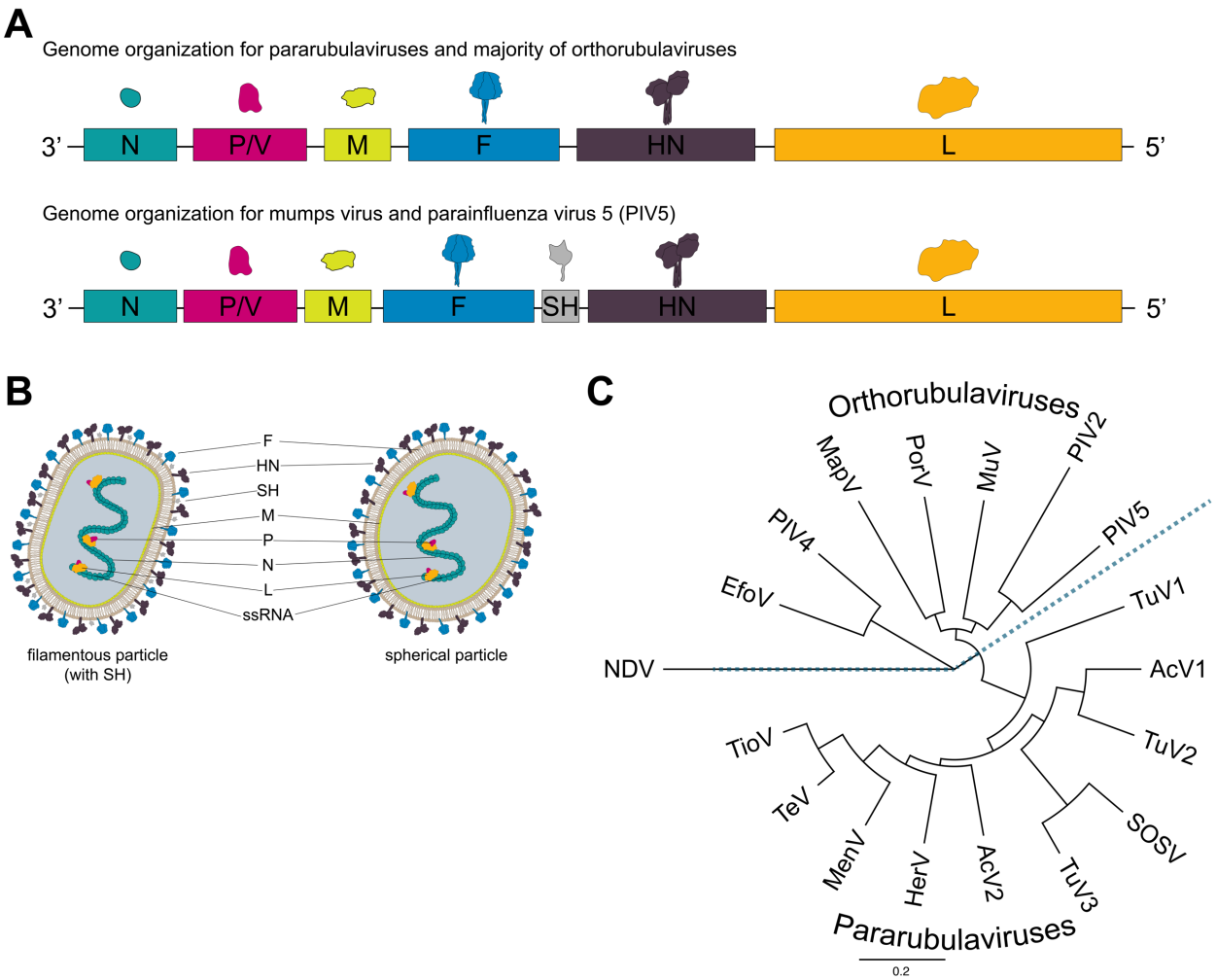

Figure 1.3. Overview of *Rubulavirinae* subfamily. (A) Genome organization of rubulaviruses, PIV5 and mumps encode an additional protein compared to many other rubulaviruses. **(B)** Filamentous and spherical morphology diagrams of paramyxoviruses. Adapted from Payne (2017) (5). **(C)** Phylogeny of rubulaviruses using N protein sequences the division of the subfamily into the two separate genera: *Orthorubulavirus* and *Pararubulavirus*. Rubulavirus genomes deposited in GenBank and the N, F, and HN protein sequences taken. The tree builder tool of Geneious Prime software (Biomatters, version 2023.0.3, Mac OS) was used with a BLOSUM 62 substitution matrix to generate the phylogeny with the Newcastle Disease Virus (NDV) N protein sequence serving as an outgroup. GenBank accession numbers for viral genomes used for collecting N, F, and HN protein sequences: Newcastle disease virus (NDV; FJ754271.2), mumps (MuV; JX287385.1), human parainfluenza virus 2 (PIV2; AF533012.1), human parainfluenza virus 4 (PIV4; KF878965.2), parainfluenza virus 5 (PIV5; JQ743318.1), Mapuera virus (MapV; NC_009489.1), porcine rubulavirus (PorV; NC_009640.1), *Eptesicus fuscus* orthorubulavirus (EfoV; MZ355765.1), Achimota virus 1 (AcV1; NC_025403.1), Achimota virus 2 (AcV2; NC_025404.1), Sosuga virus (SOSV; NC_025343.1), Teviot virus (TeV; NC_039198.1), Tioman virus (TioV; NC_004074.1), Menangle virus (MenV; NC_039197.1), Tuhoko virus 1 (TuV1; NC_025410.1), Tuhoko virus 2 (TuV2; NC_025348.1), Tuhoko virus 3 (TuV3; NC_025350.1), and Hervey virus (HerV; KU672593.1).

Sosuga pararubulavirus

The isolation and discovery of Sosuga virus (SOSV) is a particularly fascinating story because it was a fellow scientist who became infected while on a field-study conducted by the Center for Disease Control and Prevention. In 2012, a female wildlife biologist and bat expert from the United States of America went to South Sudan and Uganda to collect bat and rodent samples as part of an ecological research project (17). Only days after returning home from the 6-week study, the researcher became ill with an severe acute febrile disease and required hospitalization (17). Over the course of the 2-week hospital stay, the researcher experienced a wide range of symptoms including a skin rash, fever, oropharynx ulcerations, diarrhea (with occult blood), bloody vomit, and petechia (bleeding under the skin) at sites of pressure (17). Additionally, all of the diagnostic tests that included screens for members of multiple different viral families, rickettsiae, and malaria had all returned negative (17). Ultimately a pathogen-discovery program using deep-sequencing on cDNA was used on blood samples taken from the researcher and discovered a novel paramyxovirus that was named Sosuga virus for South Sudan and Uganda—the two countries visited during the study (17). Fortunately, the researcher survived the near fatal experience with the fever ending on day 9, and most of the symptoms healed at time of discharge (day 14) although some conditions such as fatigue, malaise, headaches persisting months after discharge (17). Since the researcher participated in donating PBMCs to our group, she will be referred to as the "SOSV donor" for the majority of this body of work.

Analysis of the genome showed that SOSV was a rubulavirus most closely related to Tuhoko virus 3 (17), placing SOSV in the *Pararubulavirus* genus as discussed

above. Screening of the bat and rodent samples collected during the study, as well as archived samples indicated that Egyptian fruit bats (*Rousettus aegyptiacus*) were the likely reservoir host (23). This case is particularly interesting as the researcher was both experienced, had appropriate safety equipment for the study, and was not the sole person participating in the work—yet was the only member of the group to become infected. Information on the additional group members was not discussed in the literature. However, considering the age of the SOSV donor, 25 years old (17), at the time of the study I think it is likely that the SOSV donor was one of the younger members if not the youngest. We also know the donor had received many vaccinations for this travel and was on medications to help prevent malaria (17), meaning that one of the youngest and presumably healthiest members to participate in the expedition is the individual who became infected. This case opens up many research questions in both the virology and epidemiology of SOSV. For example: what is the route of transmission, did it happen while wearing personal protection equipment (PPE), did it even occur during sample collection and/or processing, was there an underlying condition that caused the SOSV donor to be more susceptible to the virus? There are also the questions of whether this is truly the first case of SOSV infection, or if serological studies of people living around the collection sites would reveal previous zoonosis events. The symptoms of infected individuals may also vary in regions where SOSV, and likely other pararubulaviruses yet to be discovered, are circulating in bats compared to the naïve donor from the United States. For instance, while the SOSV donor had a broad range of symptoms and a systemic infection, an individual who has been routinely exposed to SOSV or related viruses may have milder symptoms and/or a localized

infection determined by SOSV's tissue tropism. Studying the humoral immune response through mAbs from SOSV donor presents opportunities in better understanding the immune response to novel paramyxoviruses such as SOSV as well as the potential to produce useful reagents or therapeutics for continued research on SOSV and rubulaviruses.

CHAPTER II

Isolation of the first human monoclonal antibodies to Sosuga virus

Disclaimer: part of the data and information presented in this chapter were adapted from the following:

Parrington HM, Kose N, Armstrong E, Handal LS, Diaz S, Reidy J, Dong J, Stewart-Jones GBE, Shrivastava-Ranjan P, Jain S, Albariño CG, Carnahan RH, Crowe JE. 2023. Potently neutralizing human monoclonal antibodies against the zoonotic pararubulavirus Sosuga virus. JCI Insight https://doi.org/10.1172/jci.insight.166811.

Chapter II Introduction

Since I was interested in studying bat-borne viruses, I wanted to isolate antibodies against SOSV so that they could be used for learning more about the virus and had the potential to be clinically relevant if ever necessary. In order to isolate mAbs, I needed blood from the only known case of human infection. Fortunately, the SOSV survivor (17) donated peripheral blood mononuclear cells (PBMCs) to our laboratory before the start of this project and about five years after recovering from SOSV infection. Before I could begin to make hybridomas though, I needed to develop a screening assay in order to identify SOSV-specific B cells. There are a variety of assays that can be used to accomplish such screens such as enzyme linked immunosorbent assays (ELISAs) with soluble proteins (60), virus-like particles (VLPs) (61), or whole virus (62); viral neutralization assays (63); or cell-surface displayed antigen detected by

flow cytometry (64). Any assay requiring live or whole virus was unable to be used as our lab did not have the safety requirements to safely grow and purify SOSV, which is a BSL-3 pathogen (65). ELISA assays with VLPs would be similar to authentic virus, however, known methods of producing VLPs for other rubulaviruses requires the use of the matrix (M) and nucleoprotein (N) structural proteins (66). The presence of these structural proteins in the screen may lead to isolation of SOSV-specific B cells that are non-reactive to either of the glycoproteins. Since it is known that the mumps vaccine-induced antibody response is predominantly to the N protein (43, 45), I was concerned that the immune response to SOSV may be similar and chose to not pursue VLPs. Using soluble proteins in an ELISA would ensure that only glycoprotein-specific B cells would be identified. However, given the novelty of SOSV, I could not be certain that the modified proteins would be conformationally correct or even be expressed. Cell-surface display allows wildtype, transmembrane proteins such as the SOSV glycoproteins to be expressed and displayed on the cell surface. Since paramyxoviruses fuse at physiological pH and replicate in the cytoplasm (5, 7, 67), of the potential screening options, I reasoned that cell-surface display would provide the most virus-like expression of the SOSV proteins without introducing potential off-target proteins. In this chapter I will go over the cell-surface display screening methodology and the necessary reagents to identify and isolate SOSV-reactive human B cells. The following work describes how we were able to go from having donor PBMCs and viral glycoprotein sequences deposited in GenBank, to a panel of 24 human monoclonal antibodies specific to a novel paramyxovirus.

Chapter II Results

Design and expression of SOSV glycoproteins

Coding sequences for the SOSV F and HN glycoproteins were obtained from GenBank where the complete cDNA genome was deposited under accession number NC_025343.1 after the discovery of SOSV in 2012 (17). The first-generation SOSV (Gen1) constructs used the wildtype sequence for SOSV F, while the SOSV HN sequence was identical to wildtype except for the addition of a codon for a glycine residue that was inserted into the HN protein following the start to create a stronger Kozak sequence (**Figure 2.1A**). Sequences were human codon-optimized and synthesized by Twist Biosciences and cloned into the pTwist-CMV-BetaGlobin WPRE Neo mammalian expression vector. These constructs will be referred to as SOSV-F.1 and SOSV-HN.1.

The second-generation constructs (Gen2) started with taking full-length wildtype SOSV sequences from GenBank (NC_025343.1) and adding a DYKDDDDK (FLAG®) tag to the cytoplasmic tails of the F and HN sequences. The constructs (SOSV F-FLAG and SOSV HN-FLAG) were human-codon optimized, synthesized by Twist, and cloned into the mammalian expression vector pTwist-CMV. Identical constructs switching the FLAG-tag for a 6xHis-tag were similarly made (**Figure 2.1B**). Since reduction of plasmid size may increase transfection efficiency (68, 69), the pTwist-CMV vector was chosen for the Gen2 constructs. Using the FLAG-tagged constructs as the template DNA, polymerase chain reaction (PCR) amplification was used to restore the SOSV WT sequences using primers that removed additional residues and added restriction

enzyme sites outside of the protein coding regions for cloning into an empty pTwist-CMV backbone which was ~2kB smaller from the Gen1 backbone. Once cloning was completed, DNA sequencing was used to confirm that both the HN and F (SOSV F-WT and SOSV HN-WT) protein sequences were restored to match the wildtype sequences found in GenBank (SOSV F, YP_009094032.1; and SOSV HN, YP_009094033.1).

To confirm expression of the SOSV proteins, both Gen1 and Gen2 constructs were transfected into adherent cells (HEp-2 or Vero) to check for syncytia formation in single or co-transfected wells. The presence of syncytia would verify that the proteins are being expressed, trafficked to the cell-surface, and triggering the fusion process—an indication of functionality. The Gen1 constructs produced syncytia when the F and HN glycoproteins were co-transfected, but syncytia did not form during individual protein transfections or mock conditions (**Figure 2S.1**). Similarly, the Gen2 constructs only had syncytia formation in the co-transfection conditions (**Figure 2.2A**) while single-protein transfections (**Figure 2.2B**) as well as the mock transfection (**Figure 2.2C**) did not produce syncytia. Since VSV-G is another viral glycoprotein capable of inducing syncytia formation and served as another negative control because despite protein expression and syncytia formation, VSV-G should not stain with either anti-SOSV or anti-FLAG antibodies. As expected, the VSV-G transfection looks similar to the mock transfection condition, with no fluorescent syncytia (**Figure 2.2C**). Additionally, syncytia formation occurred independently of staining with anti-SOSV mAbs as shown by the presence of syncytia in the anti-FLAG stained wells (**Figure 2.2A**).

Figure 2.1. Protein sequences for synthetic constructs of SOSV F and HN transmembrane glycoproteins. GenBank accession numbers YP_009094032.1 (SOSV F) and YP_009094033.1 (SOSV HN) were used as the reference sequences for designing synthetic cDNA for protein expression. **(A)** Gen1 SOSV-F1 is identical to the reference sequence while SOSV-HN1 has an additional residue inserted at the second amino acid position. **(B)** Gen2 constructs show the addition of tags to the cytoplasmic tails of the proteins. Tags are added to the carboxy terminus of the F protein while tags are added to the amino terminus of the HN proteins. The SOSV F-WT and SOSV HN-WT sequences are identical to the reference proteins.

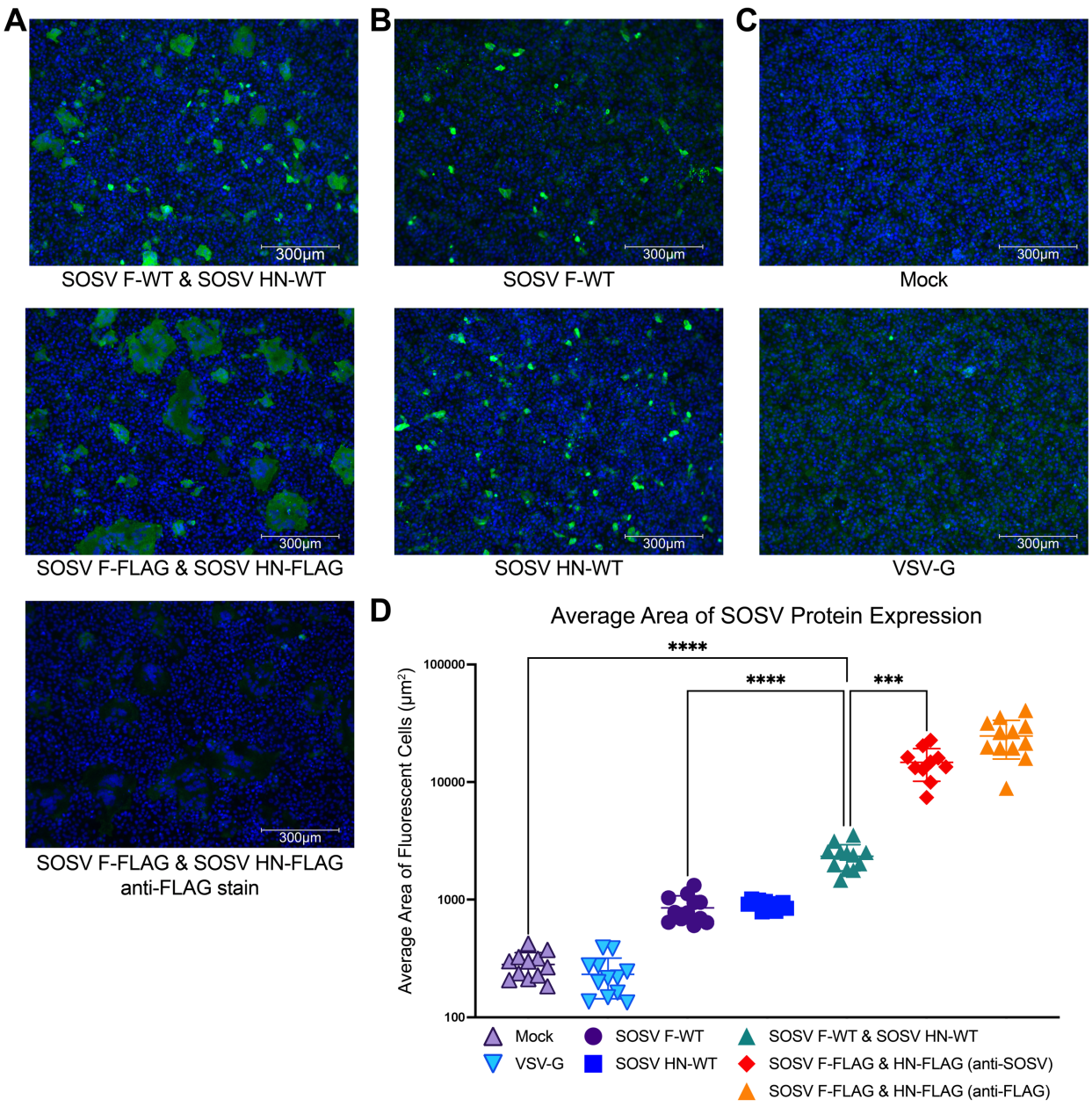

Figure 2.2. Co-transfection of cDNAs encoding SOSV F and HN proteins causes robust syncytia formation in cell culture monolayers. Representative field of view (10× objective) of transfected Vero cell culture monolayers. Nuclei were stained with 4′,6-diamidino-2-phenylindole (DAPI; blue) and SOSV proteins were stained with a polyclonal mix of six anti-SOSV mAbs (three anti-HN and three anti-F) or mouse anti-FLAG antibody with goat anti-human IgG with Alexa Fluor 488 dye or goat anti-mouse IgG with Alexa Fluor 488 dye antibodies as secondary antibodies. **(A)** Syncytia producing transfections: Co-transfection of SOSV F-WT + SOSV HN-WT, co-transfection of SOSV F-FLAG + SOSV HN-FLAG, or co-transfection of SOSV F-FLAG + SOSV HN-Flag constructs stained with anti-FLAG antibodies. **(B)** Non-syncytia producing transfections: cDNA encoding SOSV F-WT or SOSV HN-WT were transfected individually. **(C)** Controls: mock transfection or VSV G-WT transfection. **(D)** Average area of fluorescently stained clusters (cells or syncytia). One-way Anova with Tukey's Multiple Comparison with a P-value threshold of < 0.05, four asterisks (****) indicate $p < 0.0001$, three asterisks (***) indicate $p < 0.001$.

Production of human hybridomas from donor PBMCs

Leukapheresis samples from the only known human case of SOSV infection were obtained five years after infection following informed written consent. Peripheral blood mononuclear cells that had previously been isolated were thawed from cryopreservation and transformed with Epstein-Barr virus (EBV) to form lymphoblastoid cell lines (LCLs). LCLs that displayed reactivity to SOSV F or HN proteins through cell-surface display screening using an iQue Screener PLUS high-throughput flow cytometer (Sartorius) were expanded and then fused with a non-secreting myeloma cell partner (HMMA2.5 cells) to make stable hybridoma lines. Single-cell sorting flow cytometry was used to isolate the clonal hybridoma lines to ensure that ultimately a monoclonal line would be produced. Throughout this process, cell supernatants were routinely screened for binding to cell-surface expressed SOSV glycoproteins, using non-transfected cells to set the negative threshold for non-binding. The frequent screening helped ensure that the final monoclonal hybridoma lines were secreting SOSV-specific antibodies.

Since these were the first ever antibodies against SOSV being discovered, I attempted to have a broad selection of hybridomas—selecting wells or cell-lines for expansion with a range of wells from weakly positive to strongly positive. Additionally, at early screening stages I wanted to err on the side of false-positives so wells that had ambiguous results would typically be expanded so that they could be screened again. Due to the large volume of plates for screening at earlier stages, live-dead staining was typically not used until after the single-cell sorting phase when positive cells were expanded out of 384-well plates. The gating strategy used for setting the cut-off between negative and positive reactivity was done using Forecyt software

accompanying the iQue flow cytometer (Sartorius). First, cells were gated out of the events by examining the SSC-H by FSC-H, doublets were excluded by looking at the FSC-H versus FSC-A and gating on the singlets, if live-dead staining was used the dead cells were excluded by gating on the negative stained population, and the SOSV-reactive cells were selected by gating on the positive-stained population of the appropriate channel for the fluorescent secondary antibody used—typically a PE-conjugated secondary for these assays (**Figure 2.3A**). The untransfected cells helped to establish the threshold level for positive and negative SOSV-reactivity (**Figure 2.3B**). The cell-surface display screening method was used during all steps of hybridoma production, and fluorescence-activated single-cell sorting (FACS) was used to go from a mix of hybridoma lines to monoclonal lines. Once monoclonal cell lines were established, cells were pelleted and submitted for sequencing by 3′ or 5′ RACE using a Sequel instrument from PacBio (60).

In total, 24 SOSV-reactive mAbs were isolated, with 18 binding to F protein and 6 binding to HN protein (**Table 1**). The sequencing data revealed that the antibodies are predominantly of the IgG1 subclass, with two mAbs (SOSV-2 and -32) being IgG3. Most (19 of the 24) mAbs use a κ light chain, while five clones (SOSV-13, -21, -64, -83, and -85) use a λ_1 or λ_2 light chain. Recombinant versions of each member of the mAb panel were synthesized by Twist Biosciences by inserting the variable genes into a human IgG1 expression vector. Therefore, all recombinant mAbs (rmAbs) are of the IgG1 isotype. The rmAbs each exhibited the ability to bind the appropriate cell-surface displayed viral antigen, as expected, and were used in all future assays of this work.

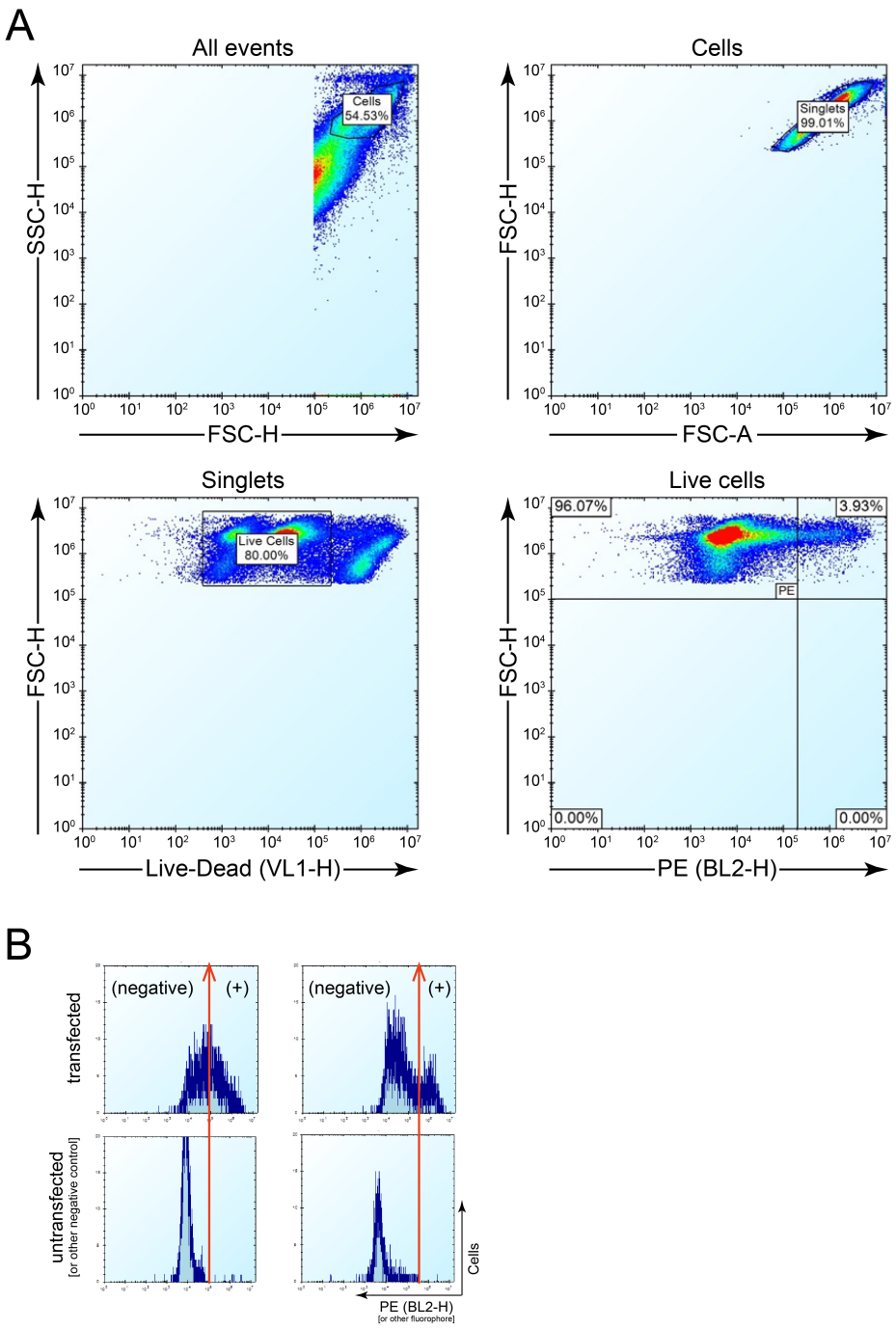

Figure 2.3. Gating strategies and threshold controls for screening B cell supernatants. B cell supernatants were used as primary stain against transfected cells displaying SOSV glycoproteins on the surface or against untransfected control. After staining cells with B cell supernatants and labelling with a goat anti-human PE secondary. Cells were analyzed on an iQue Screener PLUS flow cytometer (Sartorius). **(A)** SSC-H, FSC-H, and FSC-A were used to remove debris or cell clumps from the population so that only single-cells were analyzed. When used, live-dead staining removed dead cells from the population. Lastly, intensity of the secondary stain was used to determine which cells were labelled with antibodies. **(B)** Untransfected cells show the level of background fluorescent intensity, B cells, hybridomas, or purified mAbs are considered reactive for SOSV when the fluorescent intensity peak shifts past the threshold set by the untransfected cells.

Table 2.1: Isolated anti-SOSV mAbs and their isotypes and antigen specificity			
mAb name	Heavy chain isotype	Light chain isotype	SOSV protein specificity
SOSV-2	IgG3	Igκ	F
SOSV-5	IgG1	Igκ	
SOSV-10	IgG1	Igκ	
SOSV-21	IgG1	$Ig\lambda_2$	
SOSV-23	IgG1	Igκ	
SOSV-32	IgG3	Igκ	
SOSV-35	IgG1	Igκ	
SOSV-38	IgG1	Igκ	
SOSV-39	IgG1	Igκ	
SOSV-44	IgG1	Igκ	
SOSV-53	IgG1	Igκ	
SOSV-59	IgG1	Igκ	
SOSV-64	IgG1	$Ig\lambda_2$	
SOSV-66	IgG1	Igκ	
SOSV-68	IgG1	Igκ	
SOSV-73	IgG1	Igκ	
SOSV-77	IgG1	Igκ	
SOSV-85	IgG1	$Ig\lambda_1$	
SOSV-13	IgG1	$Ig\lambda_2$	HN
SOSV-19	IgG1	Igκ	
SOSV-24	IgG1	Igκ	
SOSV-29	IgG1	Igκ	
SOSV-83	IgG1	$Ig\lambda_2$	
SOSV-84	IgG1	Igκ	

Table 2.1: Isolated anti-SOSV mAbs and their isotypes and antigen specificity. Name isotype (heavy and light), and SOSV-protein specificity for all 24 isolated anti-SOSV mAbs. 18 of the mAbs recognize the SOSV F protein while the remaining 6 bind to SOSV HN. Antibodies were discovered and isolated using SOSV donor PBMCs and a protocol for making human hybridomas from memory B cells. Antibody sequences were obtained through 5′ or 3′ RACE sequencing of hybridoma cell pellets. Antigen specificity was determined through flow cytometric screening of cell-surface displayed SOSV F or HN proteins.

Chapter II Discussion

The SOSV F and HN constructs successfully expressed the SOSV glycoproteins, also syncytia formation only occurred when both F and HN were transfected and expressed together (**Figure 2.2, Figure 2S.1**). The necessity of both F and HN for syncytia (or fusion) to occur is consistent with the *Rubulavirinae* fusion model (6, 9, 70, 71). Additionally, the lack of syncytia when F is transfected alone indicates that the metastable F protein of SOSV is relatively more stable in the prefusion state compared to viruses like RSV where the F protein alone can cause fusion (6). The absence of syncytia was a highly beneficial outcome as antibodies targeting the prefusion F state are expected to be better at neutralizing the virus (72–75), thus keeping F and HN expressed separately in the cell-surface display screening would likely identify prefusion F-specific B cells. Although, at the time of screening we could not verify the conformational state of the displayed F proteins or the conformational specificity of the B cell or hybridoma supernatants.

Overall, the cell-surface display method was successful and 24 mAbs were discovered. 18 of the 24 mAbs were specific to the F protein while the remaining 6 were isolated against the HN protein. All of the antibodies are in the IgG class as it was known that the SOSV donor had a high IgM and IgG immune response (76), so IgG secreting B cells were specifically targeted in the screening assays. The majority of the isolated mAbs used the IgG1 heavy chain isotype and Igκ was the most used light chain isotype (**Table 2.1**). These results were typical of a standard primary immune response (77, 78), which was the case for the SOSV donor. Recombinant antibodies were

synthesized to allow for better yields and faster production as hybridoma lines were highly variable in yield and growth time between different mAbs.

It is important to note that the number of isolated mAbs reactive to each glycoprotein does not reflect the prevalence of the mAbs in the donor. In fact, there were so many LCL supernatants reactive to both F and HN that the SOSV B cell frequency could not be calculated. More F-reactive B cells were specifically selected for expansion and fusion for two reasons. First, since neutralizing mAbs were desired and we could not confirm conformational state specificity of the Abs at the time of screening we wanted a larger panel to increase the odds of identifying prefusion-specific mAbs. Secondly, at the start of this project I was thinking closer to work done on RSV than on rubulaviruses like mumps. Historically, RSV and the other pneumoviruses were members of *Paramyxoviridae* (6, 79–81) until reclassification separated them into two separate families (5, 81). RSV is also extensively studied as it is the leading cause of severe lower respiratory tract infections in children (82, 83), potentially causing up to almost 80,000 hospitalizations a year in the United States of America (82). Since RSV F is the main target for vaccines and therapeutic mAbs (72, 74), increased attention was given to SOSV F-specific B cells at the start of this project.

In conclusion, the work presented in this chapter establishes the cell-surface display assay as a useful tool identifying SOSV-specific B cells and covers the isolation of the first human mAbs against SOSV.

Chapter II Materials & Methods

Immune cells.

In 2012, a 25-year-old, otherwise healthy individual was infected with SOSV during occupational exposure while handling wild bats as part of a research project (17). In 2017, approximately 5 years post-infection, the SOSV survivor provided written informed consent to participate in donating blood. A leukapheresis pack was obtained from the individual and the peripheral blood mononuclear cells (PBMCs) were isolated from the product. The PBMCs aliquoted into 1-2 mL vials at a density of 10 or 25 million cells/mL and cryopreserved in the vapor phase of liquid nitrogen until use. The studies were approved by the Vanderbilt University Medical Center Institutional Review Board.

SOSV F and HN transmembrane glycoprotein constructs.

Coding sequences for the SOSV F or HN proteins were obtained from the 2012 human isolate sequences (GenBank NC_025343.1). The HN sequence was modified to include an additional glycine residue at the second amino acid position, the F sequence was kept as wildtype. Sequences were codon-optimized for human expression, and cDNA was synthesized by Twist Bioscience and inserted into pTwist-CMV-Betaglobin-WPRE-Neo expression vector for use in cell-surface expression assays. These first generation (SOSV-F1 and SOSV-HN1) constructs were used in all antibody discovery screens. Constructs of the HN and F wildtype (GenBank) coding sequences were generated with the same sequences as above but with the addition of cDNA encoding a DYKDDDDK (FLAG®) tag or 6x His-tag on the cytoplasmic domain of the proteins

(carboxy terminus for the F protein and amino terminus for the HN protein) and synthesized by Twist Biosciences. These second generation constructs (SOSV F-FLAG, SOSV HN-FLAG, SOSV F-6xHis, and SOSV HN-6xHis) were synthesized into pTwist-CMV mammalian expression vector.

PCR cloning to generate constructs of SOSV F-WT and SOSV HN-WT in pTwist-CMV.

The SOSV F-FLAG and SOSV HN-FLAG constructs were used as the DNA template for PCR cloning of the wildtype F and HN genes. Primers were designed in such a way as to not include the FLAG-tags and generate necessary restriction sites to insert into pTwist-CMV. The forward (Fwd) and reverse (Rev) primer sequences were as follows: SOSV-HN-Fwd (5′-TTAAGCGGCCGCGCCACCATGCACGCCAGAAACTCATCAGTATCC-3′), SOSV-HN-Rev (5′-CCTGCGGATCCTTATTTGATGAGG-3′), SOSV-F-Fwd (5′-TACCATCCACTCGACACACCC-3′), SOSV-F-Rev (5′-AATTGGATCCATTGACACTGTCAATGCTGAACAGAC-3′). Primers were synthesized by Integrated DNA Technologies (IDT) using standard desalting. The SOSV-HN-Fwd primer included a tail containing NotI restriction site while the SOSV-F-Rev primer added a BamHI restriction site. The SOSV-HN-Rev and SOSV-F-Fwd primers were designed to include amplification of a BamHI and NotI restriction site (respectively) that were already in the template sequences. PCR was performed using the Platinum SuperFi II green PCR master mix (Invitrogen, cat. # 12369010) following manufacturer's recommendations and melting temperature based on primer sequences. The PCR

amplified products were purified using a GenJET gel extraction and DNA cleanup microkit (Thermo Fisher Scientific, cat. K0831) and digested with NotI and BamHI. Digested amplicons were ligated to empty pTwist-CMV (digested with NotI and BamHI) using T4 DNA ligase (New England Biolabs, cat. # M0202S) following manufacture's protocol. The newly assembled vectors were transformed into competent *E. coli* and single colonies isolated. DNA from 3 clones of each construct (SOSV HN-WT and SOSV F-WT) were sequenced using a PacBio Sequel instrument (Pacific Biosciences) and glycerol stocks made from sequence-verified clones.

Microscopy of SOSV F and HN expression in cultured cells.

HEK293T/17 (ATCC, cat #CRL-11268) cells were seeded at 20,000 live cells/well into a clear-bottomed, black 96-well plate (Greiner Bio-One, cat. #655090) in DMEM + 10% FBS + 1% PSG. While in suspension, cells were transfected with 10 μL of Lipofectamine 3000 (Thermo Fisher Scientific, cat. #L3000015) transfection mix containing plasmids encoding SOSV F-WT, SOSV HN-WT, SOSV F-WT & SOSV HN-WT, SOSV F-FLAG & SOSV HN-FLAG, VSV-G (pCAGGS-G-Kan; Kerafast, cat. # EH1017), or no DNA (mock), with 10-12 replicate wells for each condition. Transfection mixes were prepared following the manufacturer's protocol using ~0.15 μL of Lipofectamine 3000 reagent and ~100 ng total DNA per well. The plate was incubated at 37°C in 5% CO_2 for 45 hr, after which the medium was removed, and the cells were fixed in 100 μL of 4% PFA for 1 hr. Cells were washed several times with DPBS before blocking and permeabilizing with 150 μL/well of permeabilization buffer (5% nonfat dry milk, 0.1% saponin, in 1X PBS-T) or 60 min at room temperature (RT). A pooled mix of

anti-SOSV mAbs was made by mixing 3 HN mAbs and 3 F mAbs; the anti-SOSV mix was diluted to 1:250 in permeabilization buffer while monoclonal anti-FLAG M2 (Sigma-Aldrich, cat. # F3165) was diluted 1:500 in permeabilization buffer. Cells were stained with 50 μL of anti-SOSV or anti-FLAG primary (half the plate) and incubated ~1 hr at RT, after which the primary stain was removed, and the plate washed with DPBS. The cells were then stained with 50 μL of the secondary mix (goat anti-human IgG-AF488 (SouthernBiotech, cat. #2040-30) and goat anti-mouse Alexa Fluor 488 IgG (H + L) (Invitrogen, cat. #A11001) both diluted to 1:1,000) in permeabilization buffer and incubated 1 hr at RT, protected from light. Cells were then washed with DPBS before being stained with 50 μL/well of DAPI (4,6-diamidino-2-phenylindole, dihydrochloride) (Invitrogen, cat. #D1306) diluted to 5 μM in DPBS for 15 min. Cells were then washed several times and then kept in 250 μL/well of DPBS for imaging. Imaging was done on an EVOS M5000 instrument (Invitrogen, cat. #AMF5000) with a 10× objective with four fields of view imaged for 3 replicate wells of each transfection condition. Area of stained cells/syncytia was measured using Fiji (84), and the data were analyzed in Prism (GraphPad Software, version 9.3.1 for Mac OS X).

EBV transformation of cell lines from human blood.

Vials of cryopreserved PBMCs were thawed at 37°C and washed in ClonaCell™-HY Medium A (STEMCELL Technologies, cat. #03801). Epstein-Barr virus (EBV) was obtained by collecting the supernatant of the marmoset lymphoblastoid cell line (LCL) B95-8 (85) (formerly available from the American Type Culture Collection as ATCC® CRL-1612). B cells were transformed with EBV by combining washed PBMCs with

prepared stocks of filtered B95-8 cell supernatant, using 4.5 mL to transform 8 to 10 million PBMCs in B cell growth medium (Medium A containing CpG (86) [Invitrogen, oligo ZOEZOEZZZZZOEEZOEZZZT] at the 10 µmole scale [desalted], cyclosporin A [Sigma-Aldrich, cat. #C1832], and Chk2 inhibitor II [Sigma-Aldrich, cat. # C3742]). Cells were plated at 50 µL/well in one 384-well plate for each suspension of 8 to 10 million PBMCs. Cells were incubated at 37°C in 7% CO_2 for 6 to 12 days until LCLs were clearly visible and forming colonies. The plates of transformed B cells were expanded to four 96-well plates in B cell expansion medium (Medium A, CpG, Chk2i II, and 10 million irradiated human PBMCs per plate from an unrelated healthy donor [Nashville Red Cross]). The plates were incubated at 37°C in 7% CO_2 for 4 to 7 days before screening antibodies in LCL supernatants for binding to SOSV antigen expressed in cells using a high-throughput flow cytometry assay.

Production of human hybridoma cell lines from transformed B cells.

Once positive SOSV-reactive wells of LCLs were identified, the B cells from these wells were transferred to microcentrifuge tubes and washed three times with BTX medium (300 mM sorbitol [Fisher Scientific, cat. # BP439], 0.1 mM calcium acetate [Fisher Scientific, cat. # AC21105-2500], 0.5 mM magnesium acetate [Fisher Scientific, cat. #AC42387-0050], and 1.0 mg/mL bovine serum albumin [Sigma-Aldrich, cat. # A3294]). The B cell pellets were resuspended in BTX medium, combined with the HMMA2.5 human-mouse myeloma fusion partner cell line (87) and electroporated in a 0.2 µm cuvette (BTX, cat. # 45-0125). After fusion, cells were left in cuvettes in 7% CO_2 at 37°C for at least 30 min before transferring to hypoxanthine-aminopterin-thymidine

(HAT) selection medium (88–90) (20% ClonaCell™-HY Medium E [STEMCELL, cat. # 03805], 80% Medium A, HAT media supplement [final concentrations: 100 µM hypoxanthine, 0.4 µM aminopterin, 16 µM thymidine (Sigma-Aldrich cat. # H0262-10VL)], and 150 µL of 1 mg/mL ouabain octahydrate [Sigma-Aldrich, cat. #O3125; final concentration 0.33 µg/mL]). Fused cells were plated by limiting dilution in 384-well plates with 50 µL/well volumes. The plates were incubated for 2 to 3 weeks, feeding with 25 µL/well of Medium E after 1 week, before screening for binding to recombinantly expressed viral antigens by high-throughput flow cytometry to identify wells with hybridomas secreting SOSV-reactive antibodies. SOSV-reactive hybridomas were expanded to 48-well plates with 500 µL/well Medium E and screened again.

Isolation of human mAbs secreted from hybridoma cell lines.

The hybridoma cell lines secreting SOSV-reactive antibodies were cloned using single-cell sorting on a BD FACSAria III cytometer (BD Biosciences) or SH800 Cell Sorter (Sony Biotechnology) into 384-well plates containing Medium E and incubated in 7% CO_2 at 37°C for 1 to 2 weeks for the cells to expand in number. Supernatants from 384-well plates (one plate for each hybridoma line) were screened by high-throughput flow cytometry using cell-surface expressed SOSV antigens to identify hybridoma cell clones secreting SOSV-specific antibodies. The cloned hybridoma cell lines with antigen-reactive supernatants were scaled up gradually in 48-well, 12-well, T-25, and T-75 plates or flasks with screening for antibody binding to cell-surface displayed antigens by high-throughput flow cytometry at each expansion step. The cells from T-75 flasks were used to make frozen stocks of the mAb-secreting cloned hybridoma cell lines by

freezing cells in freezing medium (50% cell culture medium, 40% fresh Medium E, and 10% dimethyl sulfoxide).

Sequence analysis of antibody variable genes.

Cell pellets from clonal hybridoma cell lines were processed for RNA extraction and amplification of antibody variable genes by 5′RACE or 3′RACE procedures, and DNA sequence analysis of cDNA using a Sequel instrument (Pacific Biosciences) as previously described (60). The recombinant versions of each of the 24 anti-SOSV mAbs were created by synthesizing a cDNA encoding the antibody variable gene regions and cloning by Gibson assembly into a human IgG1 expression vector (with κ or λ light chain as appropriate) as previously described (91–93) using Twist Biosciences to synthesize the DNA.

Purification of mAb proteins from hybridoma.

Ab IgG proteins in supernatants of cloned hybridoma cell lines were prepared by washing cells from T-75 flasks in serum-free Hybridoma-SFM Medium (Thermo Fisher Scientific, cat. # 12045076) and seeding 3 to 6 wells of a 6-well G-Rex plate (Wilson Wolf, cat. # 80240M) with the mAb-secreting lines in Hybridoma-SFM medium. The G-Rex plates were incubated in 7% CO_2 at 37°C, with the supernatant typically being harvested and cells split every one to two weeks. The G-Rex wells were reseeded up to a maximum of 3 times. MAb supernatants were collected and clarified through a 0.2 μm filter, and then mAbs were isolated by fast protein liquid chromatography (FPLC) on an ÄKTA pure system (Cytiva) using HiTrap Protein G High Performance (Cytiva, cat. # 17-

0404-01) or HiTrap MabSelect SuRe (Cytiva, cat. # 11-0034-95) columns.

Purification of mAb proteins.

Plasmids encoding the recombinant mAbs were expressed using the ExpiCHO expression system (Thermo Fisher Scientific, cat. # A29130). Cultures of ExpiCHO cells (Thermo Fisher Scientific, cat. # A29127) were transfected at a density of around 6 x 10^6 live-cells/mL in flat-bottomed Erlenmeyer flasks following manufacturer's protocol. Cells were cultured at 37ºC, 7% CO_2 with shaking at 125 RPM and harvested 8-10 days post-transfection. The recombinant mAb supernatants were collected and clarified through a 0.2 µm filter, and then mAbs were isolated by fast protein liquid chromatography (FPLC) on an ÄKTA pure system (Cytiva) using HiTrap Protein G High Performance (Cytiva, cat. # 17-0404-01) or HiTrap MabSelect SuRe (Cytiva, cat. # 11-0034-95) columns. Eluants were collected and concentrated using Amicon Ultra-15 Centrifugal Filters with Ultracel-10 Membrane (Millipore Sigma, cat. # UFC901024) and buffer exchanged to DBPS with Zeba™ Spin Desalting Columns (7K MWCO, 10 mL, Thermo Fisher Scientific, cat #89894. Antibody stocks were diluted to a concentration of 1 mg/mL, aliquoted, flash-frozen using dry-ice and ethanol bath, before being stored at -80ºC until needed. When thawed, antibody stocks were maintained at 4ºC.

High-throughput flow cytometric detection of binding to cell-associated viral antigens.

Expi293F cells were transfected with DNA plasmids encoding either full-length SOSV F or HN constructs as described. Cells were seeded in flat-bottomed flasks at 2.5

x 10^6 cells/mL, using the volume of the culture size used to scale the transfection mix. The transfection mix was prepared by combining cold Opti-MEM™ I Reduced-Serum Medium (Thermo Fisher Scientific; 0.1 mL/mL of cells), DNA (1 µg/mL of cells), and 2.7 µL/mL of cells Expifectamine 293 reagent (in Thermo Fisher Scientific kit, cat. # A14524) mixing 3 to 5 times by pipetting and incubating at RT for 20 to 30 min. Flasks of cells first were swirled before adding the transfection mix to ensure even spreading of the transfection mix. Cells were incubated at 37°C in 7% CO_2 with shaking at 125 RPM for 24 to 48 hr. The day after transfection, ExpiFectamine™ 293 Transfection Enhancer 1 and Enhancer 2 were added at 0.5% or 5% scale of transfection, respectively. Transfected cells were plated at 50,000 to 70,000 live-cells/well in 96-well V-bottom plates, washed with flow cytometry buffer (DPBS without calcium and magnesium, 2% low-IgG FBS, 2 mM EDTA), and stained with antibodies in the supernatants of transformed B cells or hybridoma cells, or purified mAb, at 30 to 50 µL/well at 4°C for 30 min as the primary stain. The primary stain was washed off with flow cytometry buffer, and the cells were stained with 50 µL/well of a 1:1,000 dilution of goat anti-human IgG-PE (Southern Biotech, cat. # 2040-09) secondary antibodies for 30 min at 4°C. The secondary antibodies were removed by washing with DPBS and cells were fixed with 50 to 100 µL of 4% paraformaldehyde (PFA) in DPBS for 10 min at RT. For screening for binding of antibodies in hybridoma supernatants or suspensions of purified mAbs, cells were also stained with LIVE/DEAD™ Fixable Violet Dead Cell Stain (Invitrogen, cat. # L34963) for 30 min at 4°C prior to fixation. The fixative was washed off with flow cytometry buffer and cells resuspended in 25 µL of FACS buffer and analyzed on an iQue Screener PLUS flow cytometer with the violet, blue, and red (VBR) three-laser,

thirteen-colour system (Sartorius). Live-dead staining was not performed on all assays. Data was analyzed in Forecyt (Sartorius)

Statistical analyses.

A one-way ANOVA followed by a Tukey's multiple comparisons test was used in Prism (GraphPad Software, version 9.3.1 for Mac OS X) to analyze the differences in cell average area of the fluorescent cells transfected with control conditions or SOSV glycoproteins (**Figure 2.2**). The P-value threshold used was <0.05.

Chapter II Supplemental Information

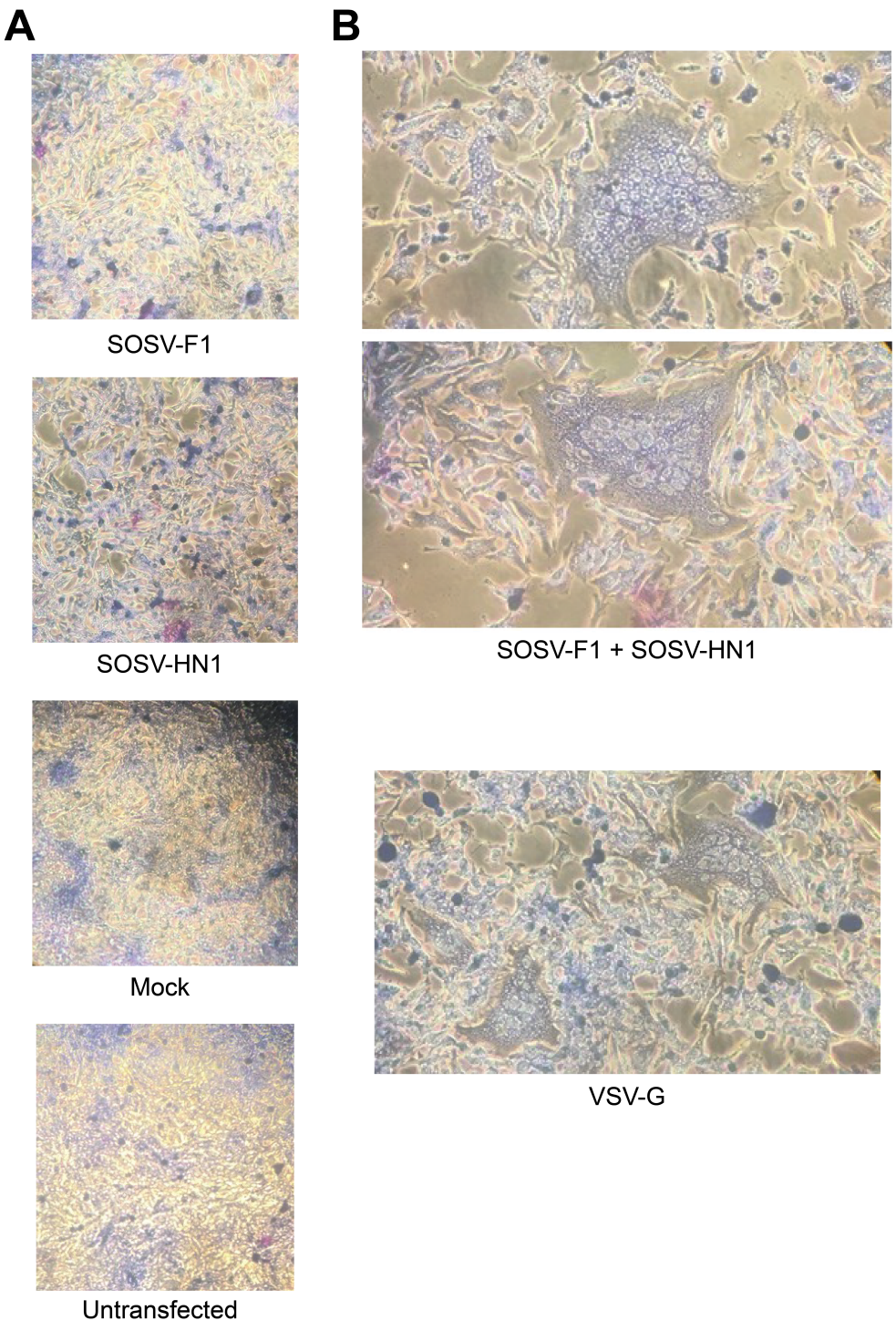

Figure 2S.1. Wright-Giemsa stain of HEp-2 cells transfected with viral glycoproteins. HEp-2 cells were transfected with plasmids expressing viral proteins and incubated for 4 days at 37°C, 5% CO_2. Cells were fixed with cold methanol and then stained with Wright-Giemsa. Cells were imaged with a bright-field microscope at 20×. **(A)** Non-syncytia producing transfections. SOSV-F1 and SOSV-HN1 expressed alone did not induce syncytia as neither did the mock or untransfected conditions. **(B)** Syncytia-inducing transfections. SOSV-F1 and SOSV-HN1 induced large syncytia formation when co-transfected. VSV-G served as a positive control for syncytia formation.

2S.1 Materials and methods.

HEp-2 cells (ATCC, CCL-23) were seeded in 24-well plates at 20,000 live-cells/mL and incubated overnight at 37°C, 5% CO_2 in growth medium (Opti-MEM I [Gibco, cat. # 31985088] + 5% FBS [Gibco, cat. # A3840102] + 1% PSG [Gibco, cat. # 10378016]). The next day cells were transfected with Lipofectamine 3000 (Invitrogen, cat. # L3000015) following manufacturer's protocol. Transfection conditions included: SOSV-F1, SOSV-HN1, SOSV-F1+SOSV-HN1, VSV-G, mock, and untransfected. SOSV-F1 and SOSV-HN1 are expressed with pTwist-CMV-Betaglobin-WPRE-Neo while VSV-G is in pCAGGS. Four days post-transfection growth media was removed, and monolayers were washed in DPBS (Corning, cat. # 21031CM). Wright-Geimsa stain (Electron Microscopy Sciences, cat. # 26149-01) was added to the monolayers at 500 μL/well and incubated at room temperature for 30 min. Wright-Geimsa was removed and carefully discarded in chemical waste (contains methanol). Excess stain was removed by rinsing wells with DPBS. Wells were filled with ~1 mL DPBS and imaged with a standard bright-field microscope.

CHAPTER III

Characterization of anti-SOSV recombinant monoclonal antibodies

Disclaimer: part of the data and information presented in this chapter were adapted from the following:

Parrington HM, Kose N, Armstrong E, Handal LS, Diaz S, Reidy J, Dong J, Stewart-Jones GBE, Shrivastava-Ranjan P, Jain S, Albariño CG, Carnahan RH, Crowe JE. 2023. Potently neutralizing human monoclonal antibodies against the zoonotic pararubulavirus Sosuga virus. JCI Insight https://doi.org/10.1172/jci.insight.166811.

Chapter Acknowledgements:

Dr. Guillaume Stewart-Jones formerly of the Vaccine Research Center (VRC), of the National Institute for Allergy and Infectious Disease (NIAID), of the National Institutes of Health (NIH), Bethesda, Maryland, USA: designed the secreted pre- and postfusion SOSV F proteins. Dr. Stewart-Jones also provided some samples of purified proteins that he had made which were used in initial studies.

Dr. Elad Binshtein of the Vanderbilt Vaccine Center, Vanderbilt University Medical Center (VUMC), Nashville, TN, USA performed the negative-stain electron microscopy on the antigen and Fab samples that I provided. Dr. Binshtein also produced the 3D and 2D images that were used in Figures 3.11-12.

Dr. Jinhui Dong formerly of Vanderbilt Vaccine Center, Vanderbilt University Medical Center (VUMC), Nashville, TN, USA designed the soluble SOSV-HN_{ecto} construct.

Chapter III Introduction

This chapter expands on the panel of antibodies discovered in Chapter II by further characterizing their specificity to protein domains or conformations. From the cell-surface display screening, only the glycoprotein specificity of the anti-SOSV mAbs was known. While the cell-surface display system is a useful tool for expression of whole, viral transmembrane proteins, on its own cell-surface display cannot give more refined specificity. For example, as SOSV F protein, like all paramyxovirus F proteins, can be in either in the prefusion or postfusion conformational states (1, 6, 7). Without having methods to control for the different states, I could not tell which conformation any given anti-F mAb was recognizing. Currently there are no human mAbs to *Rubulavirus* F or HN proteins. Mouse mAbs may be commercially available for some viruses but target structural proteins such as N rather than the glycoproteins so there were not any antibodies that had already been characterized available for controls. Thus, to further refine the specificity of the anti-SOSV mAbs I needed a different system. Fortunately, work in structural biology had solved a crystal structure for SOSV HN (94), and we also started a collaboration with a researcher who had made prefusion-F stabilized versions of parainfluenza viruses 1-4 (95) and had already been extending that knowledge to SOSV. From these structural studies and collaborations, some of the challenges briefly mentioned in Chapter II around soluble protein production were alleviated. Using soluble SOSV F and HN proteins I sought to further characterize the anti-SOSV mAbs

and begin the process of determining their epitopes.

One of the major questions I sought to address in this project was the possibility of cross-reactive antibodies between SOSV and other members of *Rubulavirinae*, and to discover any epitopes of cross-reactivity. Cross-neutralizing antibodies may provide protection against a broad group of viruses (63, 75, 96–100) which can have direct therapeutic applications. However, even non-neutralizing cross-reactive antibodies can have uses in diagnostic assays for viruses with highly variable strains or as reagents in scientific research. The evolutionary relationship between paramyxoviruses, particularly rubulaviruses, (4, 35, 101) means that there is the high likelihood of more pararubulaviruses being discovered in the future, and having a cross-reactive antibody could help in studying such novel viruses. In this chapter I will discuss the protein domain/conformation specificity of the anti-SOSV mAbs, their competition-binding groups, and cross-reactivity to other members of *Rubulavirinae*.

Chapter III Results

Expression of recombinant HN SOSV antigens for production of soluble proteins.

We developed two soluble constructs of the HN proteins, using the wildtype HN sequence as a template. The first construct was intended to make tetrameric HN proteins and included the majority of the protein's ectodomain (residues 75-582) and was designated as HN_{ecto}. The second construct was following the design first described by Stelfox & Bowden (94), which contains the globular head domain and a very small

portion of the stalk domain and produces a dimeric molecule. We used the same portion of the HN molecule as Stelfox & Bowden (94), residues 125-582, and termed this construct HN_{head}. A human CD5-signal peptide sequence was added along with a thrombin-cleavable 6x His-tag to the amino terminus of the proteins (**Figure 3.1A**). Additional constructs that used the same HN sequences as HN_{ecto} and HN_{head} were also made to help reduce contamination in the purified protein product for use in electron microscopy. These constructs included a mouse IL-2 signal sequence and a thrombin-cleavable 8x His-tag and Twin-Strep-tag® (102); these constructs were designated $HN_{ecto\text{-}TS8H}$ and $HN_{head\text{-}TS8H}$ (**Figure 3.1A**). All constructs were human codon-optimized and synthesized by Twist Biosciences into pTwist-CMV expression vectors. Soluble HN proteins were expressed in Expi293F cells for 5 to 7 days and purified from cell supernatants using an ÄKTA pure system (Cytiva), and the eluate was concentrated and buffer-exchanged into Dulbecco′s Phosphate Buffered Saline (DPBS) or Tris-saline (140 mM Tris-HCl, 20 mM NaCl, pH ~8). The final purified proteins were about 70 kDa in apparent molecular weight. Negative-stain electron-microscopy (NS-EM) showed that the HN_{ecto} construct produced proteins in various oligomeric states but predominantly tetramers and dimers, while the HN_{head} construct produced dimers (**Figure 3.1B**).

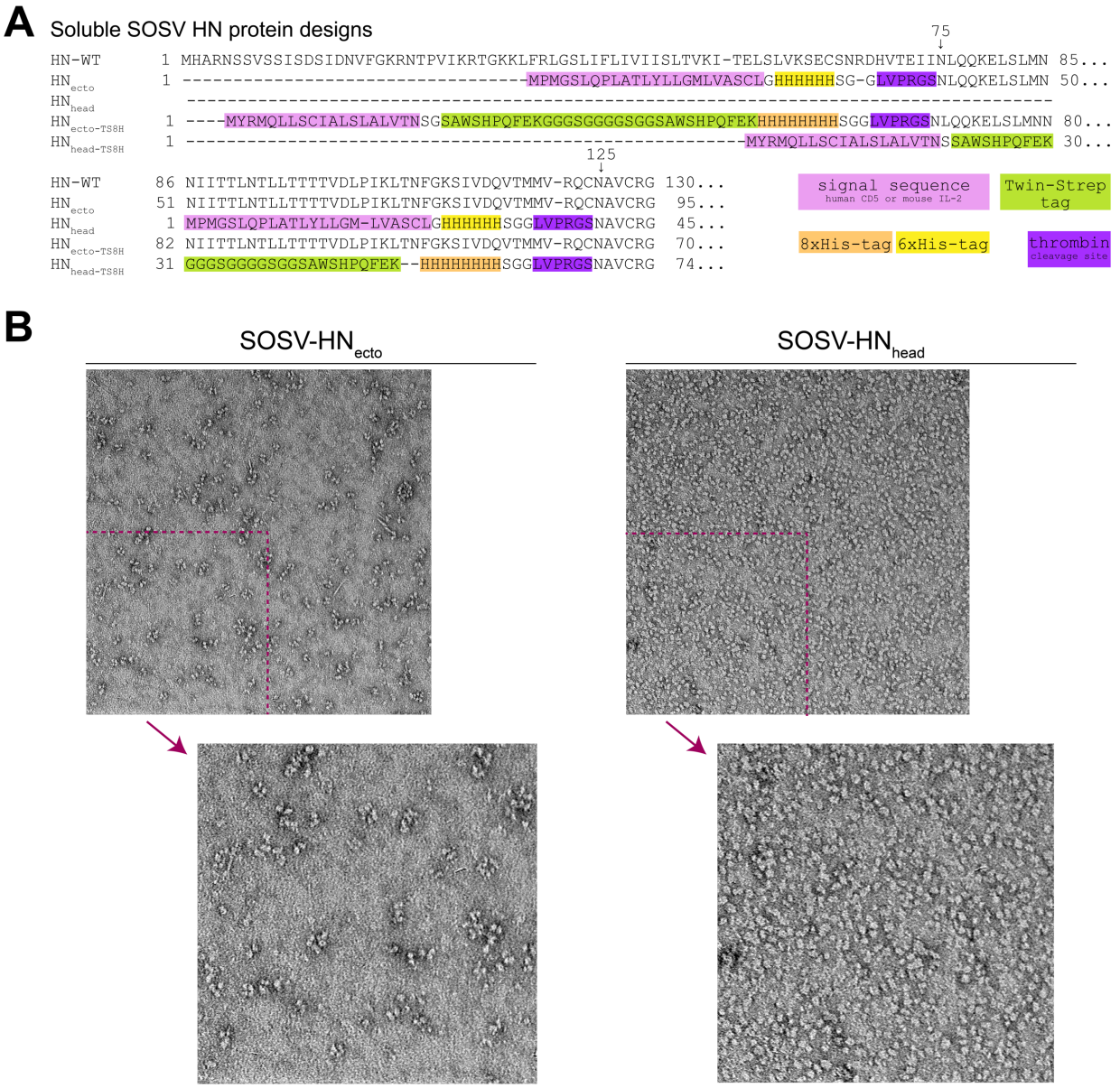

Figure 3.1. Soluble constructs of SOSV HN protein can produce oligomeric proteins. (A) Amino acid sequence comparison between SOSV-WT and the soluble constructs HN_{ecto}, HN_{head}, $HN_{ecto\text{-}TS8H}$, $HN_{head\text{-}TS8H}$. The 'ecto' proteins use 75-582 while 'head' proteins use residues 125-582, which excludes the cytoplasmic and transmembrane domains. Signal peptide sequences (pink), His-tags (6x yellow, 8x, peach), and Twin-strep-tags (green) were all placed at the amino terminus of the HN proteins with a thrombin cleavage site (purple) between the tags and HN sequences. **(B)** NS-EM images of purified HN_{ecto} and HN_{head}. Areas enclosed in the pink lines was expanded for easier viewing. Visible tetrameric and dimeric proteins can be seen in the HN_{ecto} image.

Expression of recombinant F SOSV antigens for production of soluble proteins.

Dr. Guillaume Stewart-Jones of the Vaccine Research Center (VRC) designed soluble forms of the SOSV F protein using similar work done for parainfluenza viruses (95). Both a prefusion-stabilized (preF-tHS) and postfusion (postF-tHS) conformations (**Figure 3.2A**) were synthesized and cloned into the mammalian expression vector pVRC4800 by Dr. Stewart-Jones, who graciously sent purified plasmid DNA of the constructs to use in this work. The DNA was transformed into Stellar competent cells (Takara Bio) and grown with kanamycin selection, miniprep DNA was isolated from 3 clones (single colonies) of each construct and sequence verified. The pre- and postfusion F protein constructs contain a mouse IL-2 signal sequence at the amino terminal, followed by the SOSV F protein sequence from residues 15 to 476, and an engineered, trimeric coiled-coil domain of the yeast transcriptional activator GCN4 leucine zipper (GCNt (103)) replacing the transmembrane and cytoplasmic domains and lastly a thrombin-cleavable 6x His-tag and Strep-tag II (104) the carboxy terminus. To help stabilize the prefusion conformation, the poly-basic furin cleavage site was disrupted site by replacing three residues (from 101-103) with a soluble glycine linker and adding a stabilizing disulfide bond between residues 206 and 223 (95). Soluble protein was generated by expressing the constructs in Expi293F cells for 5 days before purification by FPLC on a AZURA P 6.1L (Knauer), eluate fractions were combined, concentrated, and buffer-exchanged into Dulbecco′s Phosphate Buffered Saline (DPBS) or Tris-saline (140 mM Tris-HCl, 20 mM NaCl, pH ~8). The final protein product had an apparent molecular weight of about 55 kDa. NS-EM of the postF-tHS product revealed postfusion molecules that assembled into rosettes, while the preF-tHS construct

produced proteins predominantly in the prefusion state but with postfusion molecules still present and rosettes were not observed (**Figure 3.2B&C**)

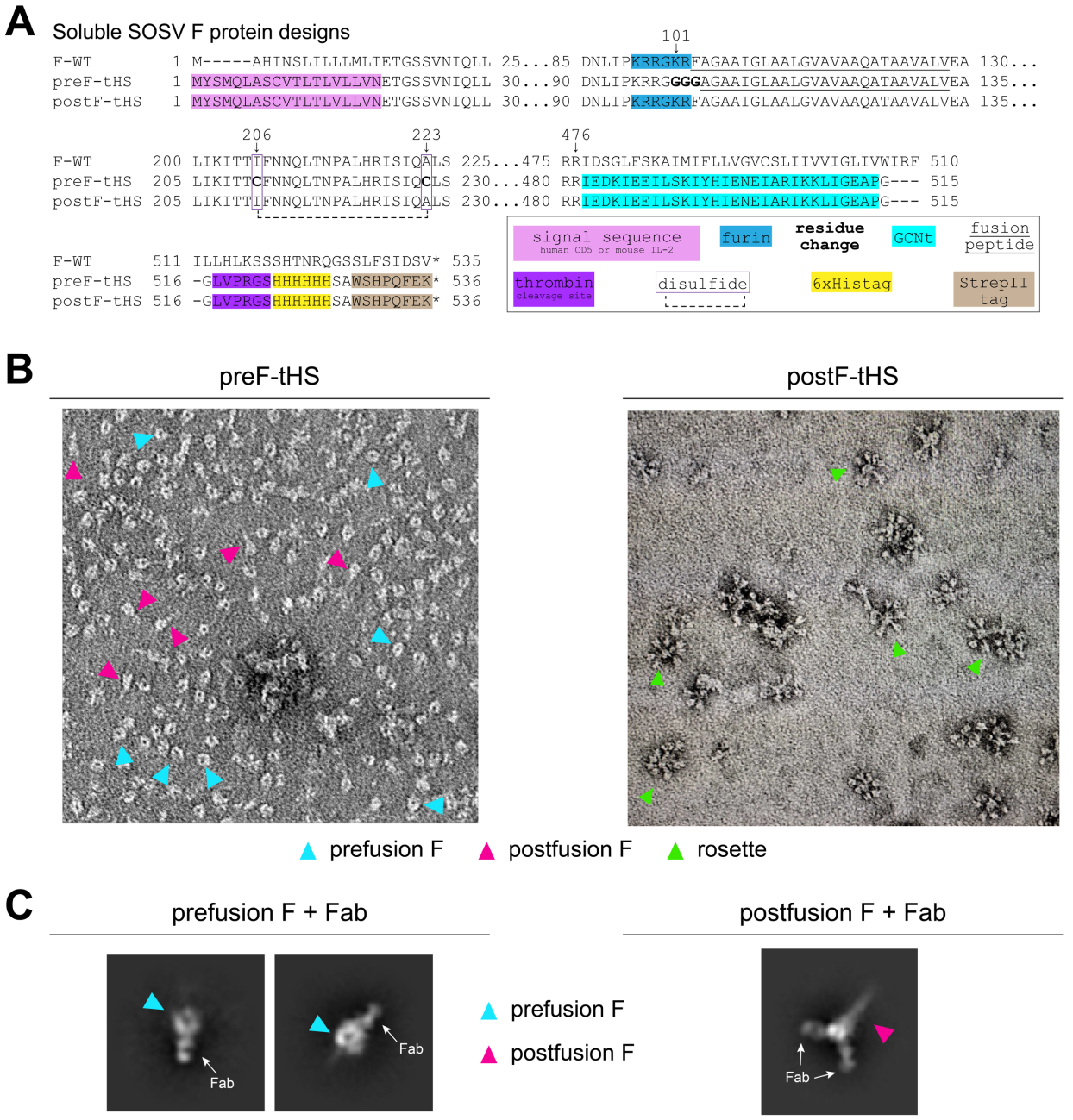

Figure 3.2. Soluble constructs of SOSV HN protein can produce oligomeric proteins. Soluble SOSV pre- and postfusion F constructs were expressed in Expi293F cells and purified on FPLC. NS-EM was performed on purified proteins. (A) Comparison of the SOSV preF-tHS (prefusion), postfusion F (postF-tHS), and wildtype (F-WT) sequences. Both soluble designs F protein use residues 15-476 of the wildtype sequence, this removes the native signal sequence and the cytoplasmic and transmembrane domains. A mouse IL-2 signal sequence is put at the N-terminal while a GCNt trimerization domain, 6x His-tag, and Strep-tag II are added to the C-terminal. Additional, stabilizing modifications to the preF-tHS sequence are a soluble linker at residues 101-103 and point mutations at residues 206 and 223 to cysteines. **(B)** NS-EM images of purified protein from preF-tHS and postF-tHS constructs. The preF-tHS produces a mix of prefusion (blue arrows) and postfusion (magenta arrows) molecules. The postF-tHS construct produce postfusion molecules that form rosettes (green arrows). **(C)** 2D class images of prefusion (blue arrows) and postfusion (magenta arrow) F molecules bound by anti-SOSV Fabs (white arrows).

Domain specificity of HN-reactive mAbs.

Since the two constructs for soluble HN had differing portions of the stalk domain, the two forms of protein were used to determine the domain-specificity (stalk or head) of the anti-HN mAbs. ELISA assays were used to assess binding of the mAbs to the HN_{head} protein and the tetrameric/dimeric HN_{ecto} protein in ELISA. All six of the HN-reactive mAbs (rSOSV-13, -19, -24, -29, -83, and -84) bound to both HN antigens (**Figure 3.3**), indicating that the binding sites for all mAbs were likely located in the globular head domain of the HN protein. The half-maximal effective concentration (EC_{50}) values for binding of the rmAbs to soluble HN proteins ranged from 22 to 92 ng/mL (**Table 3.1**). For comparative purposes, two of the mAbs (rSOSV-84 and rSOSV-24; selected at random) were purified as IgG from hybridoma cell line supernatants and tested in ELISA to verify similarity in binding between recombinant and hybridoma versions of the mAbs (**Figure 3S.1**). The HN-reactive rmAbs also were tested in a competition-binding ELISA (**Figure 3.3**), revealing that the anti-HN mAbs could be divided into 4 competition-binding groups. The groups were labelled: Group 1: rSOSV-84, Group 2: rSOSV-83, rSOSV-29, and rSOSV-24, Group 3: rSOSV-19, and Group 4: rSOSV-13. Four competition-binding groups were identified consistently whether testing for competition-binding to HN_{head} (**Figure 3.4A**) or HN_{ecto} proteins (**Figure 3.4B**).

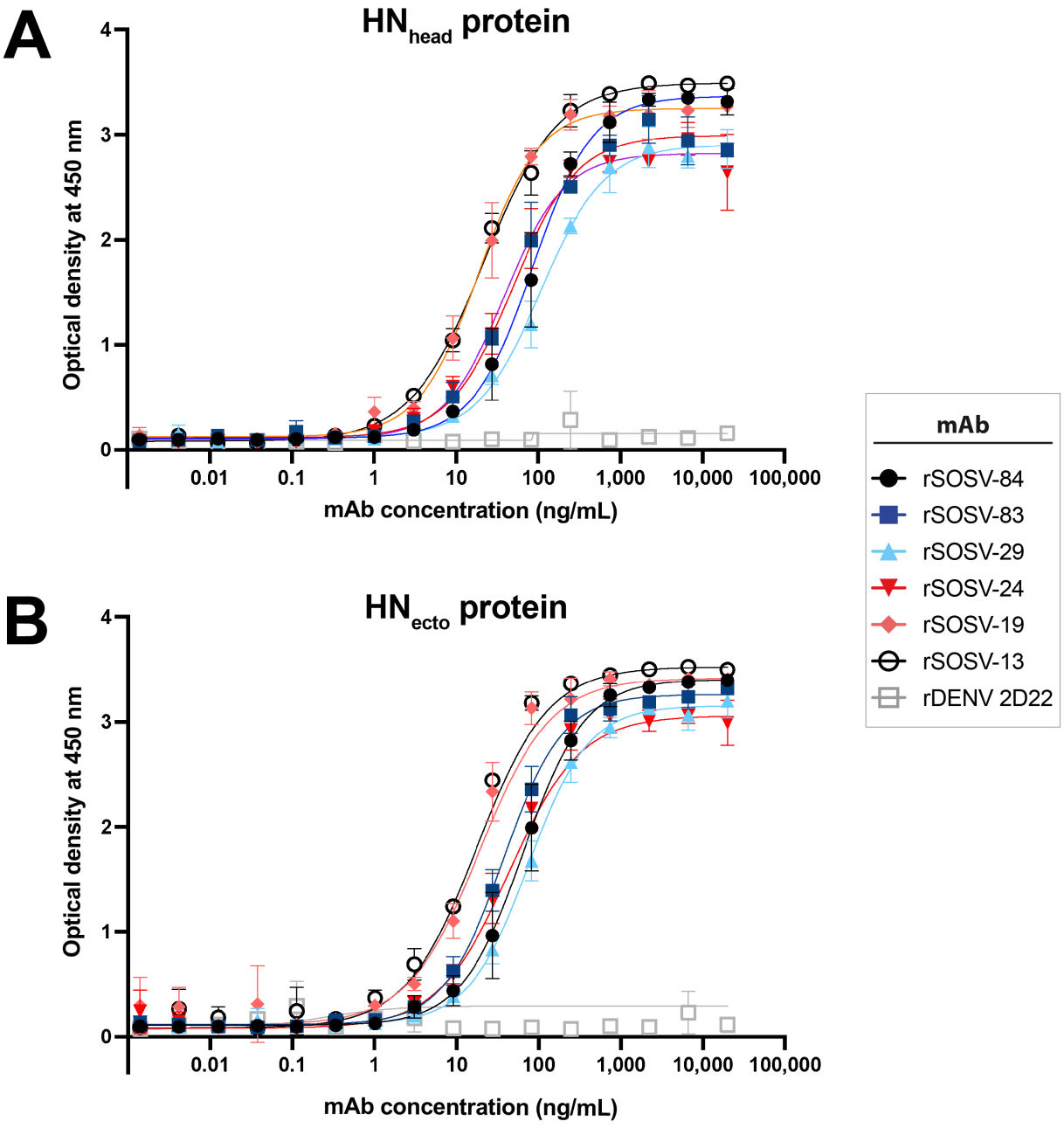

Figure 3.3. Representative ELISA for binding of anti-HN rSOSV mAbs to soluble HN antigens. Representative data of three biological replicates performed using anti-HN rmAbs. Graphs are shown as the average of three technical replicates plotted with standard deviation. **(A)** Anti-HN rSOSV mAbs against HN_{head} proteins. **(B)** Anti-HN rmAbs against and HN_{ecto}.

Table 3.1 Half-maximal effective concentration (EC_{50}) values for antibody binding soluble HN proteins in ELISA		
MAb (rSOSV-)	**EC_{50} value for binding (ng/mL) to indicated protein antigen (± SD)**	
	HN_{ecto} protein	**HN_{head} protein**
13	38.9 ± 27	29.5 ± 8.7
19	28.1 ± 9.6	22.0 ± 5.7
24	66.4 ± 41	64.0 ± 26
29	78.8 ± 24	92.2 ± 21
83	67.3 ± 27	63.7 ± 20
84	105.7 ± 38	66.8 ± 23

Table 3.1. Half-maximal effective concentration (EC_{50}) antibody binding soluble HN proteins in ELISA. The relative EC_{50} values were obtained for each of the six anti-HN SOSV mAbs against HN_{ecto} and HN_{head}. EC_{50} values were calculated for each biological replicate (3 total) each consisting of 3 technical replicates per antibody and averaged with standard deviation. Additionally, a negative control mAb (rDENV-2D22) in each assay to confirm non-specific binding did not occur throughout the assays.

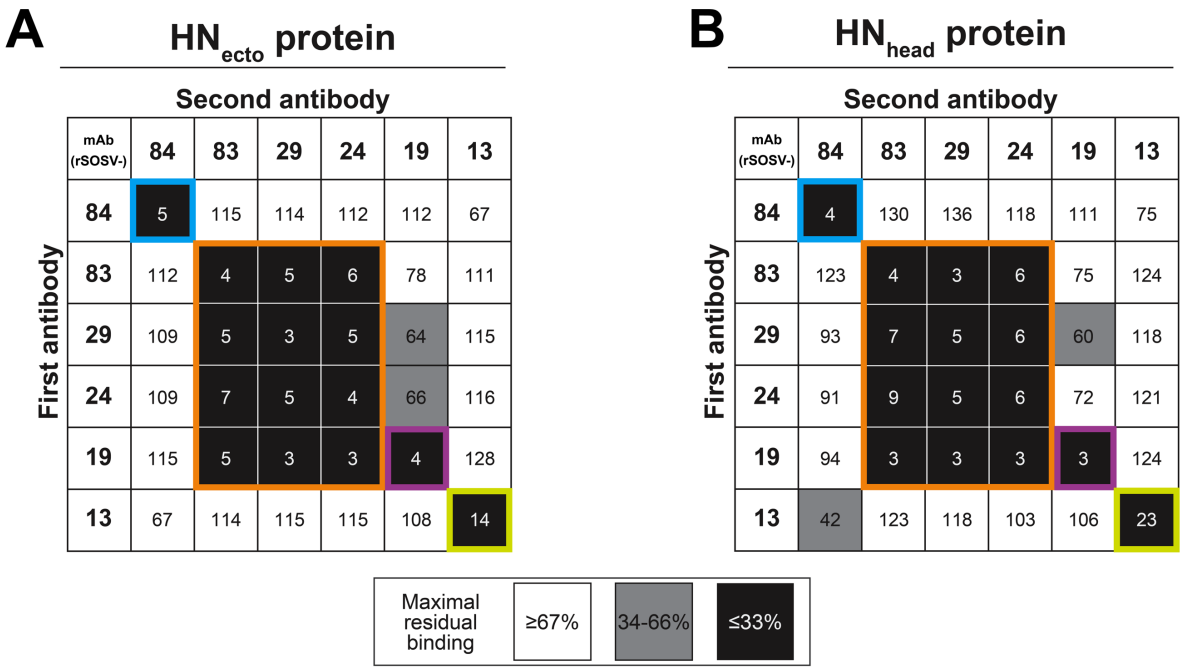

Figure 3.4. Competition-binding assay for anti-HN rmAbs. Unlabelled primary (first) mAb was bound to antigen-coated plates in saturating conditions (10 μg/mL) with second, biotinylated antibodies added at a final concentration of 100 ng/mL. Detection of biotinylated rmAbs accomplished using mouse anti-biotin AP. Data were converted to percent binding relative to the maximal non-competing binding of the second antibody (lacking a primary mAb). Assays were repeated in triplicate with quadruplicate technical replicates. A representative assay for each antigen/mAb set tested is shown. **(A)** Binding data of mAbs against HN_{ecto} as antigen. **(B)** Binding data of mAbs against HN_{head} as antigen.

Conformational specificity of anti-F mAbs.

As paramyxovirus fusion proteins only metastable in the prefusion state (6, 7, 105), I needed to determine if the anti-F mAbs were postfusion or prefusion specific. To accomplish this, I used ELISA assays and the preF-tHS and postF-tHS proteins. Additionally, ELISAs were performed with pre- and postfusion protein samples provided by Dr. Stewart-Jones to help verify the conformational specificity of each mAb (**Figure 3S.2**). A single mAb (rSOSV-85) was specific to the postfusion conformation while seven mAbs (rSOSV-10, -21, -38, -39, -64, -66, and -73) were specific to the prefusion conformation (**Figure 3.4**). Eight mAbs (rSOSV-2, -5, -23, -32, -44, -53, -68, -77) recognized both the pre- and postfusion proteins (**Figure 3.4**). The mAbs rSOSV-35 and rSOSV-59, did not detectably bind to either antigen during the ELISAs (**Figure 3.4**), though they still bound to cell-surface displayed, WT protein. For grouping purposes, these two antibodies were included with the prefusion-specific set, bringing that class up to 9 antibodies (rSOSV-10, -21, -35, -38, -39, -59, -64, -66, and -73). The relative half-maximal effective concentration (EC_{50}) values for binding of the rmAbs are summarized in (**Table 3.2**). The EC_{50} values for the prefusion binding ranges from 15.7 ng/mL to 54.2 ng/mL. The EC_{50} values for binding to postfusion protein ranged from 1.5 ng/mL to 42.7 ng/mL. Similarly, to the anti-HN mAbs, the anti-F mAbs were also assessed for competition-binding groups using ELISA. Since the conformational-specificity of the mAbs already divided them into 3 classes (prefusion, postfusion, and pre- & postfusion), antibodies were competed within their respective class except for the single, postfusion specific mAb which was included with the pre- & postfusion class. Additionally, the pre- & postfusion mAbs were tested in competition-binding ELISAs against prefusion and

postfusion F to confirm that the binding groups was not dependent on conformational state. The data (**Figure 3.5**) revealed that there are approximately eight distinct competition-binding groups: Group 1) rSOSV-73; Group 2) rSOSV-66, -64, and -38; Group 3) rSOSV-39 and rSOSV-10; Group 4) rSOSV-21; Group 5) rSOSV-59 and rSOSV-35; Group 6) rSOSV-77, -68, -53, -44, -5; Group 7) rSOSV-32, -23, -2; and Group 8) rSOSV-85. Competition-binding was also examined using cell-surface display flow cytometry with wildtype F protein and gave similar results and helped confirm the members of Group 5 (rSOSV-59 and rSOSV-35) (**Figure 3S.3**).

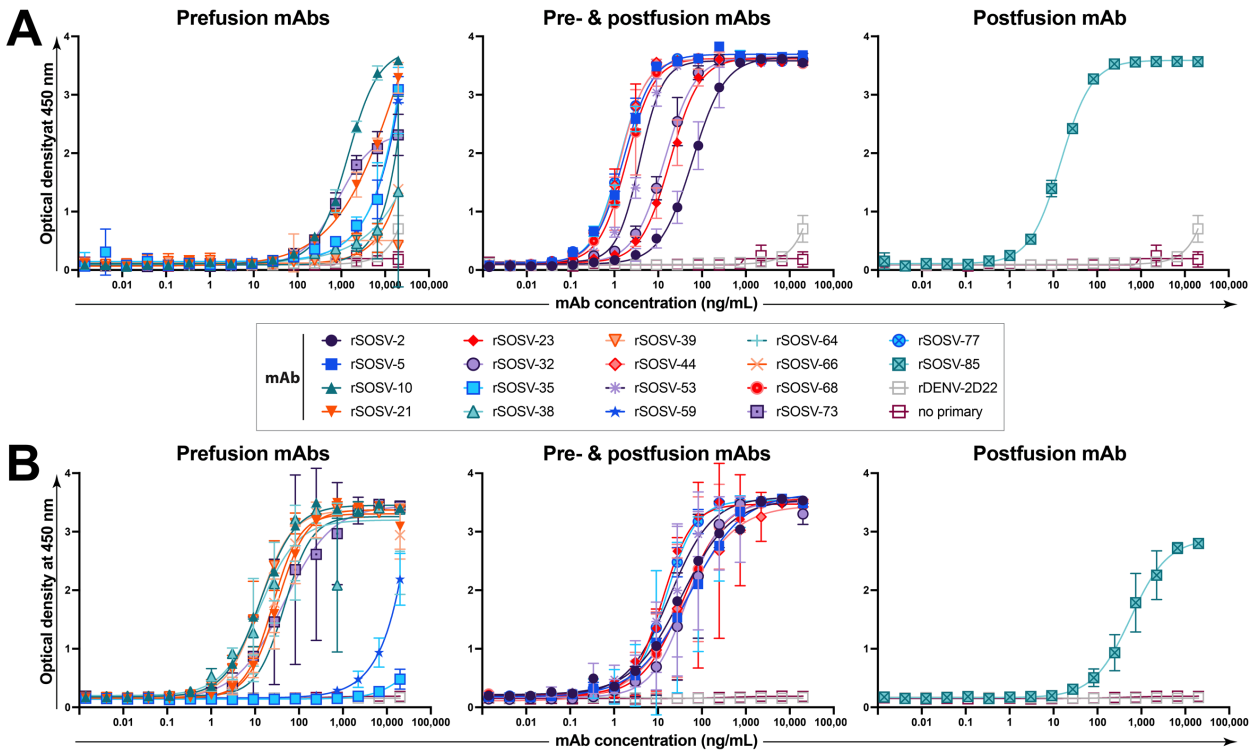

Figure 3.5. Representative ELISA data for anti-F rmAbs against prefusion and postfusion F. Shown here is a single, representative set of data of the three biological replicates that were performed. Curves show the average of three technical replicates plotted with standard deviation. The anti-F rmAbs are divided into 3 subsets: prefusion, pre- & postfusion, or postfusion, although all the rmAbs were tested simultaneously. **(A)** Anti-F rSOSV mAbs against postfusion SOSV F. **(B)** Anti-F rSOSV mAbs against SOSV pre-fusion F construct.

Table 3.2. Half-maximal effective concentration (EC_{50}) of anti-F rmAbs to pre- and postfusion protein		
MAb (rSOSV-)	**EC_{50} value for binding (ng/mL) to indicated protein antigen (± SD)**	
	Pre-fusion F	**Postfusion F**
2	26.5 ± 9.4	42.7 ± 18.5
5	25.4 ± 23.0	1.7 ± 0.8
10	23.4 ± 14.9	N/A
21	37.7 ± 11.5	N/A
23	19.4 ± 6.6	18.5 ± 2.0
32	42.0 ± 14.0	17.0 ± 3.5
35	N/A	N/A
38	19.3 ± 2.3	N/A
39	28.3 ± 14.8	N/A
44	20.9 16.6	1.0 ± 0.3
53	19.1 ± 3.9	1.8 ± 1.8
59	>10,000	N/A
64	54.2 ± 20.1	N/A
66	31.8 ± 7.5	N/A
68	23.3 ± 15.3	1.5 ± 0.4
73	48.5 ± 9.2	N/A
77	15.7 ± 5.3	1.0 ± 0.4
85	N/A	12.6 ± 5.6

Table 3.2. Half-maximal effective concentration (EC_{50}) of anti-F rmAbs to pre- and postfusion protein. EC_{50} values were obtained for each of the 18 anti-F rmAbs against both prefusion protein (preF-tHS) and postfusion (postF-tHS) F proteins. Assays were performed as 3 technical replicates per antibody and repeated 3 times (3 biological replicates). The EC_{50} value of reach biological replicate was calculated, then the EC_{50} values between all 3 biological replicates were averaged with standard deviation. A negative control mAb (rDENV-2D22) (not shown) tested in triplicate on each plate to confirm non-specific binding did not occur throughout the assays. Entries of N/A reflect mAb binding curves that did not reach plateau and EC_{50} values could not be accurately calculated.

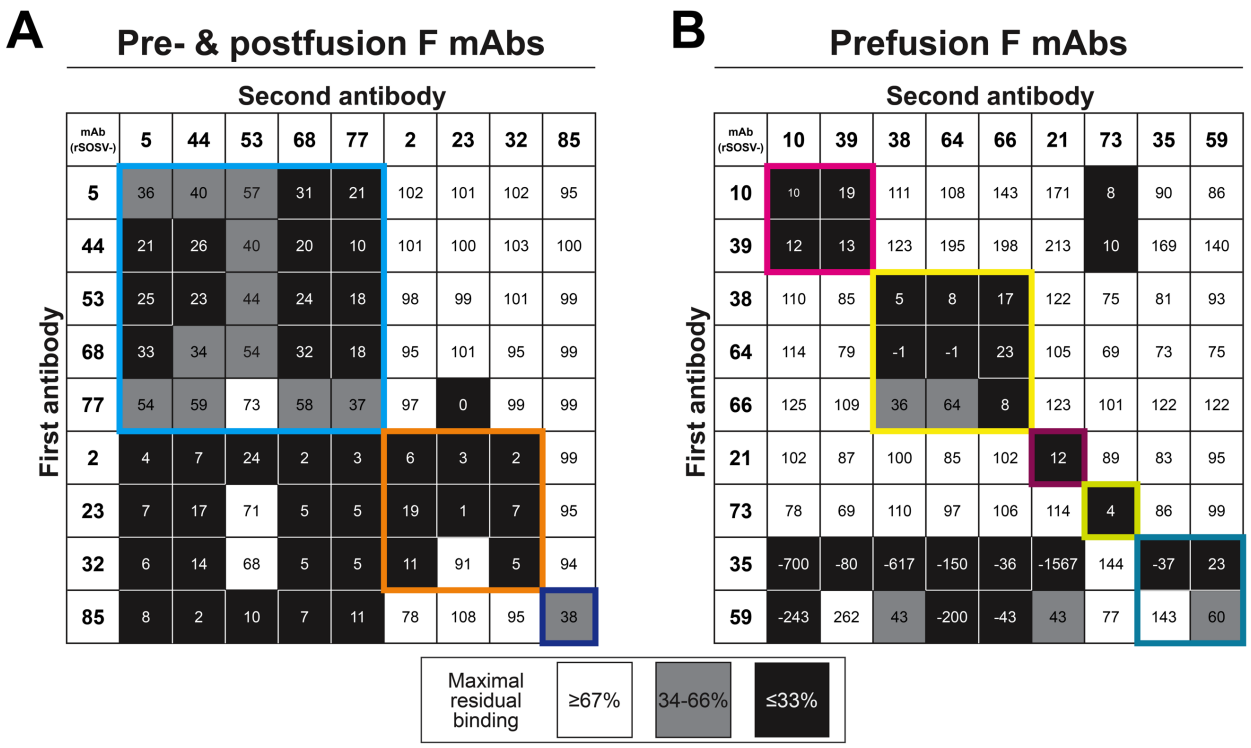

Figure 3.6. Competition-binding assay for anti-F rmAbs. Unlabelled primary (first) mAb was bound to antigen-coated plates in saturating conditions (10 μg/mL) with second, biotinylated antibodies added at a final concentration of 500 ng/mL in the layout shown. Detection of biotinylated rmAbs accomplished using a streptavidin-HRP. Data were converted to percent binding relative to the maximal non-competing binding of the second antibody (lacking a primary mAb). Assays were repeated in triplicate with quadruplicate technical replicates. A representative assay for each antigen/mAb set tested is shown. **(A)** Binding data for pre- & postfusion anti-F mAbs (rSOSV-2, 5, 23, 32, 44, 53, 68, & 77) and the postfusion mAb (rSOSV-85) against pre-fusion F protein. **(B)** Binding data for pre-fusion F specific mAbs (rSOSV-10, 21, 35, 38, 39, 59, 64, 66, & 73) against prefusion F antigen.

Cross-reactivity of anti-SOSV mAbs.

Cross-reactivity has been observed for mouse mAbs against some of the orthorubulaviruses (106) or between orthorubulaviruses and respiroviruses (107). Protein sequence similarity between SOSV and other rubulaviruses varies from 49-77% similarity for the F protein (**Figure 3.7A**) and 35-69% for the HN protein (**Figure 3.7B**). To test for cross-reactivity between various viruses, plasmids encoding human-codon optimized cDNA for wildtype F and HN proteins of Menangle virus (MenV), Tuhoko virus 3 virus (TuV3), and human mumps virus genotype G (Iowa 2006 strain) (MuV) were synthesized by Twist Biosciences using pTwist-CMV for the vector backbone. To quickly screen for cross-reactivity, polyclonal mixes of F or HN mAbs were made to use in cell-surface display flow cytometry. The HN polyclonal mix included all 6 rmAbs, while the anti-F mix used 10 rmAbs in total with randomly selected rmAbs from the different conformation classes (prefusion, postfusion, and pre- & postfusion). The anti-HN polyclonal mix did not react to any non-SOSV proteins (**Figure 3.8**). The anti-F polyclonal mix showed strong reactivity to Tuhoko virus 3 and weak reactivity to mumps (**Figure 3.8**). Based on these results, we further tested the anti-F SOSV mAbs individually to identify individual cross-reactive mAbs using fluorescent microscopy (**Figure 3.9-10**). Cells were counted and the percent of SOSV-F-stained cells was given as a percentage of total cells in the well (**Figure 3.10**). rSOSV-77 bound to both SOSV and mumps virus while rSOSV-10, -35, -38, and -39 cross-reacted with Tuhoko virus 3—the closest related virus to SOSV (17).

A

% AA similarity	SOSV	MenV	TeV	TioV	TuV1	TuV2	TuV3	HerV	AcV1	AcV2	MuV	PIV2	PIV4	PIV5	MapV	EfoV	PorV	NDV
SOSV		58	59	59	56	64	77	60	60	57	53	49	54	53	53	53	52	45
MenV	58		75	75	60	61	57	70	62	62	54	49	50	54	54	52	53	45
TeV	59	75		92	62	61	58	69	62	63	54	52	50	56	55	52	54	45
TioV	59	75	92		63	60	59	70	62	63	54	52	48	56	55	52	54	46
TuV1	56	60	62	63		61	56	60	62	60	55	51	50	56	55	49	52	46
TuV2	64	61	61	60	61		64	65	72	65	56	51	52	54	54	53	55	44
TuV3	77	57	58	59	56	64		61	62	56	52	50	50	53	54	52	54	46
HerV	60	70	69	70	60	65	61		62	65	55	51	49	55	55	51	56	43
AcV1	60	62	62	62	62	72	62	62		62	53	49	49	55	54	52	53	43
AcV2	57	62	63	63	60	65	56	65	62		57	53	51	57	55	54	56	47
MuV	53	54	54	54	55	56	52	55	53	57		58	52	60	60	58	58	47
PIV2	49	49	52	52	51	51	50	51	49	53	58		53	65	55	53	58	47
PIV4	54	50	50	48	50	52	50	49	49	51	52	53		56	56	75	55	49
PIV5	53	54	56	56	56	54	53	55	55	57	60	65	56		58	56	60	47
MapV	53	54	55	55	55	54	54	55	54	55	60	55	56	58		58	67	48
EfoV	53	52	52	52	49	53	52	51	52	54	58	53	75	56	58		55	48
PorV	52	53	54	54	52	55	54	56	53	56	58	58	55	60	67	55		45
NDV	45	45	45	46	46	44	46	43	43	47	47	47	49	47	48	48	45	

B

% AA similarity	SOSV	MenV	TeV	TioV	TuV1	TuV2	TuV3	HerV	AcV1	AcV2	MuV	PIV2	PIV4	PIV5	MapV	EfoV	PorV	NDV
SOSV		42	46	45	40	55	69	48	52	47	37	36	37	37	36	34	36	36
MenV	42		67	67	37	38	41	51	39	42	31	32	31	34	32	31	29	30
TeV	46	67		84	38	39	43	51	39	42	33	32	32	34	34	30	31	30
TioV	45	67	84		38	40	43	52	40	43	31	34	32	32	34	31	30	30
TuV1	40	37	38	38		40	40	42	40	43	35	34	33	35	35	33	34	33
TuV2	55	38	39	40	40		52	44	60	47	38	39	36	37	38	33	33	34
TuV3	69	41	43	43	40	52		48	53	49	37	35	37	34	36	36	37	34
HerV	48	51	51	52	42	44	48		43	47	35	35	36	38	37	34	34	33
AcV1	52	39	39	40	40	60	53	43		46	36	35	36	35	36	35	34	31
AcV2	47	42	42	43	43	47	49	47	46		40	39	40	38	39	37	39	34
MuV	37	31	33	31	35	38	37	35	36	40		54	50	58	51	53	53	44
PIV2	36	32	32	34	34	39	35	35	35	39	54		54	64	51	53	55	44
PIV4	37	31	32	32	33	36	37	36	36	40	50	54		55	51	66	52	43
PIV5	37	34	34	32	35	37	34	38	35	38	58	64	55		53	54	56	44
MapV	36	32	34	34	35	38	36	37	36	39	51	51	51	53		49	59	43
EfoV	34	31	30	31	33	33	36	34	35	37	53	53	66	54	49		52	43
PorV	36	29	31	30	34	33	37	34	34	39	53	55	52	56	59	52		43
NDV	36	30	30	30	33	34	34	33	31	34	44	44	43	44	43	43	43	

Figure 3.7. Percentage of amino acid similarity between various members of *Rubulavirinae*. F or HN protein sequences were aligned in Geneious Prime software (Biomatters, version 2023.0.3) using the Geneious multiple-sequence alignment algorithm with a BLOSUM-45 substitution matrix. The F and HN sequence from NDV (subfamily *Avulavirinae*) was used as an outgroup to show similarities to a similar, non-rubulavirus paramyxovirus. Heat map was used to indicate percent similarity; dark colours being higher percentage of similar residues between the proteins. **(A)** amino acid similarities between F proteins of rubulaviruses and NDV **(B)** amino acid similarities between HN proteins of rubulaviruses and NDV.

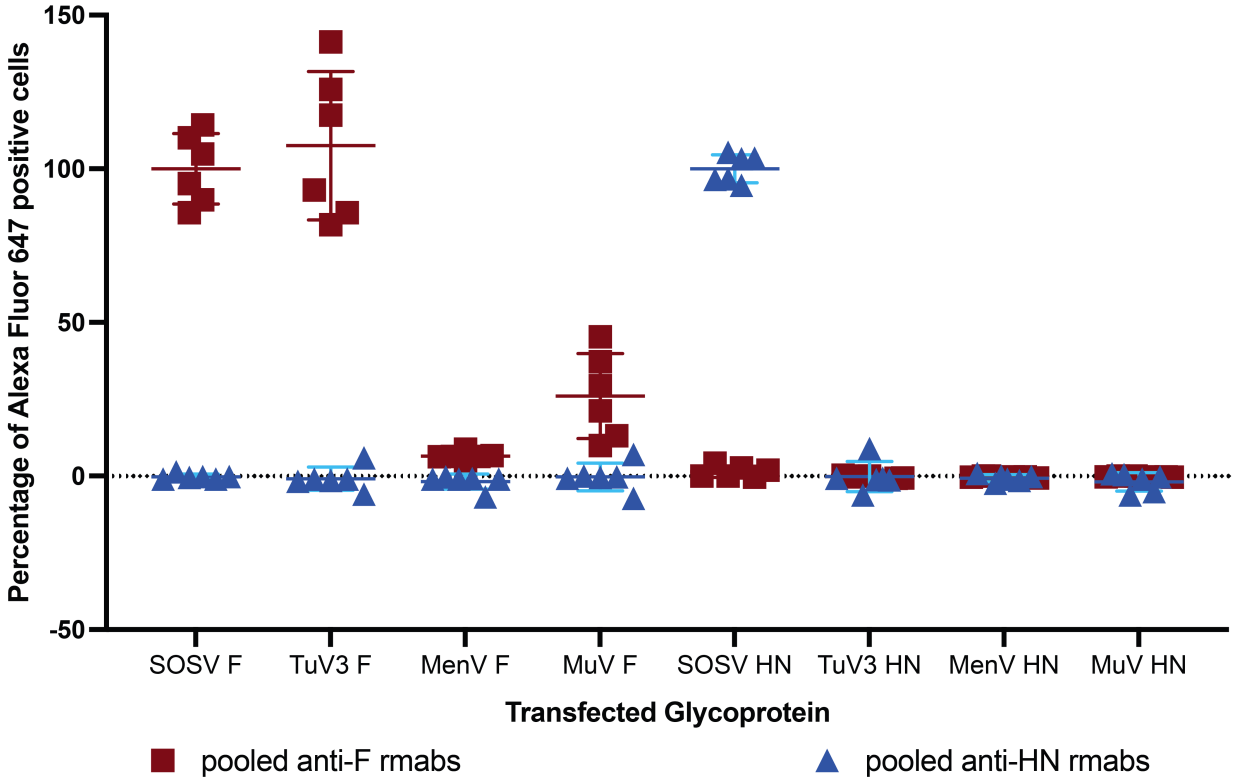

Figure 3.8. Cross-reactivity of pooled anti-SOSV rmAbs against cell-surface displayed rubulavirus glycoproteins. Transfected Expi293F cells were stained with mixes of SOSV anti-F (10 rmAbs) or anti-HN (6 rmAbs) and then goat anti-human Alexa Fluor 647 as the secondary stain. Cells were analyzed using flow cytometry (iQue screener) and the percentage of positive cells to each antigen. Percentages were scaled to put SOSV proteins at 100%. The assay was repeated 3 times with 2 technical replicates and the data plotted as average and standard deviation using Prism (GraphPad).

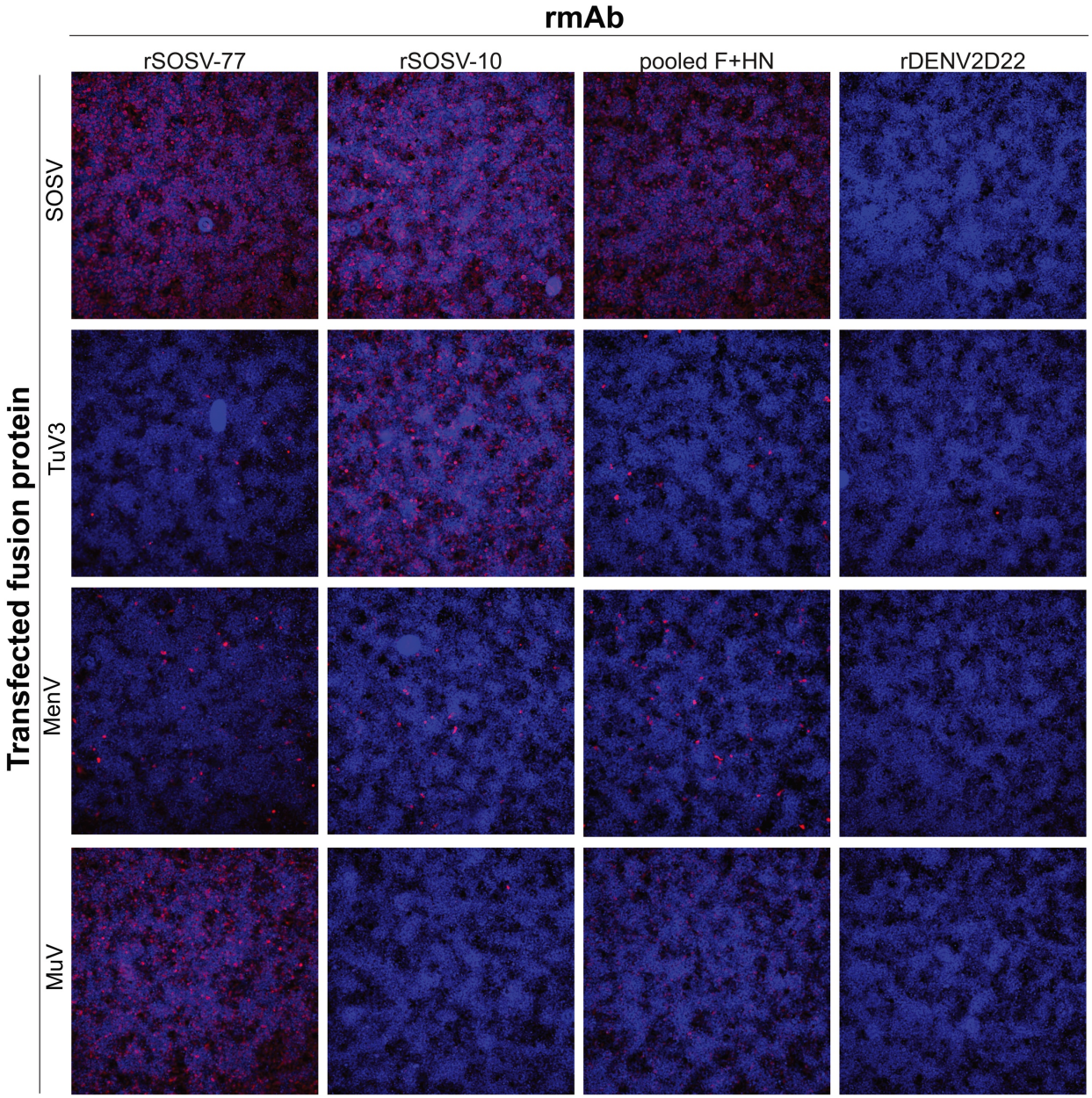

Figure 3.9. Representative images for select anti-F rSOSV mAbs against four different rubulavirus fusion proteins. HEK293T/17 cells were transfected in 96-well plates with the fusion protein from four different rubulaviruses (Sosuga, SOSV; Tuhoko virus 3, TuV3; Menangle virus, MenV; and mumps virus, MuV). Negative transfection controls used were VSV-G, SOSV HN, and untransfected cells. Cells were fixed and stained with DAPI and individual anti-F rmAbs, with goat anti-human Alexa Fluor 568 used as the secondary. Pooled F and HN rmAbs were used as a positive control for staining, and rDENV-2D22 and no primary were used as negative controls for the background signal levels. Plates were imaged on an ImageXpress high-throughput microscope (Molecular Devices) and analyzed with accompanying software (MetaXpress).

Percent postive cells stained with individual anti-F rmAbs						
mAb / antigen	rSOSV-85	rSOSV-77	rSOSV-73	rSOSV-68	rSOSV-66	rSOSV-64
SOSV F	1.1	65.5	63.9	62.6	62.0	57.0
MuV F	0.0	46.2	0.5	0.4	0.2	0.0
TuV3 F	0.0	0.7	1.4	1.0	5.4	0.9
MenV F	0.0	2.5	3.1	2.9	1.8	2.4
eGFP	0.1	0.1	0.4	0.2	0.1	0.0
SOSV HN	0.2	0.2	0.5	0.3	0.1	0.0
untransfected	0.0	0.0	0.3	0.1	0.0	0.0
mAb / antigen	rSOSV-59	rSOSV-53	rSOSV-44	pooled F+HN	rDENV-2D22	no primary
SOSV F	63.5	63.6	66.6	65.4	2.1	0.0
MuV F	0.3	0.3	0.4	22.6	0.1	0.1
TuV3 F	0.6	0.6	0.8	1.1	0.0	0.0
MenV F	2.4	2.6	1.6	3.8	0.0	0.0
eGFP	0.1	0.0	0.1	0.1	0.1	0.0
SOSV HN	0.0	0.1	0.1	55.9	0.0	0.0
untransfected	0.0	0.0	0.1	0.0	0.0	0.1
mAb / antigen	rSOSV-39	rSOSV-38	rSOSV-35	rSOSV-32	rSOSV-23	rSOSV-21
SOSV F	70.0	62.5	63.1	55.0	71.3	55.6
MuV F	0.1	0.0	0.5	0.6	0.3	0.2
TuV3 F	26.8	26.3	47.7	1.0	1.1	0.9
MenV F	2.6	3.4	1.6	3.1	4.0	2.4
eGFP	0.0	0.7	0.4	0.6	0.1	0.4
SOSV HN	0.1	0.1	0.9	1.0	0.5	0.3
untransfected	0.0	0.1	0.1	0.2	0.1	0.1
mAb / antigen	rSOSV-10	rSOSV-5	rSOSV-2	pooled F+HN	rDENV-2D22	no primary
SOSV F	65.4	67.2	68.1	60.6	0.2	0.1
MuV F	0.5	0.0	0.2	0.7	0.8	0.0
TuV3 F	53.8	0.7	0.5	0.7	0.0	0.0
MenV F	2.4	1.7	2.1	2.0	0.0	0.0
eGFP	0.2	0.0	0.1	0.1	0.0	0.0
SOSV HN	0.6	0.0	0.2	38.3	0.1	0.0
untransfected	0.1	0.0	0.1	0.0	0.1	0.0

Figure 3.10. Cross-reactivity analysis for panel of 18 anti-F rmAbs. MetaXpress software was used to analyze the collected ImageXpress microscopy data to count the total number of cells (DAPI stain) and the number of rSOSV-stained cells (DAPI and Alexa Fluor 568) and calculate the percentage of positively stained cells for each transfection condition. The pooled F and HN data serves as a positive control while staining with rDENV-2D22 or no primary mAb serve as the negative controls.

Negative-stain electron microscopy of anti-SOSV Fabs bound to soluble antigens.

To get an idea of where some of the epitopes for the anti-SOSV mAbs are we used low-resolution negative-stain electron microscopy (NS EM). A FabALACTICA Fab kit (Genovis, cat. # A2-AFK-025) was used to purify Fab fragments from the rSOSV-24, -10, and -77 mAbs. Purified SOSV preF-tHS and $HN_{head\text{-}TS8H}$ proteins were incubated with their respective Fabs, with one Fab at a time, and the resulting complexes were imaged with an electron microscope. 2D classes were averaged and 3D reconstructions made using structures of prefusion PIV5 F (PDB: 4SWG (108)), postfusion PIV3 F (PDB: 1ZTM, (11)), and SOSV-HN_{head} (PDB: 6SG8 (94)) as models. The rSOSV-24 Fab binds at the top of one of the globular head domains, somewhat close to the dimer interface (**Figure 3.11**). rSOSV-10 Fab binds to the upper tip of the prefusion trimer (**Figure 3.12A**), both rSOSV-24 and rSOSV-10 were unable to accommodate the binding of another Fab molecule. In contrast, rSOSV-77 Fab, which was imaged binding to postfusion F, binds to the side of one of the monomers allowing for up to 3 Fabs binding at once (**Figure 3.12B**).

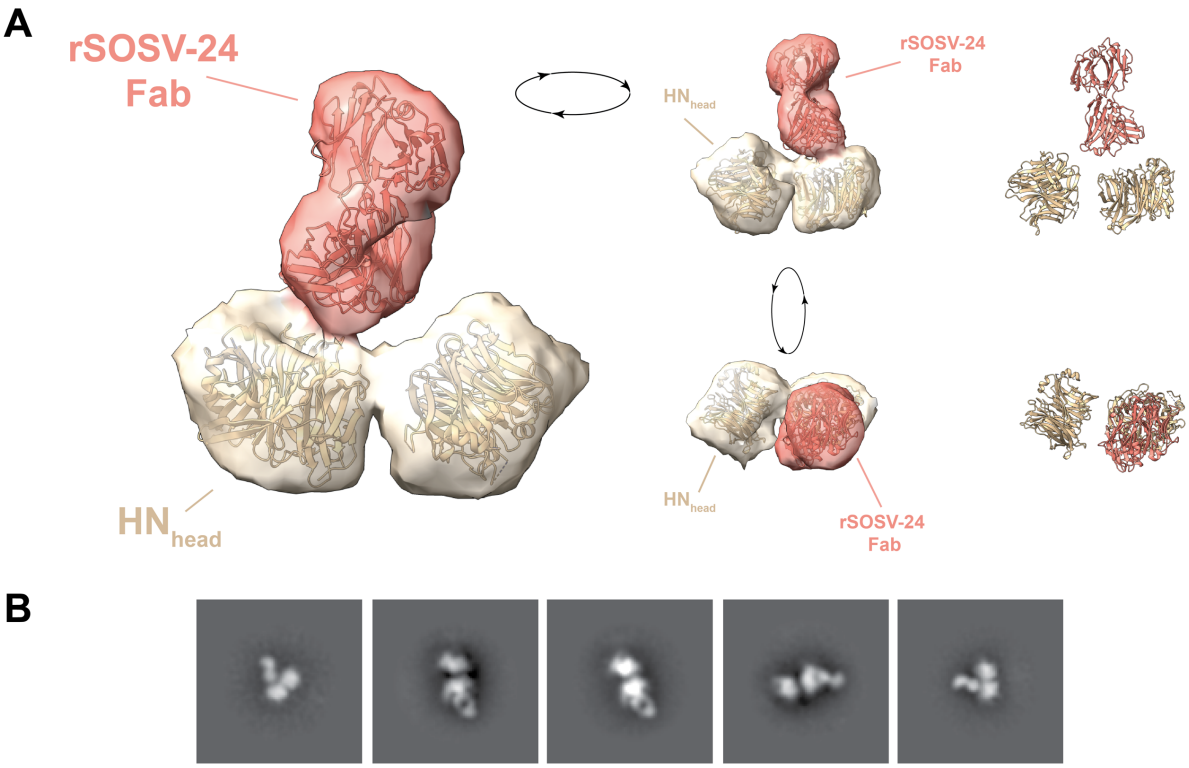

Figure 3.11. Low-resolution NS-EM shows rSOSV-24 Fab binds to top of globular head near dimer interface. rSOSV-24 IgG was digested into Fab fragments and incubated with purified $SOSV_{head\text{-}TS8H}$. Fab-antigen mix was placed on mesh copper grids and stained with uranyl formate, images were taken with a transmission electron microscope, 2D class averages were determined and used in 3D reconstruction. Chimera/ChimeraX (USCF) were used to create the protein images. **(A)** 3D reconstruction of rSOSV-24 Fab binding to $SOSV_{head\text{-}TS8H}$. Side and top-down views show Fab binding close, but not in, the dimer interface. **(B)** Representative 2D class images of the Fab-antigen complex.

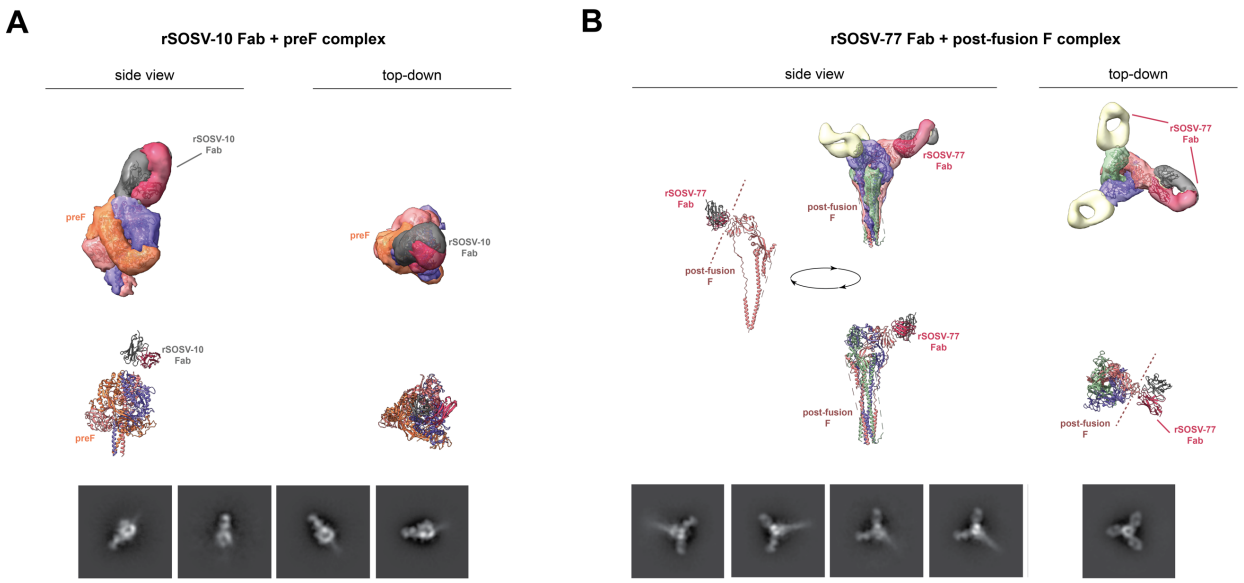

Figure 3.12. Low-resolution NS-EM of rSOSV-10 and rSOSV-77 against SOSV F protein. rSOSV-10 and rSOSV-77 IgG was digested into Fab fragments and incubated with purified with prefusion protein (preF-tHS). Fab-antigen mixes were stained with uranyl formate on copper grides and imaged with a transmission electron microscope. The 2D class averages were taken and used for 3D reconstruction. Protein images were created using Chimera/ChimeraX (USCF) **(A)** 3D reconstruction of rSOSV-10 Fab binding to a prefusion F protein. Only a single Fab was shown binding to the F protein. Representatives of the 2D class images are shown below. **(B)** 3D reconstruction of rSOSV-77 binding to a postfusion F protein. Side and top-down views show the binding of up to 3 Fabs. Representative 2D class images are shown below.

Chapter III Discussion

Using secreted SOSV F and HN proteins, I was able to provide further characterization on the binding of the anti-SOSV rmAbs. All of the anti-HN rmAbs bound to the globular head domain of the HN protein. Despite all binding to the same protein domain, the panel of 6 anti-HN mAbs could be separated into 4 distinct competition-binding groups. Further refinement of these epitopes may help reveal the mechanisms of neutralization. For example, based on the NS-EM of rSOSV-24 Fab (**Figure 3.11**), it is possible that this antibody is blocking receptor attachment though further assays would be necessary to confirm this, especially without knowing what the receptor is or where it binds.

As discussed in Chapter I, the F protein of paramyxoviruses can exist in two very distinct conformations, prefusion and postfusion, and we were able to produce soluble forms of both (**Figure 3.2**). Consistent with these two forms of protein, the panel of 18 F-specific mAbs could be divided into the three broad groups: mAbs that recognized 1) prefusion, 2) both conformations, 3) or postfusion. Only a single postfusion anti-F mAb was isolated, this was a nice result as I had preferably wanted to isolate neutralizing antibodies and postfusion specific F antibodies have a higher likelihood of being non-neutralizing, as the postfusion conformation of F is mainly present after virus-host cell fusion. The prefusion conformation of the F protein, however, is a potential neutralizing target since antibodies that block the triggering of the prefusion F protein may prevent virus-cell fusion. Since in total 17/18 anti-F mAbs could bind to the prefusion protein, and 10/18 were exclusively prefusion-specific (**Figure 3.4**), it was promising that at least

some of the anti-F mAbs would be neutralizing. In Chapter II, I had hypothesized that the cell-surface display system would predominantly present prefusion F. The low amount of isolated postfusion mAbs is supportive of this. Additionally, rSOSV-35 and rSOSV-39 did not bind well during ELISA (**Figure 3.5**), but do bind in cell-surface display (**Figure 3S.3**) indicating that the epitope for these antibodies is either absent or altered in the soluble F proteins. Had ELISA screening been used to discover SOSV-reactive B cells, it is likely that the resulting panel would have lost some epitope diversity as mAbs like rSOSV-25 and rSOSV-59 would not be identified.

Similar to the anti-HN proteins, the anti-F mAbs could also be divided into competition-binding groups, for which there was a total of 8 for the panel. While competition-binding is useful for getting a broad sense of the epitope diversity of a panel, it is not refined enough to give exact epitope information. This is noticeable in the panel of anti-F rmAbs as antibodies recognizing the exact same epitope should have similar properties. However, rSOSV-77 is grouped with 4 other antibodies (rSOSV-5, -44, -53, and -68) (**Figure 3.6**) yet only rSOSV-77 and none of the other rmAbs showed cross-reactivity to mumps (**Figure 3.9-10**). Thus, the actual epitope diversity of the panel may be higher than the groups identified through competition-binding assays.

While rSOSV-77 should be able to bind pre- and postfusion F (**Figure 3.5**), the NS-EM studies only found rSOSV-77 Fab complexed with postfusion F (**Figure 3.12**). The preF-tHS protein used EM studies is still only metastable in the prefusion form so it is not surprising to have some binding to postfusion F as it will always be present. It is possible that the preparation process for the NS-EM increases fusion-triggering, and because rSOSV-77 binds both conformations there was no stabilization of the F protein

by the Fab, unlike what rSOSV-10 may have done. Alternatively, the rSOSV-77 Fab may have higher affinity for the postfusion F. Further testing would be needed to verify, but the initial data of rSOSV-77 Fab looks similar to the binding of anti-RSV Fabs to RSV antigenic site IV (98). While rSOSV-77 could have one Fab binding per F-monomer, rSOSV-10 only had a single Fab bound to the prefusion F proteins at any time (**Figure 3.12**). Given the placement of the rSOSV-10 Fab, it is possible that rSOSV-10 could inhibit triggering of the F and thus be a neutralizing mAb. Broadly comparing to RSV, rSOSV-10 appears to be binding in a similar manner to how the anti-RSV Fab D25 binds to the ∅ site of RSV (109).

In conclusion, the work in this chapter gave further insight into the epitope-specificities of the panel of anti-SOSV mAbs.

Chapter III Materials and methods

Soluble SOSV F and HN and wildtype rubulavirus construct designs.

Secreted forms of the SOSV HN protein were generated by adding a human CD5 signal peptide sequence and a thrombin-cleavable 6x His-tag were added to the amino ends of the HN protein, replacing the cytoplasmic and transmembrane domains. The construct encoding the majority of the ectodomain of the HN protein (HN_{ecto}) contains amino acid residues 75 to 582. The HN_{head} construct contains residues 125 to 582 as previously described (94). Additional HN constructs ($HN_{ecto\text{-}TS8H}$ and $HN_{head\text{-}TS8H}$) were similarly designed but with a mouse IL-2 signal sequence and a thrombin-cleavable

Twin-Strep-tag and an 8x His-tag). All sequences were human codon-optimized and synthesized by Twist Biosciences into the mammalian expression vector pTwist-CMV. The soluble form of the prefusion F protein consisted of amino acid residues 15 to 476 of the SOSV F sequence with the following modifications: amino acid changes I206C, A223C, K101-F103GGG were introduced, a GCNt domain was added to the C-terminus, and a mouse IL-2 signal peptide was placed into the pVRC8400 vector at the N-terminus of the protein-coding sequence. The I206C and A223C mutations create a disulfide bond, and K101-F103GGG edits the furin cleavage site. Plasmid DNA of the pre- and postfusion constructs were received from the VRC (Bethesda, MD) and ~ 2 ng of each plasmid was transformed into 50 µL Stellar chemically competent *E. coli* (Takara Bio, cat. # 636763) following manufacturer's protocol with the 60 s heat-shock at 42°C in a 1.75 mL microcentrifuge tube. Cultures were plated on LB agar + 50 µg/mL Kanamycin (Molecular Cell Biology Resource Core, Vanderbilt University Medical Center) and grown overnight at 37°C. 3 single colonies were selected from each construct's plate and grown overnight at 37°C, 225 rpm shaking in Millers LB Broth (Corning, cat. # 46-050-CM) with 50 µg/mL Kanamycin (Sigma-Aldrich, cat. # K0254-20ml). Bacterial cell pellets were collected and miniprep plasmid DNA extracted through alkaline-lysis with a Qiagen Plasmid Mini Kit (Qiagen, cat. # 12123). Clones were sequenced verified using a Sequel instrument (Pacific Biosciences) and glycerol stocks made of the sequence-confirmed clones. Wildtype proteins sequences for F and HN were found on GenBank from the complete genome sequences for Menangle virus (NC_039197.1 (110)), Tuhoko virus 3 (NC_025350.1 (25)), and mumps virus genotype G strain Iowa 2006 (JX287385.1). cDNA of the F and HN proteins for each of the

viruses was human-codon optimized and synthesized by Twist into the pTwist-CMV mammalian expression vector.

Protein purification for recombinant SOSV soluble antigens.

Soluble forms of the SOSV antigens were purified by using the proteins' 6x-His tag or Strep-tag II tags and Expi293F cells and Expifectamine 293 expression system (Thermo Fisher Scientific, cat. # A14525) following the same transfection protocol as expression for cell-surface display. For soluble F transfections, the cells were moved to 32°C, 7% CO_2, shaking at 125 RPM after the enhancer addition on day 1 post-transfection. Cells were harvested at day 5 to 7 post-transfection, collecting the supernatant. His-tag purification was performed using an ÄKTA pure system with HisTrap™ Excel (Cytiva, cat. # 17-3712-05) columns. Strep-tagged proteins were purified with StrepTrapHP™ (Cytiva, cat. # 29-0486-53) or StrepTrapXT™ (Cytiva cat. # 29401322) columns on an AZURA P 6.1L (Knauer). Eluates were run on an SDS-PAGE gel to identify samples with the target proteins. These samples were then collected and concentrated using an Amicon Ultra-15 Centrifugal Filter with Ultracel-10 Membrane (Millipore Sigma, cat. # UFC901024) and buffer exchanged to DBPS or Tris-saline (140 mM Tris-HCl [Corning, cat. # 46-031] and 20 mM NaCl [Corning, cat. # 46-032-CV] diluted in deionized, filtered water and titrated to pH 8) with Zeba™ Spin Desalting Columns (7K MWCO, 10 mL, Thermo Fisher Scientific, cat #89894). Protein concentrations were typically diluted to ~1 mg/mL or less, aliquoted, and stored at 4°C if being used recently or -80°C after freezing in a dry-ice ethanol bath for longer-term storage.

Enzyme-linked immunosorbent assay (ELISA) to detect antibody binding to viral proteins.

ELISAs were performed by coating 384-well plates with either soluble viral glycoprotein (HN_{ecto}, HN_{head}, pre-fusion F with 6x-His tag and Strep-tag II [preF-tHS], or postfusion F with 6x-His tag and Strep-tag II [postF-tHS] at 2 µg/mL in 20 to 25 µL of DPBS. Plates were coated with antigen overnight at 4°C, washed three times with phosphate buffered saline with Tween 20 (PBS-T; Cell Signaling, cat. #9809S, 20 stock solution used to make 0.05% Tween 20 when diluted to 1X) using an EL406 plate washer dispenser instrument (BioTek), then blocked for 1 to 3 hr at RT with 50 µL/well of blocking buffer: 2% Blotting Grade Blocker (Bio-Rad cat. # 1706404) and 2% heat-inactivated goat serum (Gibco, cat. #16210-072) in PBS-T. SOSV HN mAbs were diluted in blocking buffer starting at 20 µg/mL in a 3-fold serial dilution series. After removing the blocking buffer, primary antibodies were added at 20 µL/well to the plates and incubated at RT for 1 hr. Plates were washed three times with PBS-T prior to addition of the secondary antibodies. The secondary antibody solution was prepared by diluting goat anti-human IgG horseradish peroxidase (HRP)-conjugated antibodies (SouthernBiotech, cat. # 2040-05) at 1:2,000 in blocking buffer and adding 20 to 25 µL/well, and then incubated at RT for 1 hr. Secondary antibodies were removed, and plates washed three times with PBS-T. A volume of 25 µL/well of 1-step Ultra TMB-ELISA Substrate Solution (Thermo Fisher Scientific, cat. # PI34029) was added to the plates and incubated for 5 to 10 min at RT, before being quenched with 25 µL of 1N hydrochloric acid (Fisher Scientific, cat. # SA48-1). Plates were analyzed on a BioTek

plate reader at 450 nm wavelength. Data were analyzed in Prism (GraphPad Software, version 9.3.1 for Mac OS) using a sigmoidal, four-parameter logistic, nonlinear regression model to generate the graphs and relative EC_{50} values for the mAbs.

Biotinylation of SOSV-specific antibodies.

SOSV F- or HN-reactive mAbs and a similarly prepared human mAb (rDENV-2D22) specific for an unrelated virus antigen (dengue virus envelope protein) were biotinylated. Purified IgG mAb proteins were diluted to a concentration of 1 mg/mL in DPBS, and an aliquot of 200 µL volume (containing 200 ng of antibody) was used for biotinylation. A 2 mg vial of EZ-Link™ NHS-PEG4-Biotin, No-Weigh™ Format biotin (Thermo Fisher Scientific, cat. #A39259) was reconstituted with 170 µL of DPBS or dimethyl sulfoxide and 1.33 µL of the biotin solution and added to 200 ng of each of the purified antibodies. Antibody-biotin solutions were mixed and incubated at RT for 50 min. Excess biotin was removed using Zeba™ Spin Desalting Plates, 7K MWCO (Thermo Fisher Scientific, cat. #89807). The plate columns were equilibrated with DPBS following the manufacturer's protocol. The antibody-biotin mixtures were loaded onto two columns for each mix, with ~100 µL loaded onto each column. The resulting duplicate eluates were combined.

Competition ELISA.

Competition ELISAs for the anti-SOSV mAbs were performed by coating 384-well plates overnight at 4°C with 20 µL of 2 µg/mL concentration solutions of antigen in DPBS: HN_{ecto} or HN_{head} protein for anti-HN mAbs and pre-fusion or postfusion F protein

for anti-F mAbs. Plates were washed three times with PBS-T using an EL406 plate washer (BioTek), then blocked for 1 to 3 hr at RT with 50 µL/well of blocking buffer (HN: 5% Blotting Grade Blocker, Bio-Rad cat. # 1706404 in PBS-T or F: 2% Blotting Grade Blocker and 2% goat serum, Gibco, cat. #16210-072 in PBS-T). Blocking buffer was removed by washing plates three times with PBS-T on an EL406 plate washer. The SOSV mAbs or control mAb DENV-2D22 were diluted to a concentration of 10 µg/mL in respective blocking buffers, and 20 µL of each mAb was plated into wells of a 384-well plate to give quadruplicate readings for each mAb combination. To determine the maximal binding of each mAb in the absence of competition, 20 µL of plain blocking buffer (without a primary antibody) was placed into enough wells of a 384-well plate to give quadruplicate readings for each mAb combination. Plates were incubated at RT for 1 hr. The biotinylated HN-mAbs were diluted to 500 ng/mL in blocking buffer while the F-mAbs were diluted to 2,500 ng/mL in blocking buffer, and 5 µL of biotinylated mAb was added to the 20 µL of unlabelled mAb or blocking buffer control, so that the final concentration of biotinylated antibody was 100 ng/mL for anti-HN mAbs and 500 ng/mL for anti-F mAbs. Plates were incubated at RT for 1 hr, and then were washed three times with PBS-T using an EL406 plate washer. A volume of 25 µL of a 1:1,000 dilution of mouse anti-biotin conjugated with alkaline phosphatase (AP) (Southern Biotech, cat. #6404-04) in blocking buffer was added to each of the wells of the HN plates and incubated for 1 hr at RT. For the F-coated plates, 25 µL of a 1:2,000 dilution avidin-peroxidase (Sigma-Aldrich, cat. # A7419-2ML) in blocking buffer was added to each of the wells of the plates and incubated for 1 hr at RT. The AP-labelled antibody or avidin-peroxidase was removed with three washes of PBS-T. For HN plates, 25 µL of

phosphatase substrate (Sigma-Aldrich, cat. # S0942) was diluted to 1 mg/mL in AP-substrate buffer (pH 9.6, 1M Tris Base [Tris (Hydroxymethyl) Aminomethane]; Research Products International, cat. # T60040), 0.3 mM $MgCl_2$ [Sigma-Aldrich, cat. # M1028]) and added to each well. Plates were developed in the dark at RT for 1 hr before being read on a BioTek plate reader at 405 nm wavelength. For the F plates, 25 µL/well of 1-step Ultra TMB-ELISA Substrate Solution (Thermo Fisher Scientific, cat. # PI34029) was added to the plates and incubated for 5 to 10 min at RT, before being quenched with 25 µL of 1N hydrochloric acid (Fisher Scientific, cat. # SA48-1) and read on BioTek plate reader at 450 nm wavelength. Since some anti-F mAbs (rSOSV-10, 21, 35, 38, 39, 59, 64, 66, & 73) had shown poor binding to postfusion F, these mAbs were not tested for competition-binding on the postfusion F protein. However, anti-F mAbs rSOSV-2, 5, 23, 32, 44, 53, 68, 77, and 85 were tested on both pre-fusion and postfusion F. The values obtained from quadruplicate wells were averaged, and values from the wells with the negative control mAb rDENV-2D22 were considered the nonspecific binding signal and subtracted. The averaged absorbance data then was converted to percentage relative to the maximal (without unlabelled primary mAb) data. Competing mAbs were defined as having a residual binding level equal to or below 33% of the maximal binding level, intermediate competition was defined as having 34 to 66% of the maximal binding, and non-competing mAbs were defined as having equal to or greater than 67% of maximal binding. Data was analyzed in Microsoft Excel (Microsoft, version 16.69 for Mac OS).

Sequence similarity between various members of *Rubulavirinae*.

F or HN protein sequences were aligned in Geneious Prime software (Biomatters, version 2023.0.3) using the Geneious multiple-sequence alignment algorithm (global alignment with free end gaps) with a blocks substation matrix BLOSUM 45 (gap open penalty of 12, extension penalty of 3, and 2 refinement iterations). The F or HN sequence from NDV (subfamily *Avulavirinae*) was used to show similarities to a similar, non-rubulavirus paramyxovirus. Distance matrices were calculated by Geneious setting amino acid percent similarity with a BLOSUM 90 matrix and threshold 1 to show the most minimal percent similarity. F and HN sequences were collected from genomes of rubulaviruses deposited in GenBank. The (genome) accession numbers for the viruses used are: Newcastle disease virus (NDV; FJ754271.2), mumps virus (MuV; JX287385.1), human parainfluenza virus 2 (PIV2; AF533012.1), human parainfluenza virus 4 (PIV4; KF878965.2), parainfluenza virus 5 (PIV5; JQ743318.1), Mapuera virus (MapV; NC_009489.1), porcine rubulavirus (PorV; NC_009640.1), *Eptesicus fuscus* orthorubulavirus (EfoV; MZ355765.1), Achimota virus 1 (AcV1; NC_025403.1), Achimota virus 2 (AcV2; NC_025404.1), Sosuga virus (SOSV; NC_025343.1), Teviot virus (TeV; NC_039198.1), Tioman virus (TioV; NC_004074.1), Menangle virus (MenV; NC_039197.1), Tuhoko virus 1 (TuV1; NC_025410.1), Tuhoko virus 2 (TuV2; NC_025348.1), and Tuhoko virus 3 (TuV3; NC_025350.1).

Screening for cross-reactive anti-SOSV mAbs.

For cell-surface display screening, Expi293F cells were transfected with wildtype F or HN proteins from SOSV, MenV, TuV3, or MuV individually using the same expression protocol described in Chapter II. Similarly, the flow cytometry staining

protocol was the same, including live-dead staining, apart from the secondary antibody used was goat anti-human IgG-Alexa Fluor 647 (Southern Biotech, cat. # 2040-31). The primary antibodies used were polyclonal mixes of 10 anti-F SOSV rmAbs or 6 anti-HN SOSV rmAbs. The polyclonal F mix was screened against all F and HN proteins for the 4 viruses, similarly the polyclonal HN mix was screened against all of the viral antigens as well so that each mix could serve as a negative control for the other.

The microscopy assay for screening individual anti-F SOSV rmAbs used the same transfection protocol as described in Chapter II with the following differences: HEK293T/17 (ATCC, cat # CRL-11268) cells were used instead of vero cells, the constructs transfected were the wildtype F constructs of SOSV, MenV, TuV3, or MuV as well as SOSV HN-WT to serve as a negative control going across the plates. Other controls included a plasmid encoding an eGFP reporter to serve as a positive control for the transfection procedure, and untransfected wells as another negative control. Plates were incubated at 37°C in 5% CO_2 for ~48 hr, after which the medium was removed and the cells were fixed in 100 μL/well of 4% PFA for 1 hr. Cells were washed several times with DPBS before blocking and 150 μL/well blocking buffer (5% nonfat dry milk in 1X PBS-T) for 60 min at room temperature (RT). Cells were stained 50 μL/well μL of 1 μg/mL of the 18 different anti-F rSOSV mAbs as well as rDENV-2D22 and polyclonal F+HN mix (1:1 ratio of the polyclonal F mix and polyclonal HN mix described previously) for a negative and positive control respectively. A column of wells were left unstained with primary to serve as a control for secondary background. After the primary incubation, plates were washed with DPBS and 50 μL/well of goat anti-human IgG Alexa Fluor 568 (H + L) (Invitrogen, cat. # A-21090) of secondary antibody diluted in blocking

buffer at 1:1,000. Plates were incubated in the dark for 1 hr at RT. Secondary was washed off with DBPS and cells were stained with 50 μL/well of DAPI (4,6-diamidino-2-phenylindole, dihydrochloride) (Invitrogen, cat. # D1306) diluted to 500 nM in DPBS for 15-30 m. Cells were then washed several times with DPBS to remove DAPI stain and 250 μL/well of DPBS was added to the wells. Plates were imaged on an ImageXpress high-throughput microscope (Molecular Devices) and analyzed with accompanying software (MetaXpress) to count the number of cells stained with DAPI, Alexa Fluor 568, and/or eGFP. Output data was taken as percentages. The output data was further analyzed in Microsoft Excel (Microsoft, version 16.69, Mac OS).

Negative-stain electron microscopy.

rSOSV-24, -10, and -77 IgG were digested into Fabs using the FabALACTICA Fab kit (Genovis, cat. # A2-AFK-025) and following the manufacturer's protocol. Fabs were combined with their target antigen, purified SOSV preF-tHS or $HN_{head\text{-}TS8H}$, to create complexes. 3 μL of ~15 μg/mL sample was applied to glow discharged 400 mesh copper grids with continuous carbon and allowed to absorb for ~60 s. Excess sample was blotted on filter paper, washed twice in Milli-Q water, and negatively stained with 0.75% (w/v) uranyl formate (111). Images were recorded on a 4k × 4k CCD camera using an FEI TF20 (TFS) transmission electron microscope operated at 200 keV and control with SerialEM (112). All images were taken at 50,000× magnification with a pixel size of 2.18 Å/pix in low-dose mode at a defocus of 1.5-1.8 μm. Image processing was performed using the CryoSPARC software package (113), and images were imported and preprocessed by CTFFIND4 (114). Particles were picked automatically and once

picked, particles were extracted picked, particles were extracted with a 200 pixel box size and binned to 100 pixels (4.36 Å/pix) and 2D classes averaged. The 2D class averages were used to generate initial 3D model, which was then used for 3D refinement of the data. Figures were made with Chimera/ChimeraX (University of California San Francisco).

Chapter III Supplemental Information

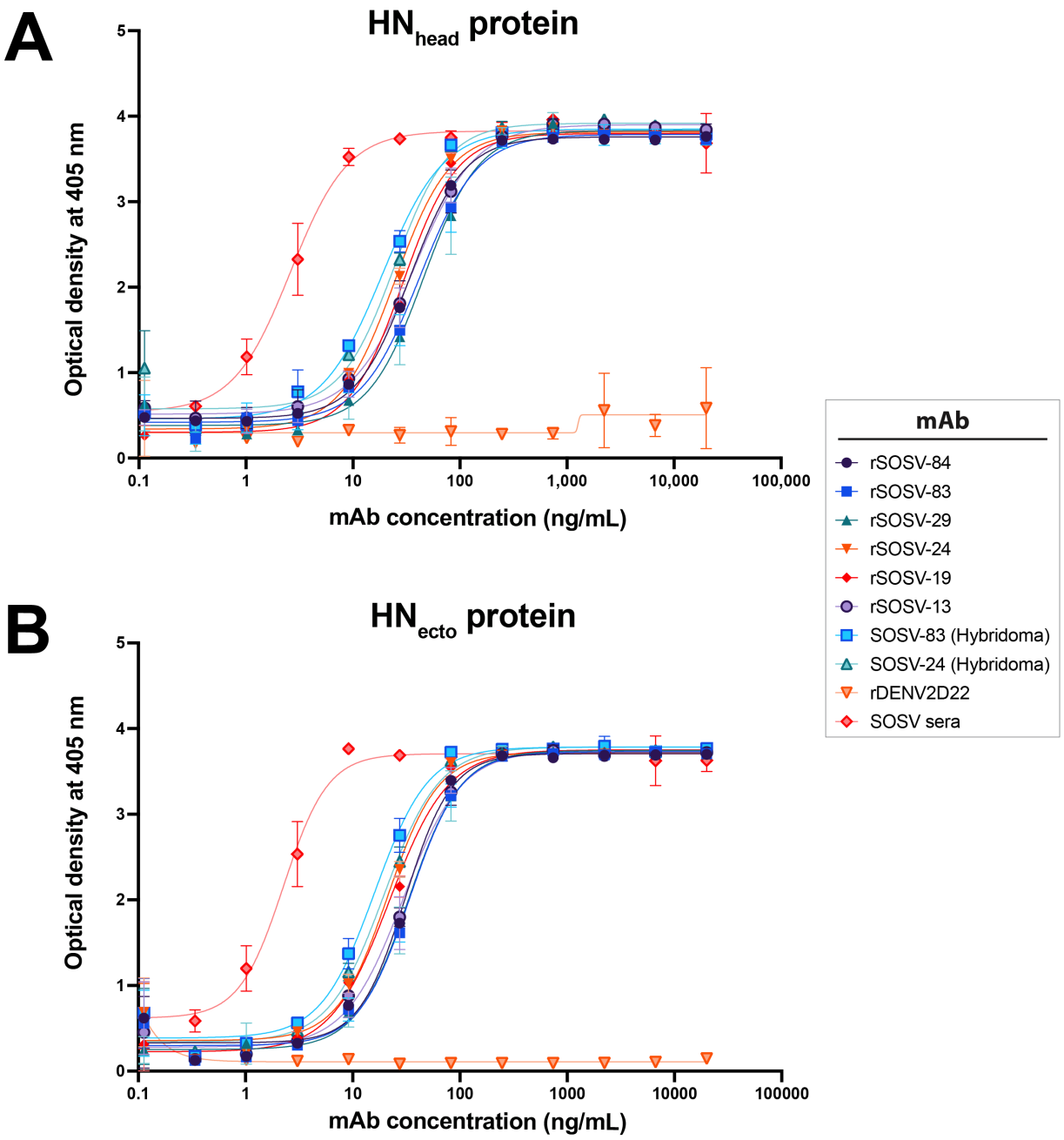

Figure 3S.1. Representative ELISA for binding of anti-HN rSOSV mAbs to soluble HN antigens. Representative data of two biological replicates performed using anti-HN rmAbs. SOSV donor sera was used as a positive. To compare between hybridoma and recombinant mAb, SOSV-83 (from hybridoma) and SOSV-24 (from hybridoma) were randomly selected to be added in the assay. Primary stain (SOSV rmAb, mAb, or sera) was detected with a goat anti-human IgG (Fc) AP secondary. Graphs are shown as the average of three technical replicates plotted with standard deviation. **(A)** Anti-HN rSOSV mAbs against HN_{head} proteins. **(B)** Anti-HN rmAbs against HN_{ecto} protein.

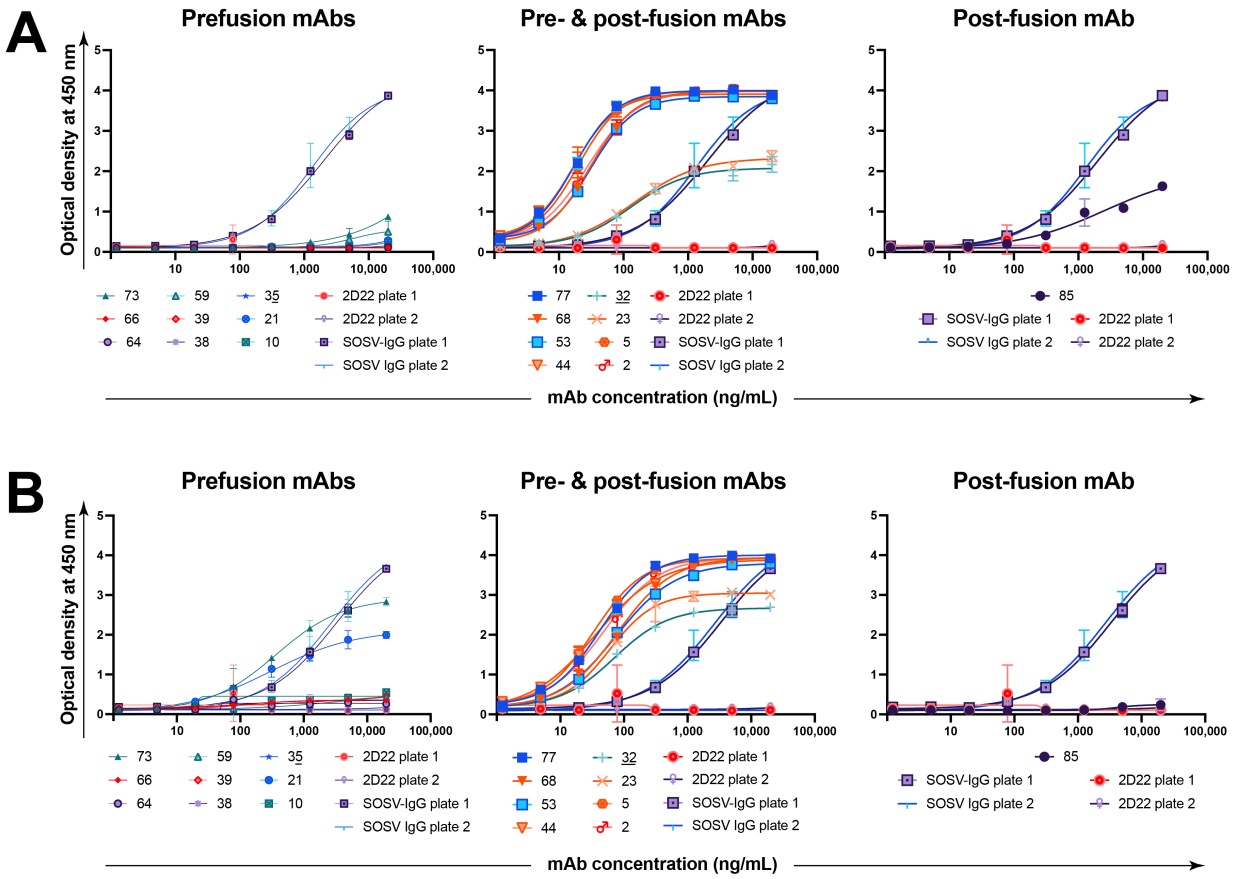

Figure 3S.2. Representative ELISA data for anti-F rmAbs against purified prefusion and postfusion F. Purified pre- and postfusion F prepared by Dr. Stewart Jones (VRC) was used to test antibody conformational specificity to the F protein. Curves show the average of three technical replicates plotted with standard deviation. The anti-F rmAbs are divided into 3 subsets: pre-fusion, pre- & postfusion, or postfusion, although all the rmAbs were tested simultaneously. **(A)** Anti-F rSOSV mAbs against postfusion SOSV F. **(B)** Anti-F rSOSV mAbs against SOSV pre-fusion F construct.

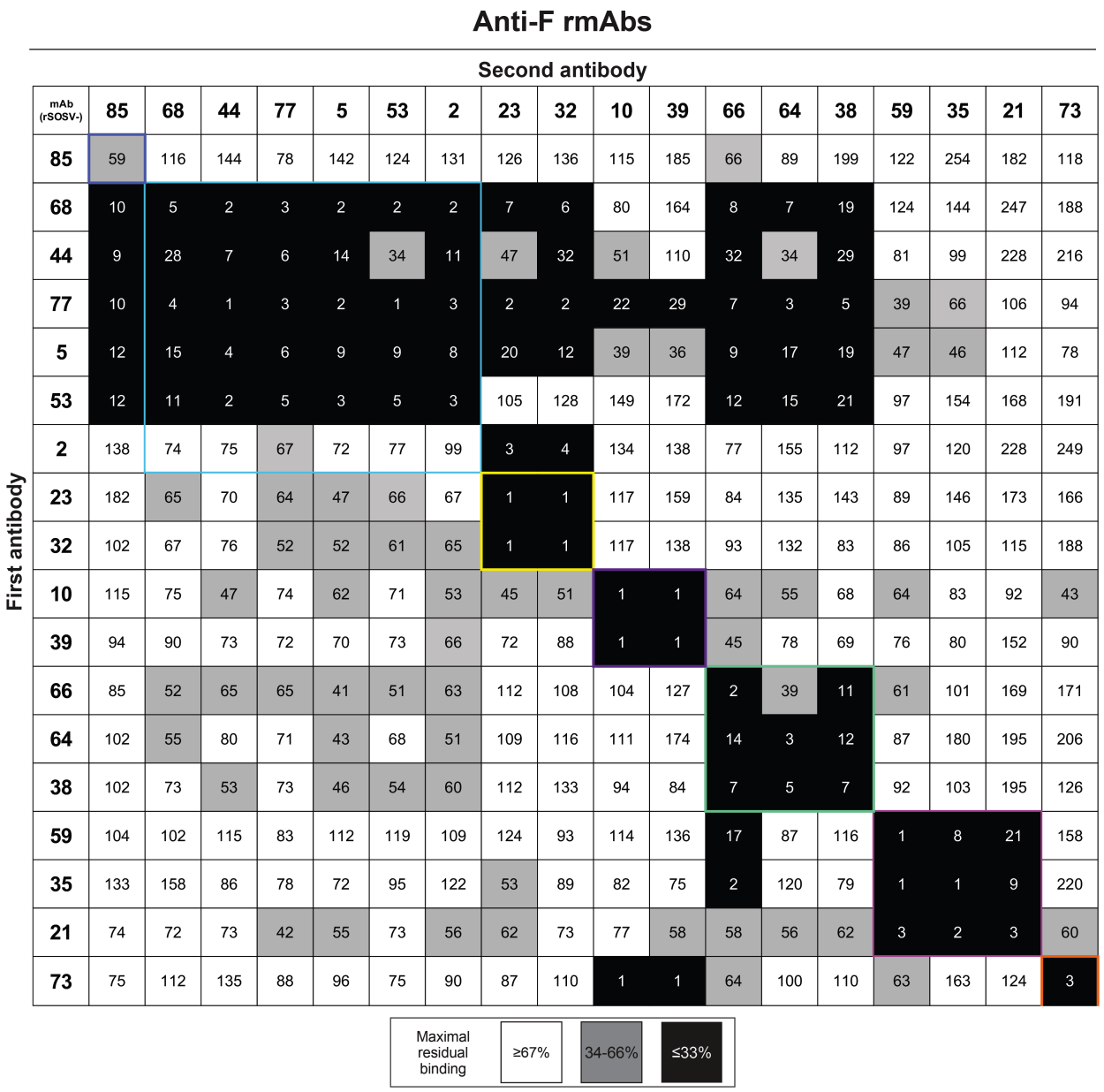

Figure 3S.3. Competition-binding assay of anti-F rSOSV mAbs using cell-surface displayed F-WT protein. Expi293F that had been transfected with SOSV F-WT were seeded in 96-well plates and stained with live-dead fixable violet, 20 µg/mL for the unlabelled mAbs and 1 µg/mL of Alexa Fluor 647 labelled mAbs (final concentration). An iQue flow cytometer (Sartorius) was used to detect fluorescent labelleing. Dead cells were removed with gating in Forecyt (Sartorius) and the median fluorescent intensity (MFI) well collected. Data were converted to percent binding relative to the maximal non-competing binding of the second antibody (lacking a primary mAb). Assay was repeated in biological duplicate with a single replicate each. Displayed is one of the biological replicates. Grouping data is very similar to the ELISA assays (**Figure 3.6**) with some differences due to poor staining of some rmAbs.

Supplemental materials and methods

Enzyme-linked immunosorbent assay (ELISA) to detect antibody binding to viral proteins

ELISAs were performed by coating 384-well plates with either HN_{ecto} or HN_{head} protein at 2 µg/mL in 20 to 25 µL of DPBS. Plates were coated with antigen overnight at 4°C, washed three times with PBS-T using an EL406 plate washer dispenser instrument (BioTek), then blocked for 3 hr at RT with 50 µL/well of blocking buffer [5% Blotting Grade Blocker (nonfat dry milk), Bio-Rad cat. # 1706404 in PBS-T]. Sosuga HN mAbs were diluted in blocking buffer starting at 20 µg/mL in a 3-fold serial dilution. Primary antibodies were added to the plates after removing the blocking buffer at 25 µL/well and incubated at RT for 1 hr. Plates were washed three times with PBS-T prior to addition of the secondary antibodies. The secondary antibody solution was prepared by diluting goat anti-human IgG (Fc) AP antibodies (Meridian Life Sciences, cat. # W99008A) at 1:4,000 in blocking buffer and adding 25 µL/well, and then incubated at RT for 1 hr. Secondary antibodies were removed and plates washed three times with PBS-T. Phosphatase substrate (Sigma-Aldrich, cat. # S0942) was diluted to 1 mg/mL in AP-substrate buffer (pH 9.6, 1M Tris Base [Tris (Hydroxymethyl) Aminomethane] (Research Products International, cat. # T60040), 0.3 mM $MgCl_2$ (Sigma-Aldrich, cat. # M1028)) and added to the plates at 25 µL/well. Plates were left to develop in the dark for 1 hr before analysis on a BioTek plate reader at 405 nm wavelength. Data were analyzed in Prism (GraphPad Software, version 9.3.1 for Mac OS) using a sigmoidal, four-parameter logistic, nonlinear regression model to generate the graphs and relative EC_{50} values for the mAbs.

Competition assays for anti-F mAbs using cell-surface display flow cytometry.

Recombinant mAbs were conjugated with Alexa Fluor-647 NHS Ester (succinimidyl ester; Thermo Fisher Scientific, cat. # A37573) following the manufacturer's protocol. Expi293F cells were transfected with the wildtype SOSV F (F-WT) as previously discussed in Chapter II for cell-surface display. Excess cells from transfections had been cryopreserved using 10% dimethyl sulfoxide (DMSO; Sigma-Aldrich, cat. # D2650-100ML) and stored in the vapor phase of liquid nitrogen storage. Cells were thawed in a bead bath at 37°C and washed with media to remove the DMSO. Transfected cells were plated at 50,000 live-cells/well in 96-well V-bottom plates and washed with flow cytometry buffer (DPBS without calcium and magnesium, 2% low-IgG FBS, 2 mM EDTA). Cells stained with LIVE/DEAD™ Fixable Violet Dead Cell Stain (Invitrogen, cat. # L34963) for 30 min at room temperature (RT) protected from light. After washing the plates to remove the live-dead stain, 40 µL of unlabelled anti-F SOSV mAbs were added to the plates at a concentration of 25 µg/mL. Plates were incubated at RT protected from light for 30 mins. Then 10 µL Alexa Fluor-647 labelled mAbs were added at a concentration of 5 µg/mL, giving a final concentration of 20 µg/mL for the unlabelled mAbs and 1 µg/mL for the fluorescent-labelled mAbs. Plates were incubated in the dark at RT for another 30 mins. Cells were washed to remove antibodies and fixed with 4% PFA. Fixative was removed and cells resuspended in 25 µL/well of flow cytometry buffer and analyzed on an iQue Screener PLUS flow cytometer and Forecyt software (Sartorius). Using the median fluorescent intensity (MFI), maximal binding was determined by the labelled-mAb only control, while background levels were determined

by unlabelled wells without the addition of the fluorescent-conjugated mAbs. Like the ELISA competition-binding assays, the thresholds were: competing mAbs had 33% or less of the maximal binding level, intermediate competition was defined as having 34 to 66% of the maximal binding, and non-competing mAbs were defined as having equal to or greater than 67% of maximal binding. Only one technical replicate was used and the experiment was conducted twice. Data was analyzed in Microsoft Excel (Microsoft, version 16.69 for Mac OS).

CHAPTER IV

Neutralization of SOSV by human monoclonal antibodies

Disclaimers:

1. Part of the data and information presented in this chapter were adapted from the following:

   Parrington HM, Kose N, Armstrong E, Handal LS, Diaz S, Reidy J, Dong J, Stewart-Jones GBE, Shrivastava-Ranjan P, Jain S, Albariño CG, Carnahan RH, Crowe JE. 2023. Potently neutralizing human monoclonal antibodies against the zoonotic pararubulavirus Sosuga virus. JCI Insight https://doi.org/10.1172/jci.insight.166811.

2. The findings and conclusions in this report are those of the authors and do not necessarily represent the official position of the Centers for Disease Control and Prevention.

Chapter Acknowledgements:

Paul Rothlauf and Dr. Sean Whelan of the Washington University in St. Louis (WUSTL), St. Louis, MO, USA; Paul designed and created all recombinant VSV-SOSV viruses, and Dr. Whelan provided guidance.

Dr. Jiong Shi and Dr. Christopher Aiken, VUMC, Nashville, TN, USA helped in the attempts to generate HIV-SOSV pseudotyped viruses.

Dr. Punya Shrivastava-Ranja, Dr. Shilpi Jain, and Dr. César G. Albariño of the Viral Special Pathogens Branch, Centers for Disease Control and Prevention (CDC), Atlanta, Georgia, USA performed all of the neutralization assays using our anti-SOSV rmAbs against their recombinant Zs-Green SOSV virus at BSL-3. Experiments were

performed by Dr. Punya Shrivastava-Ranja & Dr. Shilpi Jain and Dr. Albariño supervised the research.

Chapter IV Introduction

From Chapter III, we know the entire panel of anti-SOSV rmAbs' protein specificity, conformation/domain specificity, and competition-binding groups. Here in Chapter IV I will discuss the neutralization abilities of the anti-SOSV rmAbs as well as BLS-2 systems for assessing neutralization and the difficulties I encountered with these systems for SOSV. One of the challenges of this thesis project, is that live SOSV is currently considered as a BSL-3 virus (65) which exceeded the biosafety levels of our laboratory at Vanderbilt. One of the potential solutions for this issue was to produce pseudoviruses—non-SOSV backbone viruses displaying (pseudotyped) SOSV F and HN proteins.

Pseudotyping allows for the generation of viral particles expressing envelope proteins of the target, BSL-3/BSL-4, viruses at BSL-2 conditions. Two of the most common systems use vesicular stomatitis virus (VSV) or lentivirus backbones (115, 116). VSV is an enveloped, single-stranded, non-segmented, negative-sense RNA virus in the family *Rhabdoviridae* (117). The virus has an 11 kb genome and encodes 5 structural proteins, of which only one—glycoprotein (G; VSV-G)—is expressed on the viral envelope and serves as both the receptor binding protein (RBP) and fusion protein (117). VSV is frequently used in pseudotyping and making recombinant viruses due to

several factors, namely its ability to readily incorporate heterologous envelop proteins into virions (117, 118). VSV has been widely used to make many pseudoviruses from a broad range of viral families (118–125), including the paramyxoviruses canine distemper virus (CDV), peste des petits ruminants virus (PPRV) (126) and human measles virus (127) of the morbilliviruses, and the henipavirus Nipah virus (128). Lentivirus systems, such as HIV-1, have also been successful at pseudotyping wide variety of viruses (129–136), including VSV (137). As a member of *Retroviridae* (genus *Lentivirus*), HIV-1 is an enveloped, positive-strand RNA virus with two copies of the viral genome (138, 139). HIV-1 has a genome of about ~9-10 kb (139) divided into 10 genes (115), 3 of which encode structural proteins such as the envelope glycoprotein (Env) (138, 139). The HIV-1 *env* gene encodes the polyprotein gp160 which is proteolytically cleaved into the RBP, gp120, which is on the outer surface of the virion and gp41 which is a transmembrane protein in the lipid bilayer that forms a complex with gp120 and serves as the fusion protein (139, 140). For simplicity, the HIV-1 envelope glycoprotein complex (gp120 and gp41) will be called HIV-Env for the remainder of this chapter. The paramyxoviruses that have been well-studied for pseudotyping with either of the VSV or lentivirus systems are henipaviruses, morbilliviruses, or respiroviruses (124, 126, 128–131, 133, 135, 136)—all members within genera of the *Orthoparamyxovirinae* subfamily (2, 21). Therefore, it is uncertain if rubulaviruses glycoproteins can be successfully pseudotyped.

Another option is to create recombinant viruses that expresses the desired proteins and often a reporter gene (58, 65, 141–143). This is fairly similar to the idea of pseudotyping, except rather than supplying the target glycoprotein genes in *trans*, they

are inserted into the backbone virus's genome in lieu of the native glycoprotein(s). Successful recombinant paramyxoviruses include the rubulavirus PIV5 (144). The resulting recombinant, chimeric viruses may be replication competent, unlike pseudoviruses, and have been used to make vaccine candidates (142, 145–147).

While a pseudovirus or recombinant virus system is ideal for being able to perform neutralization assays and other assays at BLS-2, ultimately to truly determine the neutralization capabilities of a mAb it will need to be challenged at least against its live target virus *in vitro* if not in an animal study. From previous studies, it is known that the SOSV donor formed a potent neutralizing response to SOSV with a 100% focus reduction neutralization test ($FRNT_{100}$) dilution value of 800 for convalescent human serum (148). The creation of a recombinant Sosuga virus encoding a fluorescent marker, ZsGreen, (rSOSV/ZsG) allows for screening of antivirals or mAbs using a fluorescent focus reduction neutralization test (FRNT) (65, 148). Here, I sought to determine if any of the 24 anti-SOSV rmAbs could neutralize a recombinant or pseudovirus SOSV at BSL-2 while our collaborators tested the panel of rmAbs against authentic SOSV at BSL-3.

Chapter IV results

Neutralizing activity of anti-SOSV rmAbs against rSOSV/ZsG at BSL-3.

The panel of 24 anti-SOSV rmAbs and a control rmAb, rDENV-2D22, were de-identified before being sent to Dr. Punya Shrivastava-Ranja, Dr. Shilpi Jain, and Dr.

César G. Albariño of the Viral Special Pathogens Branch, Centers for Disease Control and Prevention (CDC) so that neutralization assays would be done as a single-blind study. A standard protocol (65) for a fluorescent FRNT assay was used to measure the neutralizing activity of all the rmAbs. The rmAbs were serially diluted and incubated with virus before plating on Vero-E6 cells. After 72 hr, the fluorescent intensities of the ZsGreen were quantified to determine the amount of rSOSV/ZsG infecting the monolayer (**Figure 4.1**) and calculate the IC_{50} value for each mAb (**Table 4.1**). Almost all of the rSOSV mAbs were neutralizing, only the postfusion specific anti-F rmAb was not able to neutralize the virus to an appreciable amount. As a class, the HN-specific mAbs were more potently neutralizing than the anti-F mAbs. Of the panel of anti-F mAbs, the prefusion-specific ones tended to have lower IC_{50} values than the mAbs that bind pre- and postfusion rmAbs. Some of the anti-SOSV mAbs had ultra-potent neutralizing activity with IC_{50} values <1 ng/mL.

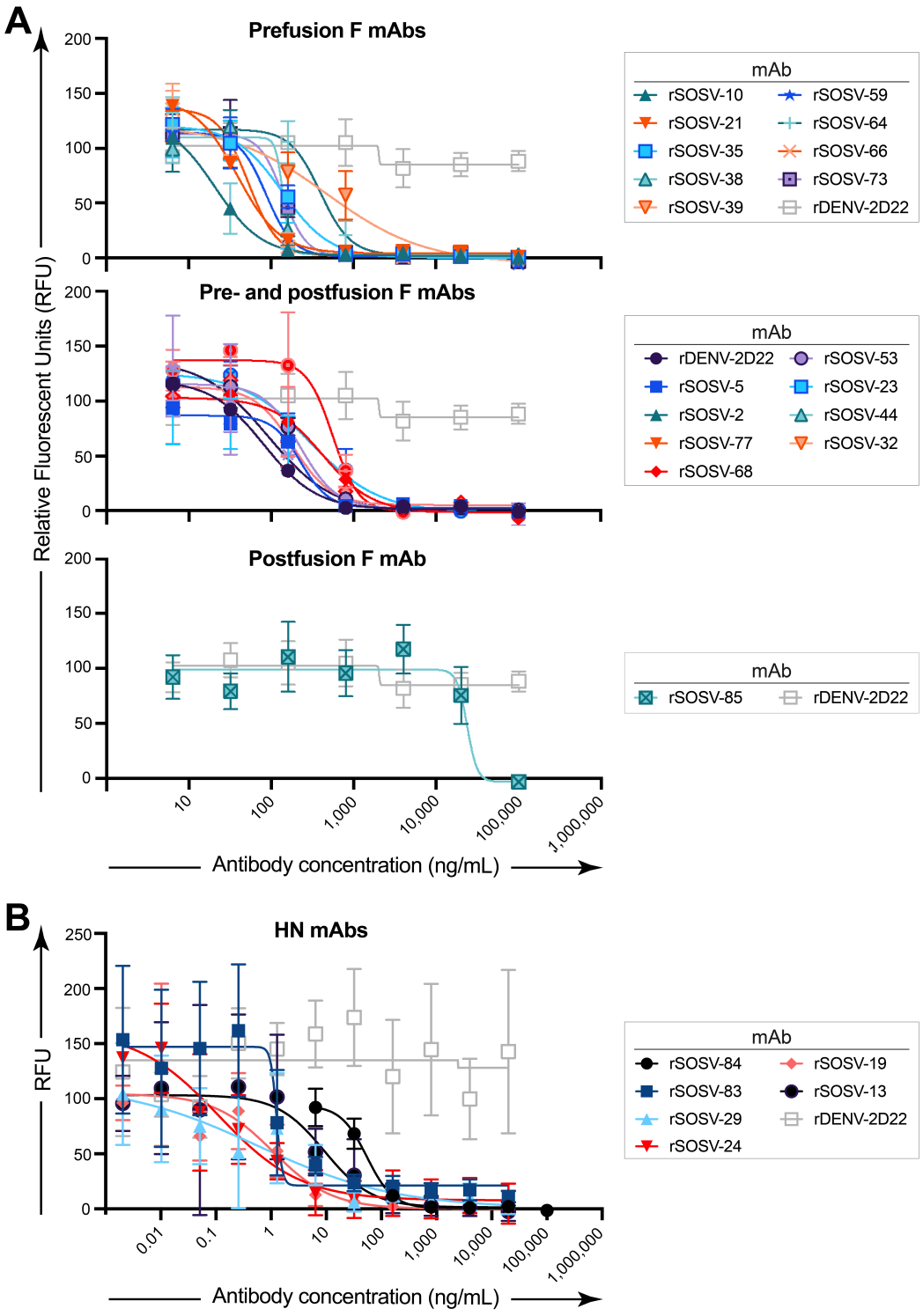

Figure 4.1. Neutralization assay of SOSV mAbs against live virus. SOSV mAbs were tested for inhibition of authentic rSOSV-ZsG in quadruplicate on Vero-E6 cell culture monolayers. **(A)** Neutralization data for anti-F mAbs. Data are grouped according to the pattern of antigen-reactivity: pre-fusion F, pre- and postfusion F, or postfusion F protein. **(B)** Neutralization data for the HN-specific mAbs.

Table 4.1. Half-maximal inhibitory concentration (IC_{50}) values for SOSV HN- or F-reactive mAbs in neutralization assay using authentic SOSV				
Targeted glycoprotein	**Domain of specificity and/or conformation specificity**	**Competition-binding group**	**mAb (rSOSV-)**	**IC_{50} (ng/mL)**
HN	Head domain	HN 1	84	55
		HN 2	24	0.4
			29	0.6
			83	1.3
		HN 3	19	1.1
		HN 4	13	9.3
F	Prefusion	F 1	73	140
		F 2	66	53
			38	140
			64	340
		F 3	10	21
			39	480
		F 4	21	39
		F 5	59	87
			35	137
	Pre- & postfusion F reactive	F 6	2	82
			53	91
			44	182
			5	226
			77	301
			68	558
		F 7	32	223
			23	422
	Postfusion	F 8	85	>10,000

Table 4.1. Half-maximal inhibitory concentration (IC_{50}) values for SOSV HN- or F-reactive mAbs in neutralization assay using authentic SOSV. Neutralization IC_{50} values were calculated for each SOSV mAb against recombinant SOSV, using 1 biological replicate consisting of 4 technical replicates per antibody. A negative control mAb (rDENV-2D22) was included in the assays to determine background levels of neutralization. Values of >10,000 reflect antibodies that had IC_{50} values exceeding 10,000 ng/mL. Antibodies are displayed by their target glycoprotein, domain (HN) or conformation (F) specificity, and their competition-binding group as determined in Chapter III.

Identification of anti-SOSV rmAbs that bind during western blot.

To aid in determining if recombinant-SOSV or pseudo-SOSV viruses were being produced at low titer, anti-SOSV rmAbs were tested for their ability to stain SOSV proteins in a western blot. The soluble fraction of lysates from cells transfected with the SOSV F-FLAG or SOSV HN-FLAG were transferred to nitrocellulose and stained SOSV mAbs as well as mouse anti-FLAG and mouse anti-PCNA as controls. Mouse primary antibodies were stained with an IRDye 680RD secondary while the SOSV rmAbs were stained with IRDye 800CW. SOSV rmAbs capable of binding in western blotting would be identified by the co-staining of the human anti-SOSV rmAbs with the mouse anti-FLAG. Antibodies were first screened in groups (**Figure 4.2**), then individual rmAbs within a group (**Figure 4.3**), and finally a confirmation screen of selected rmAbs (**Figure 4.4**). The anti-F results showed there was staining of the SOSV F protein with rmAb(s) in Group 1 (rSOSV-85, -77, -73, -68, -66, -64) that overlapped with the FLAG staining (**Figure 4.2A**). The polyclonal mix of anti-HN mAbs clearly bound to the HN protein as indicated by the overlap of anti-SOSV and anti-FLAG bands (**Figure 4.2B**). For the anti-HN mAbs, rSOSV-13 and to a lesser extent rSOSV-19 both bound to the SOSV HN-FLAG protein (**Figure 4.3A**). For the anti-F mAbs, rSOSV-77 clearly bound to the SOSV-F-FLAG protein (**Figure 4.3B**); there also appears to be some faint staining in the rSOSV-68 and rSOSV-66 wells, but as the signal was so close to background they were not counted as positive. To confirm that rSOSV mAbs were not binding to the FLAG tags, rSOSV-77 and rSOSV-13 were also tested against wildtype SOSV F and HN proteins. Both anti-SOSV rmAbs bound to their respective antigens regardless of the presence of the FLAG-tag (**Figure 4.4**), indicating that these antibodies could be

used in western blot assays to detect SOSV proteins on pseudoviruses.

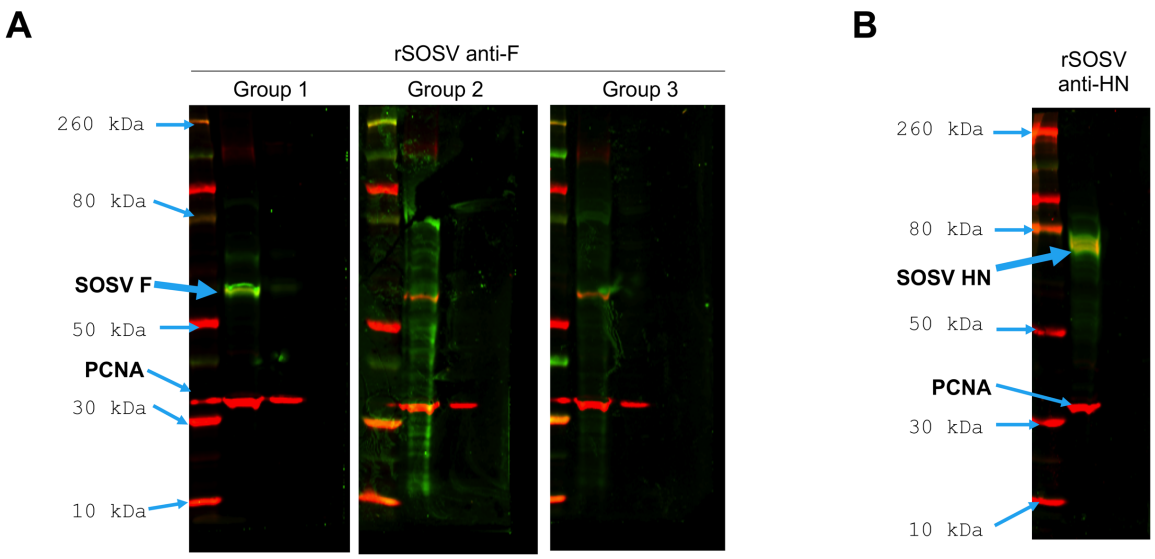

Figure 4.2. Groups rSOSV-mAbs bind to FLAG-tagged SOSV glycoproteins in western blotting. Lysates from HEK293T/17 cells transfected with SOSV F-FLAG or SOSV HN-FLAG were separated on a 4-12% polyacrylamide gels and transferred to nitrocellulose membranes. rSOSV-mAbs were divided into groups of 6, and each group was used as primary stain against its target antigen along with mouse anti-FLAG and mouse anti-PCNA as positive controls. Primary antibodies were detected with goat anti-human IRDye800CW (green) and goat anti-mouse IRDye680 (red) Nitrocellulose membranes were imaged on a LI-COR Odyssey using the 700 nm (red) and 800 nm (green) channels which were then merged to create an overlay. Blue arrows point to select bands of the molecular weight marker, as well as the PCNA and SOSV glycoproteins. **(A)** SOSV F-FLAG lysates stained with panel of 18 anti-F rmAbs pooled into 3 groups; (Group 1: rSOSV-85, -77, -73, -68, -66, -64; Group 2: rSOSV-59, -53, -44, -39, -38, -35; Group 3: rSOSV-32, -23, -21, -10, -5, -2). **(B)** SOSV HN-FLAG lysates stained with mix of all 6 anti-HN rmAbs together.

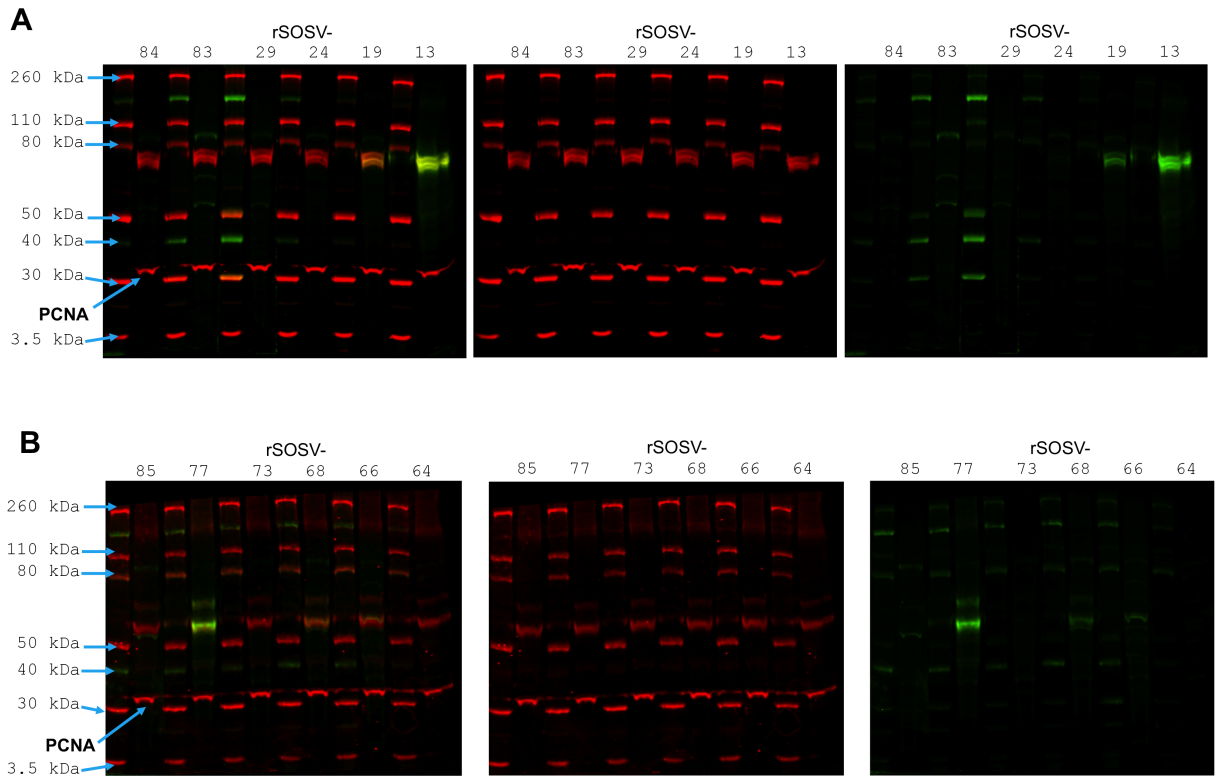

Figure 4.3. Individual anti-SOSV rmAbs can bind to target antigen in western blotting. SOSV F-FLAG or SOSV HN-FLAG proteins from cell-lysates were stained with individual anti-F and anti-HN rmAbs that had previously been identified in groups, as well as mouse anti-FLAG and anti-PCNA. Goat anti-human IRDye800CW (green) and goat anti-mouse IRDye680 (red) were used as secondaries. Membranes were imaged on a LI-COR Odyssey at 700 nm and 800 nm. The merged overlay of both colours is shown in the left-most panels followed by individual colour channels (700 nm then 800 nm). Arrows indicate select bands of the molecular weight marks, which are in every-other lane. The rSOSV-mAbs **(A)** Anti-HN mAbs (rSOSV-84, -83, -29, -24, and -13) and **(B)** Anti-F mAbs (rSOSV-85, -77, -73, -68, -66, -64) used in the primary stain are labelled above the lanes.

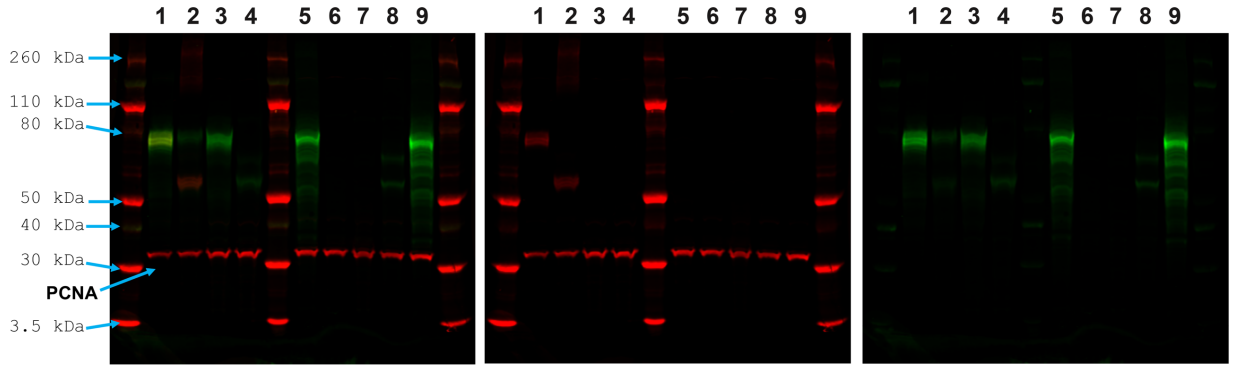

Figure 4.4. rSOSV-13 and rSOSV-77 bind to linearized SOSV HN or SOSV F respectively. Lysates from HEK293T/17 cells transfected with SOSV or VSV glycoproteins as follows: (1) SOSV HN-FLAG + SOSV F-6xHis, (2) SOSV HN-6xHis + SOSV F-FLAG, (3) SOSV HN-6xHis, (4) SOSV F-6xHis + SOSV HN-6xHis, (5) SOSV F-WT + SOSV HN-WT, (6) VSV-G, (7) untransfected, (8) SOSV F-WT, (9) SOSV HN-WT. Proteins were separated through SDS-PAGE on a 4-12% gel and transferred to nitrocellulose. The membrane was stained with mouse anti-FLAG, mouse anti-PCNA, rSOSV-13, and rSOSV-77 followed by goat anti-human IRDye800CW and goat anti-mouse IRDye680 secondaries. The membrane was imaged with a LI-COR Odyssey using the 700 nm (red) and 800 nm (green) channels which were then merged to create an overlay (far left). Single colour channels are shown as 700 nm in the center and 800 nm on the far right.

Recombinant VSV-SOSV failed to replicate.

Two recombinant VSV-SOSV viruses were generated by inserting wildtype SOSV F and HN cDNA into the genome of a rVSV-ΔG-eGFP. In the first construct (rVSV-SOSV$_{WT}$-eGFP), the SOSV F and HN genes were put into a single ORF with a DNA coding a T2A polypeptide cleavage site (149) in-between the two genes (**Figure 4.5**). Attempts to rescue the recombinant viruses were not yielding success, so unpurified samples both recombinant viruses were assessed for SOSV protein expression through western blotting and fluorescent microscopy.

For western blotting, the viruses were briefly amplified by inoculating Vero-E6 cell monolayers and incubating for 8-48 hr. Virus was grown with and without Ara-C in the culture media. The rVSV-SOSV$_{T2A}$-eGFP virus had already destroyed the cell monolayers by 8 hr, so rVSV-SOSV$_{T2A}$-eGFP supernatants were clarified and used for the western blot with rVSV-SOSV$_{WT}$-eGFP lysates that were harvested at the same time. The remaining rVSV-SOSV$_{WT}$-eGFP wells were cultured for another 40 hr before lysates were run through on a western blot. Lysates from uninfected cells (treated with or without Ara-C) were collected at the same time to serve as negative controls. Other controls included soluble SOSV F and HN proteins (preF-tHS and HN$_{ecto}$ respectively) as well as lysates from wildtype, SOSV F, SOSV HN, or SOSV F+HN transfections. A plasmid expressing eGFP was included as a transfected cell-lysate negative control. Neither the rVSV-SOSV$_{T2A}$-eGFP nor the rVSV-SOSV$_{WT}$-eGFP had detectable expression of SOSV F or HN proteins (**Figure 4.6**), though PCNA bands were visible. Many of the control conditions did not stain either, suggesting a possible issue with the SOSV staining.

Since the western blots did not turn out very well, fluorescent microscopy was used to check for expression of SOSV proteins at a smaller scale. 2-fold serial dilutions of rVSV-SOSV$_{WT}$-eGFP and 10-fold serial dilutions of rVSV-SOSV$_{T2A}$-eGFP were used to inoculate Vero-E6 cells on a 96-well plate. Half of the plate was fixed and stained to determine the amount of SOSV protein expression on the cell-surface. The other half was fixed, permeabilized, and stained to determine total (surface and intracellular) SOSV protein expression using an ImageXpress high-throughput microscope (Molecular Devices) and analyzed with accompanying software (MetaXpress). The rVSV-SOSV$_{T2A}$-eGFP virus was more cytopathic, killing many of the cells in the 10^{-1} wells. Also, while the rVSV-SOSV$_{T2A}$-eGFP virus had detectable SOSV expression in permeabilized cells, there was no staining on the cell surface (**Table 4.2**). The rVSV-SOSV$_{WT}$-eGFP virus had a very low titer, as <2% of the cells were infected even in the wells with the highest concentration of virus, however, the virus did have cell-surface expressed SOSV proteins (**Table 4.2**).

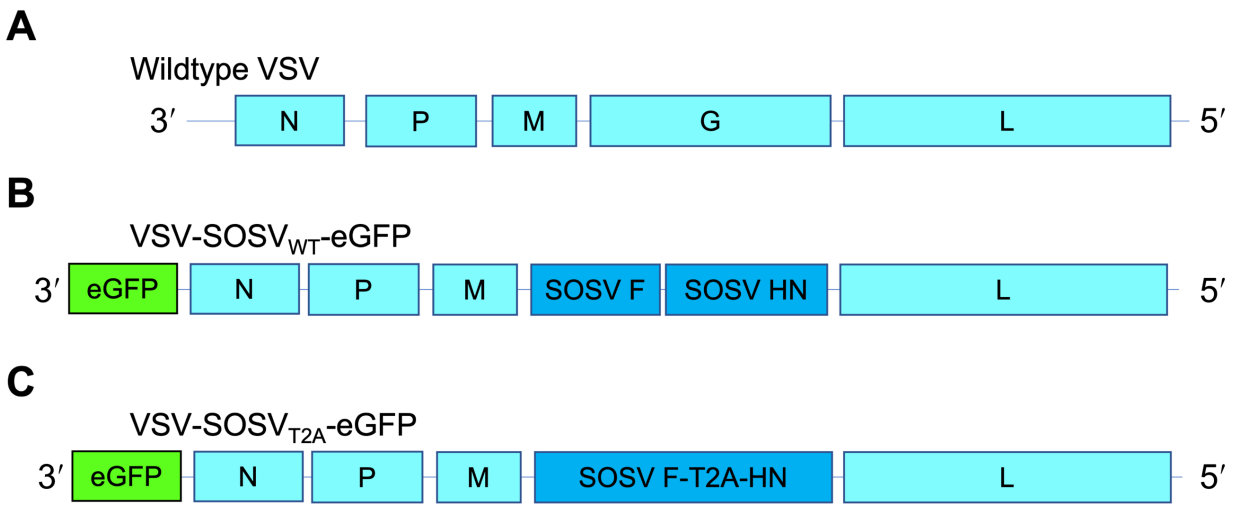

Figure 4.5. Genome organization of recombinant VSV-SOSVs compared to wildtype VSV. Diagram shows the 5 native proteins (N, P, M, G, and L) of VSV and their order in the synthetic viruses. **(A)** wildtype VSV, proteins are organized in natural order. **(B)** VSV-SOSV$_{WT}$-eGFP, eGFP gene is inserted at 3′ end of genome, also the WT sequences for SOSV F and SOSV HN replace the VSV-G gene. **(C)** VSV-SOSV$_{T2A}$-eGFP also has an eGFP gene at the 3′ end and VSV-G has been replaced by a single ORF coding for SOSV F and HN, with a T2A sequence between them.

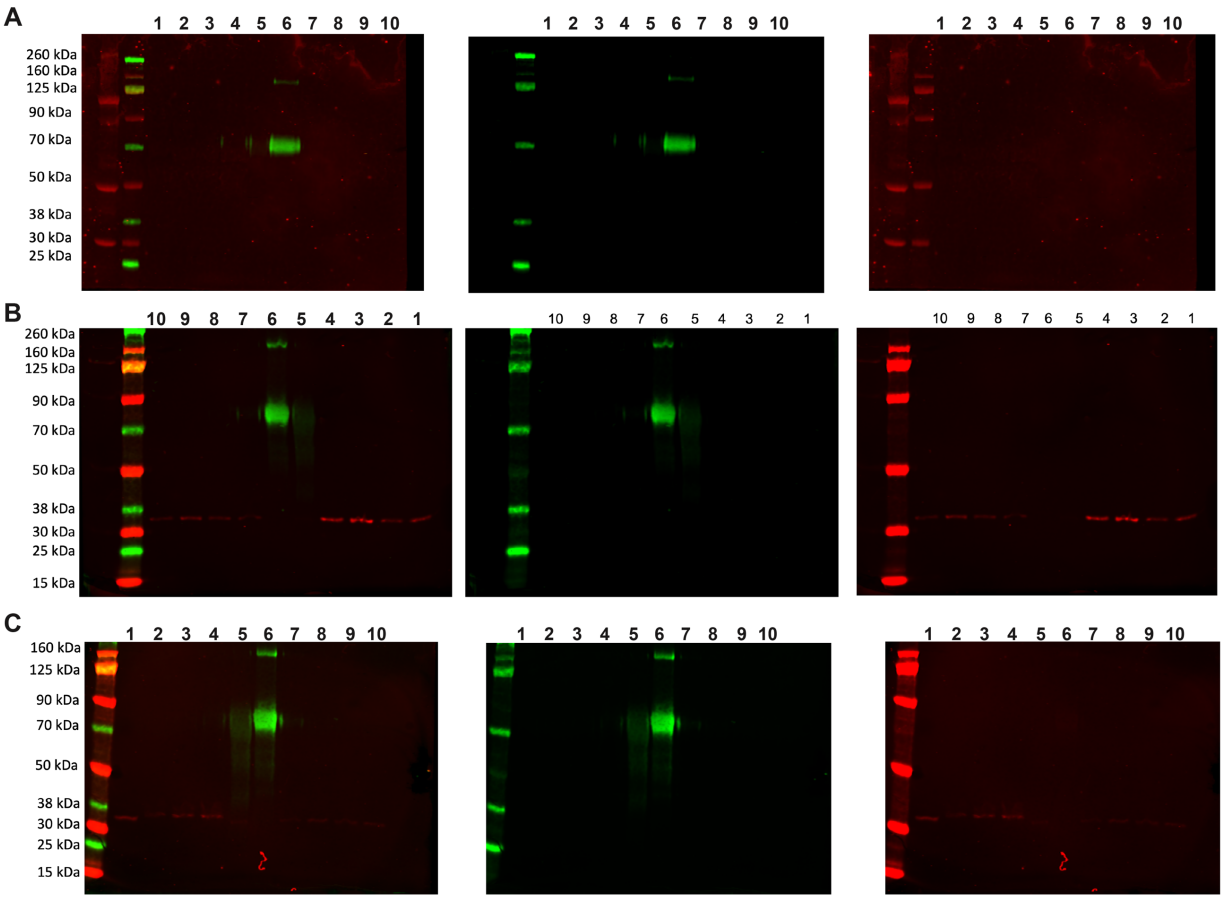

Figure 4.6. Western blots of recombinant VSV-SOSV-eGFP supernatants or lysates. Lysates, supernatants, or purified proteins were denatured before proteins were separated through SDS-PAGE. Proteins were transferred to nitrocellulose membranes using a dry-transfer and stained with mouse anti-PCNA, anti-SOSV HN (rSOSV-13), and anti-SOSV F (rSOSV-77). Membranes were imaged on an Odyssey (LI-COR Biosciences) in both the 700 nm and 800 nm channels presented in merged, green (800 nm), and red (nm). Numbers indicate which protein sample was loaded in that lane on the gel (note: in **(B)** the order is reversed), the protein samples were as follows: (1) uninfected + Ara-C, (2) rVSV-SOSV-eGFP + Ara-C, (3) uninfected, (4) rVSV-SOSV-eGFP, (5) SOSV preF-tHS, (6) SOSV HN_{ecto}, (7) SOSV F-WT, (8) SOSV HN-WT, (9) SOSV F+HN (WT), (10) eGFP. **(A)** clarified rVSV-$SOSV_{T2A}$-eGFP supernatant or uninfected cell lysates taken at 8 hr post-inoculation (p.i.) **(B)** rVSV-$SOSV_{WT}$-eGFP or uninfected cell lysates at 8 hr p.i. **(C)** rVSV-$SOSV_{WT}$-eGFP or uninfected cell lysates at 48 hr p.i.

Table 4.2. Percentage of SOSV glycoprotein expression by two chimeric VSV-SOSV-eGFP viruses and transfection controls

Expressed protein	rVSV-SOSV$_{WT}$-eGFP	rVSV-SOSV$_{T2A}$-eGFP	Transfection controls
Total F	0.77%	7.3%	12.09%
Total HN	0.68%	8.4%	12.16%
Surface F	0.78%	0.0%	8.71%
Surface HN	0.28%	0.1%	5.23%
Total eGFP	1.15%	7.3%	N/A

Table 4.2. Percentage of SOSV glycoprotein expression by two chimeric VSV-SOSV-eGFP viruses and transfection controls. Vero-E6 cells were inoculated with rVSV-SOSV$_{WT}$-eGFP (diluted 2^{-1} to 2^{-11}) or rVSV-SOSV$_{T2A}$-eGFP (diluted 10^{-1} to 10^{-11}) in duplicate. Several wells on each plate were transfeted with SOSV F or HN proteins to serve as positive-staining controls. 24 hours post-inoculation, Half of the plates were fixed while the other half was fixed and permeabilized to determine the amount of surface versus total SOSV protein expression. All plates were stained with DAPI and SOSV proteins were detected by using a primary stain of a pooled mix of anti-SOSV F and HN rmAbs, with goat anti-human Alexa Fluor 568 used as the secondary. Plates were imaged on an ImageXpress high-throughput microscope (Molecular Devices) and analyzed with accompanying software (MetaXpress) to calculate the percentage of infected (eGFP expressing) cells also expressing SOSV proteins.

Pseudotyping with VSV or HIV-1 systems.

In an effort to produce SOSV pseudoviruses, VSV and HIV-1 pseudotyping systems were used. Recombinant VSV expressing GFP in place of the VSV glycoprotein (rVSVΔG-GFP) (118) was used for the backbone virus of the VSV system. Stocks of rVSVΔG-GFP were generated in HEK293T/17 cells by transfecting with a plasmid encoding the VSV-G protein and inoculating transfected cultures with low MOI rVSVΔG-GFP pseudoviruses (purchased from Kerafast). Inoculation was typically done around 24 hr post-transfection, following manufacturer's protocol and using work from Whitt, M. A. (2010) (118) as a reference as well as looking for signs of cytopathic effect (CPE) from the VSV-G protein. While high titers (1 x 10^8 FFU/mL) of rVSVΔG-GFP could be produced using VSV-G, pseudotyping with SOSV F and HN proteins was not successful. To troubleshoot the pseudovirus production, the time between transfection of proteins and inoculation with rVSVΔG-GFP was tested from 6 hr to 72 hr and MOIs from 0.1 to 5. Additional cell lines tested were Vero, BHK-21, and Hep-2. Viruses were titered typically on vero cells, but the other cell lines were also tested.

For HIV-1, a 2-plasmid system (psPax2 + pLV-eGFP) and single-plasmid system (pNL4-3.Luc.R.E) were used. HIV plasmid(s) and SOSV F-WT and HN-WT plasmids were co-transfected in suspension on HEK293T/17 cells. Cultures were watched for signs of CPE and harvested typically 24-48 hr post-transfection. Ratios of HIV backbone plasmids to SOSV glycoproteins were tested at 30:1, 3:1, and 1:0.3. Viruses were either titered on HEK293T/17 cells and screened with flowcytometry (GFP reporter viruses) or luciferase enzyme assay (pNL4-3.Luc.R.E). Additionally, Dr. Christopher Aiken's lab at VUMC also tried to make SOSV-pseudoviruses using their HIV-1 pseudotyping

constructs. All of the HIV-1 systems failed to produce SOSV pseudoviruses, however, the VSV-G protein could be pseudotyped (**Figure 4.7**). The SOSV-pseudovirus production attempts are summarized in **Figure 4.8** below.

A

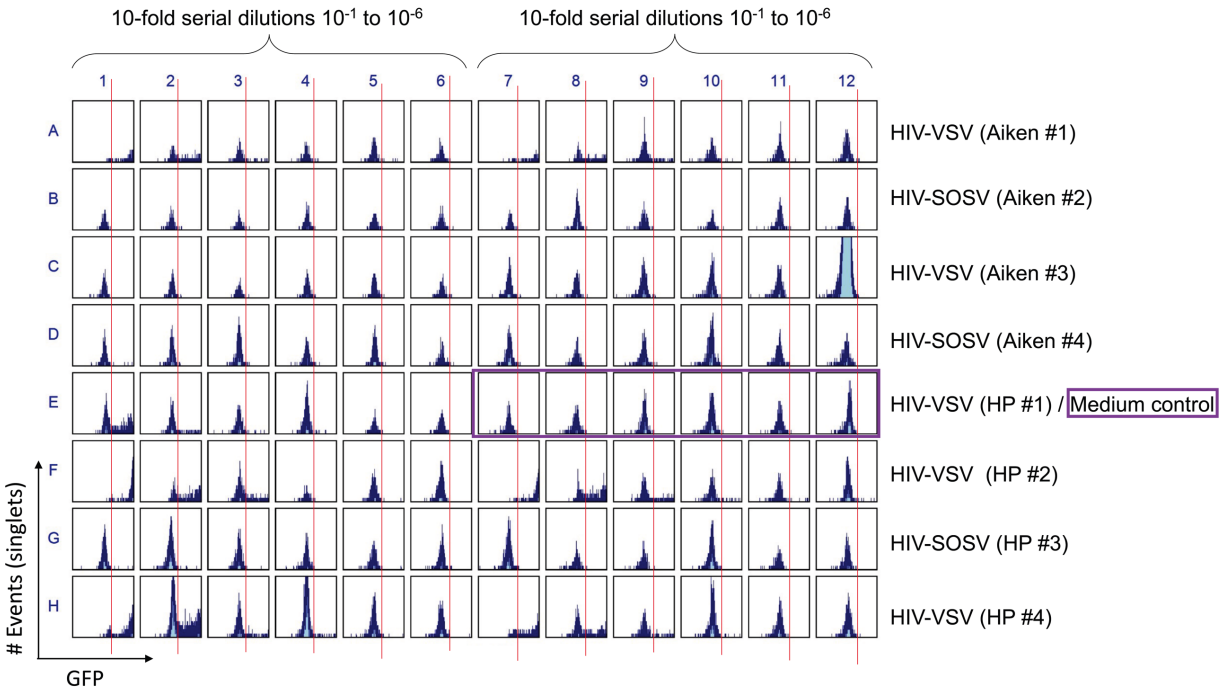

B

BHK cells	1.00E-01	1.00E-02	1.00E-03	1.00E-04	1.00E-05	1.00E-06	1.00E-01	1.00E-02	1.00E-03	1.00E-04	1.00E-05	1.00E-06	gradient
HIV-SOSV 30:1	17	22	18	16	15	21	16	24	16	23	20	23	scale
HIV-SOSV 3:1	15	17	15	14	15	24	20	14	16	19	18	18	1200
HIV-VSV 30:1	81	20	17	18	18	13	46	18	20	21	17	13	1100
HIV-VSV 3:1	52	18	19	22	18	13	24	20	21	19	18	20	1000
HIV-SOSV Aiken (#6)	18	16	17	18	14	22	25	17	15	21	21	24	900
media	16	19	16	18	17	20	19	21	16	19	20	17	800
													700
Vero Cells	1.00E-01	1.00E-02	1.00E-03	1.00E-04	1.00E-05	1.00E-06	1.00E-01	1.00E-02	1.00E-03	1.00E-04	1.00E-05	1.00E-06	600
HIV-SOSV 30:1	16	15	23	14	16	18	17	17	21	15	15	18	500
HIV-SOSV 3:1	19	17	18	17	16	18	19	22	14	13	19	17	400
HIV-VSV 30:1	1180	52	24	19	16	23	321	33	25	19	16	17	300
HIV-VSV 3:1	390	40	17	13	17	18	106	19	16	19	20	18	200
HIV-SOSV Aiken (#6)	20	17	13	24	17	19	18	22	19	16	19	21	100
media	14	17	19	14	17	22	23	19	19	14	16	16	0

Figure 4.7. HIV-pseudotyping with SOSV glycoproteins. HEK293T/17 cells were transfected with SOSV and HIV plasmid(s) and supernatants harvested at 24-48 p.t. Supernatants were diluted in series and used to inoculate 96-well plates of HEK293T/17, vero, or BHK-21 cells. **(A)** results of pseudotyping attempts with the psPax2 + pLV-eGFP system from two labs (HP and Aiken). Inoculated cells were checked for GFP expression on an iQue flow cytometer, VSV-G was used as a pseudotyping control for verification of protocol. **(B)** Results of pseudotyped HIV-SOSV using pNL4-3.Luc.R.E produced by the two groups [HP (myself) and Aiken]. 96-well plates of BHK-21 or vero cells were inoculated with the pseudotyped viruses and after 24 hr the Bright Glo luciferase assay kit (Promega) was used to virus infection of monolayers. Again, the VSV-G pseudotyped controls worked while the SOSV pseudotypes did not. Additionally, BHK-21 cells were not good for titering pseudovirus due to lack of signal even for control pseudotypes.

A

System	Backbone type	Backbone reagent(s)	Transfected glycoproteins	# Transfected plasmids	Reporter	Cell line(s)
VSV	recombinant virus particle	rVSV-SOSV$_{wt}$-eGFP	N/A	0	GFP	Vero
VSV	recombinant virus particle	rVSV-SOSV$_{T2A}$-eGFP	N/A	0	GFP	Vero
VSV	pseudotyped virus particle	rVSVΔG-GFP	SOSV F + HN	2	GFP	HEK293T/17 Vero BHK-21 Hep-2
HIV-1	2-plasmid	psPax2 pLV-eGFP	SOSV F + HN	4	GFP	HEK293T/17 Vero BHK-21
HIV-1	single-plasmid	pNL4-3.Luc.R.E.	SOSV F + HN	3	luciferase	HEK293T/17 Vero BHK-21

B

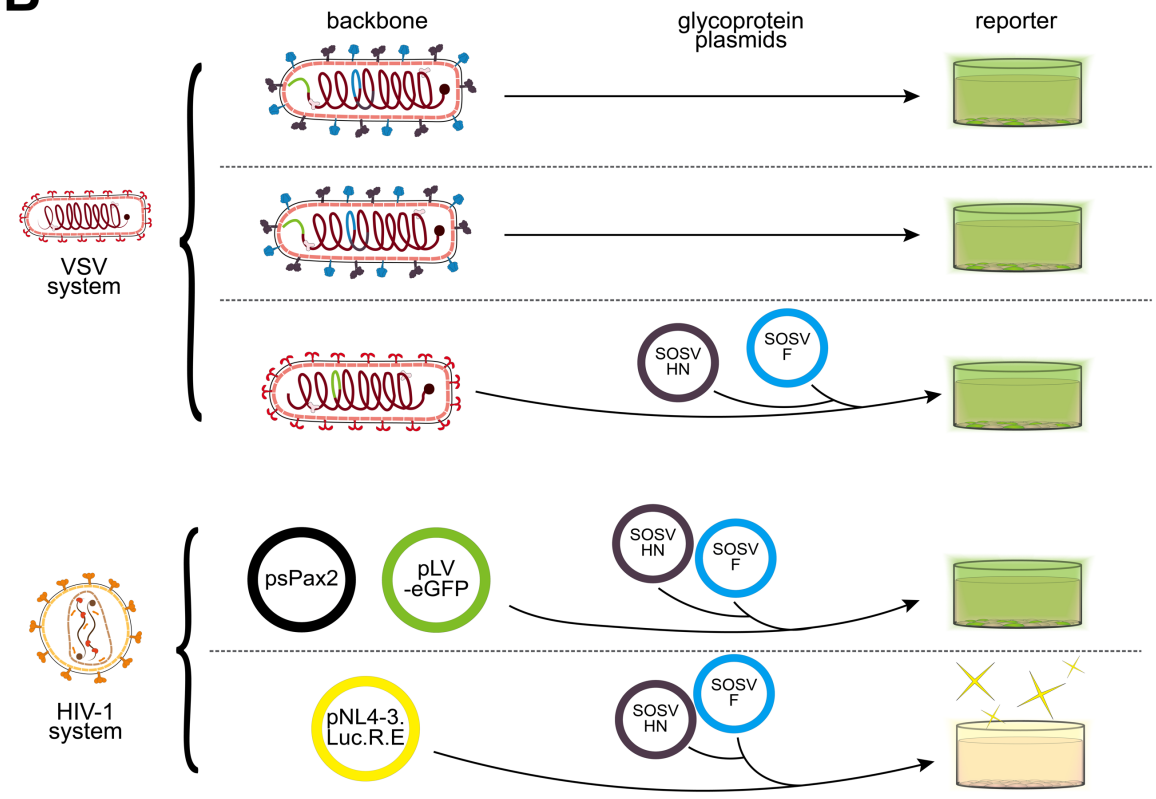

Figure 4.8. Summary of systems tested to produce recombinant or pseudotyped SOSV. Two widely successful recombinant and pseudovirus systems were used, VSV and HIV-1, however both failed to produce particles using SOSV glycoproteins. **(A)** summary of the systems, backbone plasmids or viruses, transfected plasmids, reporters, and cell lines tested. **(B)** graphical summary of systems tested.

Chapter IV Discussion

Overall, the majority of the anti-SOSV mAbs were neutralizing. The only antibody that failed to neutralize SOSV was the postfusion F-specific antibody. The anti-HN rmAbs were the most potent neutralizers with IC_{50} values ranging from 0.4 ng/mL to 55 ng/mL. Since the HN protein is the principal attachment factor and rubulaviruses do not typically fuse in the absence of HN (6, 21, 70), unlike viruses such as RSV (98), it is not unexpected that anti-HN rmAbs may be more potent. Additionally, these results are consistent with what is known of the neutralizing response to mumps virus which does predominantly target the HN protein (43, 150). It is possible that the prolonged and marked viremia induced ultra-potent mAbs may have contributed to the survival of the in this wildlife researcher but might not be elicited as commonly in humans during mild infection. An unanswered question is the seroprevalence of SOSV in people living in South Sudan or Uganda where the Egyptian rousette bats are present, or whether if SOSV infection in people living in areas endemic with pararubulaviruses would have the same susceptibility to severe disease as this U.S.-origin wildlife researcher. For the anti-F rmAbs, there was variability in the IC_{50} values for competition-binding groups within the prefusion and pre- and postfusion rmAbs confirmation groups. However, in general the prefusion-specific rmAbs had lower IC_{50} values, which is expected.

Since determining rmAbs that work in western blotting was mainly for troubleshooting, the results are not particularly meaningful to the overall body of work. It is however interesting that the cross-reactive, rSOSV-77 mAb works in western blotting and is therefore recognizing a linear epitope. Going back to the structure data in

Chapter III, this is again rather consistent with comparisons of RSV where antigenic sites II and IV contain linear epitopes (151). Therefore, structural comparisons of some known RSV antibody binding sites might help provide more specific epitope information for rSOSV-77. rSOSV-10 had the lowest IC_{50} value of the anti-F rmAbs, which lends support to the structural discussions in Chapter III that it is possible rSOSV-10 is binding to an RSV ∅-like site and functioning similar to the RSV antibody D25 (73). If this is the case, then rSOSV-10 is likely binding a quaternary epitope that locks the trimer in the prefusion state.

Between three labs and two pseudotyping systems, no SOSV pseudoviruses were successfully produced. The reasons why the pseudovirus systems did not work can only be speculated. However, myself and my collaborators suspect the cytoplasmic tails of the SOSV proteins are potentially at fault. The cytoplasmic tails for the SOSV proteins are longer than PIV5 (19 residues for HN, and ~5 residues for F) which has been successfully pseudotyped (144). Additionally, pseudotyping of other paramyxoviruses like measles and Nipah have required truncation of the cytoplasmic tails (128). It is possible that altering the SOSV tails would correct the problem, though our collaborators at WUSTL did try swapping the SOSV cytoplasmic tails with PIV5 tails and were still not able to produce SOSV pseudoviruses. Since the SOSV proteins are highly fusogenic, it is possible that a low enough amount of SOSV DNA was not tested as to prevent too much CPE for effective pseudotyping. For some of the work on SARS-CoV-2 uses the spike glycoprotein at a ratio of 0.0016 compared to the reporter plasmid (152), which is much lower than the lowest (0.3) ratio of backbone to SOSV DNA that was tested in this work.

The work in this chapter identifies ultra-potent, neutralizing rmAbs against SOSV and proposes possible mechanisms of neutralizing when combined with data from Chapter III. Additionally, this chapter covers the efforts of trying to produce HIV or VSV pseudotyped with SOSV glycoproteins.

Chapter IV Materials and Methods

Neutralizing activity of anti-SOSV rmAbs against rSOSV/ZsG at BSL-3.

The panel of 24 anti-SOSV rmAbs and a control rmAb, rDENV-2D22, were de-identified before being sent to Dr. Punya Shrivastava-Ranja, Dr. Shilpi Jain, and Dr. César G. Albariño of the Viral Special Pathogens Branch, Centers for Disease Control and Prevention (CDC) so that neutralization assays would be done as a single-blind study. A standard protocol for a fluorescent FRNT assay (65) was used to measure the neutralizing activity of all the rmAbs. Vero-E6 cells were seeded in 96-well plates (Cell Carrier Ultra plates, Perkin Elmer) at 15,000 cells/well. The next day, antibodies were serially diluted five-fold in DMEM and mixed with an equal volume (150 µL) of rSOSV/ZsG at 100 median tissue culture infectious dose ($TCID_{50}$). Virus and mAbs were incubated at 37°C for 1 hr before inoculating the Vero-E6 plates with 50 µL/well of virus-antibody mixtures. The plates were incubated for 72 hr at 37°C before fluorescent intensities were measured using a Synergy (BioTek) multi-well plate reader. Wells had been inoculated in technical quadruplicate for each rmAb concentration, along with no-virus control wells and virus-only control wells. The wells lacking virus gave the amount

of background, autofluorescence level from the cells and these values were subtracted from the virus-only and virus-rmAb treatments readings. Data was converted to a percent of the maximum signal, virus-only controls and analyzed in Prism (GraphPad) software was used to generate concentration–response plots that were fit with semi-log plots using a four-parameter equation. The maximal inhibitory concentration (IC_{50}) values were derived in Prism using the semi-log plots.

Western blotting of rSOSV mAbs.

To help aid in determining if recombinant-SOSV or pseudo-SOSV viruses were being produced at low titer, I tested anti-SOSV rmAbs for their ability to stain SOSV proteins in a western blot. HEK293F/T17 cells were seeded at 0.5 x 10^6 live-cells/well and transfected with SOSV F-FLAG or SOSV HN-FLAG in suspension using Lipofectamine 3000 (Invitrogen, cat. # L3000015) using the protocol described in Chapter II (Microscopy of SOSV F and HN expression in cultured cells). Cells were incubated at 37°C, 5% CO_2 for 24-72 hr. Cells were lysed using Radio-Immunoprecipitation Assay (RIPA) buffer RIPA (Sigma-Aldrich, cat. # R0278-50ml) by resuspending cell pellets in RIPA buffer and incubating at 4°C with agitation for 30 min. Supernatants from the lysed cell suspensions were collected and mixed 1:1 with denaturing buffer [2x Laemmli sample buffer (Bio-Rad, cat. # 1610737) + 5% 2-mercaptoethanol (Sigma-Aldrich, cat. # M6250)] and boiled at 95°C for 5-10 mins. 40-50 µL/well of lysate was loaded on a Bolt 4-12% Bis-Tris polyacrylamide gel (Invitrogen, cat. # NW04122BOX), with at least one lane per gel loaded onto 1-5 µL of Chameleon duo pre-stained protein ladder (LI-COR Biosciences, cat. # 928-60000). Gels were run

for ~35 min at 220 V in 1X NuPAGE MES SDS running buffer (Invitrogen, cat. # NP0002). Proteins were transferred to nitrocellulose membranes using an iBlot Transfer Stack mini (Invitrogen, cat. # IB301002) and an iBlot dry blotting system (Thermo Fisher Scientific) with an 8 min run time. Membranes were blocked at room temperature (RT) 1 hr to overnight in blocking buffer [Intercept (PBS) blocking buffer (LI-COR Biosciences, cat. # 92770001) + 0.2% Tween20 (Sigma-Aldrich, cat. # 9005-64-5)] with gentle shaking. Membranes were stained with primary antibodies: 1-2 µg/mL of human anti-SOSV mAb, 1:1,000 of mouse anti-FLAG clone M2 (Sigma-Aldrich, cat. # F3165), and mouse anti-PCNA clone PC10 (3F81) (eBioscience, cat. # 14-9910-82) diluted in blocking buffer; using one rmAb per membrane (often membrane was cut into strips to avoid waste). The membranes were incubated in primary stain at RT for 1 hr to overnight at 4°C with gentle shaking. The blots were washed 3x (~5 min) each with phosphate buffered saline with Tween 20 (PBS-T; Cell Signaling, cat. #9809S, 20 stock solution used to make 0.05% Tween 20 when diluted to 1X). After washing, membranes were stained with IRDye 680RD goat anti-mouse IgG (H+L) (LI-COR Biosciences, cat. # 925-68070) and IRDye 800Cw goat anti-human polyclonal antibody (LI-COR Biosciences, cat. # 926-32232) both diluted 1:15,000 in blocking buffer. After the secondary stain incubated 1 hr at RT with gentle shaking, the membranes were washed 3x (~5 min each) in PBS-T. Before imaging, PBS-T was removed and membranes rinsed and kept in DBPS until imaged. Imaging was done with an Odyssey imager (LI-COR Biosciences).

Western blots were performed with the same protocol above for the rVSV-$SOSV_{WT}$-eGFP and rVSV-$SOSV_{T2A}$-eGFP viruses with the following differences: Vero-

E6 cells (ATCC, cat. # CRL-1586) were seeded at ~50,000 live-cells/well in 24-well plates, the day before. Cell culture media was removed and 100 µL of each virus was inoculated into 4 wells, plates were incubated with virus alone for 1 hr at 37°C 5% CO_2 before adding 400 µL of virus culture media (DMEM + 1% PSG + 2% FBS). Half of those wells were treated with 25 ug/mL of cytosine β-D-arabinofuranoside (Ara-C) [Sigma-Aldrich, cat. # C1768-100MG, reconstituted to 25 mg/mL in sterile molecular biology grade water (Corning, cat. # 46-000-CI)] to help inhibit growth of vaccinia virus present with the recombinant viruses. Plates were incubated 8-48 1 hr at 37°C 5% CO_2. rVSV-SOSV$_{T2A}$-eGFP viral supernatant was collected and clarified through centrifugation, rVSV-SOSV$_{WT}$-eGFP lysates were harvested the same as transfected cells described above and stored at -20°C until all viral samples were ready to be run on a western blot. Soluble SOSV F and HN proteins as well as leftover lysates from transfections were included to serve as controls. Anti-SOSV primary stain used 2 µg/mL of rSOSV-77 and rSOSV-13.

Recombinant VSV-SOSV-eGFP viruses.

The two versions of VSV-SOSV-eGFP viruses were generated by cloning wildtype cDNA sequences of SOSV F and SOSV HN from pTwist-CMV and into a plasmid encoding cDNA for a rVSV-ΔG-eGFP virus following the same protocol as previously (144). The rVSV-SOSV$_{T2A}$-eGFP contained one ORF for both SOSV F and HN with a T2A peptide cleavage site (149) encoded between the two SOSV genes, while the rVSV-SOSV$_{WT}$-eGFP virus maintained separate F and HN genes separated by a VSV intergenic sequence (144).

Microscopy assays of recombinant VSV-SOSV-eGFP viruses.

rVSV-SOSV$_{WT}$-eGFP was diluted in a 2-fold serial dilution starting from 2^{-1} to 2^{-11} in virus culture medium (DMEM + 1% PSG + 2% FBS), while rVSV-SOSV$_{T2A}$-eGFP virus was diluted in a 10-fold series ranging from 10^{-1} to 10^{-11}. 50 µL of viral dilutions were used to inoculate 6 rows of 96-well plates (leaving 2 rows and the last column open for transfection controls) that had been seeded with 10,000 Vero-E6 live-cells/well the day before. Virus was plated so that the top half (rows A-D) and bottom half (rows E-H) being duplicates of each other. After a 1 hr incubation, 100 µL of virus growth media was added to the wells which were incubated over night at 37°C, 5% CO_2. Some of the wells that were not inoculated with virus were transfected with SOSV (SOSV F-WT, SOSV HN-WT, or SOSV F+HN WT) or a reporter plasmid (eGFP) to serve as staining controls. Approximately 24 hr post-infection, the plates were fixed and stained. One half of the plate was fixed and permeabilized using the fixation and permeabilization method described in Chapter II (Microscopy of SOSV F and HN expression in cultured cells) and the staining method described in Chapter III (Screening for cross-reactive anti-SOSV mAbs). The other half of the plate was fixed without permeabilization like the method in Chapter III. Polyclonal mixes of anti-SOSV F or HN rmAbs were used to stain individual rows and then combined to stain a single row (and transfection controls) with both F+HN anti-SOSV rmAbs. Since the viruses express eGFP, the anti-SOSV mAbs were detected with a goat anti-human Alexa Fluor 568 secondary (Invitrogen, cat. # A-21090). Plates were imaged on an ImageXpress high-throughput microscope (Molecular Devices) and analyzed with accompanying software

(MetaXpress) to count the number of cells stained with DAPI, Alexa Fluor 568, and/or eGFP. Output data was taken as percentages. The output data was further analyzed in Microsoft Excel (Microsoft, version 16.69, Mac OS).

VSV pseudovirus production.

Recombinant VSV expressing GFP in place of the VSV glycoprotein (rVSVΔG-GFP) (118) was purchased from Kerafast (cat. # EH1019-PM). Stocks of rVSVΔG-GFP were generated in HEK293T/17 cells follower manufacturer's protocol as well as work from Whitt, M. A. (2010) as a guide (118). Briefly, HEK293T/17 cells in cell growth media (DMEM + 10% FBS + 1% PSG) were seeded in 6-well plates and incubated at 5% CO_2, 37ºC overnight. When cells were ~70% confluent (typically the next day) they were transfected with VSV-G protein (pCAGGS, Kerafast, cat # EH1017) using Lipofectamine 3000 as has been previously described and incubated overnight again. The next day cells were inoculated with low (~0.1 MOI) of rVSVΔG-GFP. Supernatants from the cultures were harvested 24-48 hr post-transfection depending on CPE. Supernatants were clarified and viral stocks frozen and tittered on vero cells. For tittering, viruses were diluted in a 10-fold serial dilution and 50-100 μL of each dilution added to ~70-80% confluent monolayers of vero cells (ATCC, cat. # CCL-81) seeded the day before in 96-well plates. Since the viruses are non-replicating, the plates were only incubated overnight at 5% CO_2, 37°C. The next day cells were fixed with 4% PFA, permeabilized (1X DPBS + 0.1% saponin + 0.1% BSA), and blocked (5% nonfat dry milk + 0.1% saponin in 1X PBS-T). A mouse anti-VSV-N monoclonal (clone 10G4) (Kerafast, cat. # EB0009) was used at a dilution of 1:4,000 to stain the VSV-N protein,

primary stain was detected with a goat anti-mouse HRP conjugated secondary antibody (Thermo Fisher Scientific, cat. # 62-6520) diluted at 1:1,000. Final staining was done with TrueBlue peroxidase substrate (SeraCare, cat. # 5510-0030). Cells were imaged and counted with an Immunospot S6 Analyzer (C.T.L.). Pseudotyping with SOSV glycoproteins was done similarly but using the SOSV F and HN glycoproteins.

HIV pseudotyping with SOSV.

The pLV-eGFP lentiviral transfer plasmid was a gift from Pantelis Tsoulfas (Addgene plasmid # 36083; http://n2t.net/addgene:36083; RRID:Addgene_36083), while the psPax2 and pNL4-3.Luc.R.E. plasmids were already in our laboratory. HEK293T/17 cells were transfected in suspension with HIV plasmid(s) and SOSV F and HN glycoproteins using Lipofectamine 3000. Cells were incubated at 5% CO_2, 37°C until presence of CPE. Supernatants were harvested and clarified. Viruses were typically titered on HEK293T/17 cells that were analyzed with an iQue flow cytometer (psPax2 pLV-eGFP system) or with the Bright-Glo luciferase assay system (Promega, cat. # E2620) and read on a BioTek plate reader. VSV-G was pseudotyped as a control.

CHAPTER V

Conclusions and future directions

Disclaimer: part of the data and information presented in this chapter were adapted from the following:

Parrington HM, Kose N, Armstrong E, Handal LS, Diaz S, Reidy J, Dong J, Stewart-Jones GBE, Shrivastava-Ranjan P, Jain S, Albariño CG, Carnahan RH, Crowe JE. 2023. Potently neutralizing human monoclonal antibodies against the zoonotic pararubulavirus Sosuga virus. JCI Insight https://doi.org/10.1172/jci.insight.166811.

Conclusions

This work was intended to help address the gaps in knowledge regarding pararubulaviruses and human immune responses to them and other members of *Rubulavirinae*. At the start of this project, there were a total of three publications discussing Sosuga (17, 23, 65), and two of them were on the discovery the virus (17, 23). Also, the only reagents that existed were the virus and the donor's blood. In chapter I, I introduced the background of the *Rubulavirinae* subfamily. One of the more surprising aspects of this project was how much is not known about immunity to viruses like mumps. Since the vaccine for mumps came out in the late 1960s, I was under the impression there would be a wealth of information and characterized antibodies similar to how there is for RSV. However this was not the case, though some work on mouse mAbs against rubulaviruses was done in the 1980s. Claes Örvell of the Karolinska

Institute (Stockholm, Sweden) had generated entire panels of mouse mAbs against almost all of the mumps virus proteins, including the F and HN proteins (153). Depressingly, these antibodies appear to be lost to time though as when we reached out to contacts at the Karolinska Institute we were unable to track down these antibodies. Therefore, the work in this dissertation is not just limited to emerging, bat-borne paramyxoviruses but also advances knowledge for an entire viral subfamily.

The summation of this work is that I was able to identify the first human mAbs to Sosuga virus, which are also the first human mAbs to a rubulavirus. In total I isolated 24 human monoclonal antibodies by screening donor B cells against viral glycoproteins expressed on cell surfaces. The cell surface display assay worked remarkably well in identifying SOSV-specific B cells. As discussed in Chapter III, the use of whole viral proteins helped discover two antibodies (rSOSV-35 and rSOSV-59 that recognize an epitope on the F protein that is not present or accessible on the soluble forms of the protein. Additionally, by keeping the F and HN proteins transfected separately the cell-surface displayed F is predominantly in the prefusion state as supported by the low number of postfusion specific antibodies identified as well as the syncytia formation assays which revealed that both F and HN are required for syncytia formation (Chapter II).

At the start of this project, I was hoping to identify cross-reactive and neutralizing antibodies. Both of these were accomplished in this thesis, though to different degrees of success. The cross-reactivity results were honestly a bit disappointing. I was hoping that there would be much broader reactivity, however, most of the cross-reactivity was between SOSV and its closest relative (Tuhoko virus 3). Also, none of the anti-HN

rmAbs had cross-reactivity (**Figure 3.8**). Since the protein sequences are relatively dissimilar (**Figure 3.7**), it is not a surprising result. I was however hoping that there would be at least one cross-reactive anti-HN mAb that might have identified an epitope of the receptor binding site for pararubulavirus. rSOSV-77 which showed cross-reactivity to mumps virus was interesting however. From the characterizations in Chapters III and IV, it seems that rSOSV-77 binds to a linear epitope that is similar to either RSV site II or IV (98, 151) based on the 3D reconstructions (**Figure 3.12**). One of the broader questions of this project that I was interested in was the possibility of measles, mumps, and rubella (MMR) vaccine-induced immunity against mumps virus aiding in the protection from viruses like SOSV. It is interesting that the individual who would have most likely been the youngest and healthiest of the field-expedition group is the only person who became infected from an exposure. The age of the SOSV donor at time of infection aligns well with the immune waning against mumps virus that has been observed for MMR vaccinations in young adults (42, 51, 154). It would be interesting to learn more about the other group members on the expedition to South Sudan and Uganda to have a better idea if immunity to mumps virus, or lack thereof, played a role in the case of SOSV infection. A mumps virus recall response could also explain why there would be cross-reactivity between SOSV and MuV but not viruses in-between those two distant ones. rSOSV-77 was also a moderately potent neutralizer in the anti-F panel, with an IC_{50} of 301 ng/mL.

The isolation of neutralizing antibodies against SOSV worked out much better than expected. Only one of the antibodies could be considered non-neutralizing (rSOSV-85, postfusion specific), and all of the neutralizing antibodies had IC_{50} values

below 500 ng/mL. The anti-HN rmAbs were mostly ultrapotent with 5 out of 6 rmAbs having an IC_{50} value below 10 ng/mL. The mAbs rSOSV-19, rSOSV-24, rSOSV-29, and rSOSV-83 all had IC_{50} values below 1.5 ng/mL, which are some of the most potent mAbs discovered (155, 156). All of these anti-HN ultra-potent antibodies are within the same competition-binding group or showed partial competition between the groups (**Figure 3.4**). Due to the high potency of these antibodies which are all targeting the same or close epitopes, I suspect that these mAbs are potentially receptor blocking. The 3D reconstruction of the rSOSV-24 Fab bound to HN_{head} supports the possibility of receptor blocking as the Fab is binding to the top of the dimeric heads. It appears that only one Fab was able to bind at a time, so an entire IgG may effectively block receptor binding even if the epitope isn't the receptor binding domain itself.

The prefusion specific anti-F rmAbs were also quite potent neutralizers themselves with IC_{50} values ranging from 21 to 480 ng/mL with the average being around 160 ng/mL. rSOSV-10 was the most potent anti-F mAb with an IC_{50} value of 20 ng/mL. The 3D reconstruction for rSOSV-10 suggests binding around the very top of the trimer which may lock the F protein in the prefusion conformation. This would be similar to the antibody D25 and its epitope in the RSV site ∅ as discussed in chapter III (73). Further characterization and structural analyses of the rSOSV Fabs may help solve the mechanisms by which these highly potent antibodies neutralize the virus.

This panel of mAbs may be useful in several applications. An ultra-potent HN mAb, such as rSOSV-24, is potentially a therapeutic candidate given its extraordinarily low IC_{50} value for neutralization of 0.4 ng/mL. As there are currently no available SOSV-specific reagents, the mAbs discovered in this work also can serve as reagents for the

continued study of SOSV pathogenesis and immunity. rSOSV-85 as a postfusion-specific mAb can be used in various applications, such as to study the fusion-triggering process during the SOSV life cycle, help test the stability of potential prefusion F protein vaccine candidates, or aid in prefusion F protein purification processes by sequestering postfusion F protein during chromatographic purification protocols. Potently neutralizing prefusion-specific F mAbs like rSOSV-10 can serve as positive controls in neutralization assays for testing anti-viral compounds or vaccines. Finally, knowledge of the competition-binding groups of the HN and F proteins and preliminary data into the epitopes of select rmAbs may help in further understanding protein domains governing the paramyxovirus fusion process or in receptor discovery studies for SOSV. As SOSV and other pararubulaviruses lack the ability to bind to sialic acid but can infect human cells (94, 157), discovering the receptor for this genus of paramyxoviruses could greatly advance efforts for epidemic preparedness against this group of viruses. Also, since all of the pararubulaviruses tested so far (Teviot, Tioman, and Menangle viruses) are able to enter bat, human, and pig cells (22, 157–160) it is quite possible that the SOSV receptor may also be conserved between bats humans, and pigs—indicating potential threat to and from domestic livestock as well.

In summary, the human mAbs isolated in this study are the first SOSV-specific mAbs generated and can be used for further studies of SOSV and related viruses and as candidate therapeutic antibodies for clinical development. Additionally, the methods and approaches used in this study may be beneficial for the isolation of antibodies against other novel paramyxoviruses, particularly those in the *Rubulavirinae* subfamily.

Future directions

Receptor blocking assays using anti-HN rmAbs.

While the receptor for SOSV is unknown, cell-lines permissive for viral infection or for syncytia generation are known. To test the anti-HN rSOSV mAbs for their ability to block receptor binding then, the tagged HN_{head} and HN_{ecto} proteins can be incubated with the SOSV mAbs prior to being used as the primary stain against a suitable cell-line such as vero or Expi293F. The tags already present on the amino ends of the protein can be detected with a fluorescent-conjugated secondary and detection of binding performed by flow cytometry. Some of the pitfalls for this assay is that many cells will naturally express biotin, so choice of secondary antibody or detection agent needs to keep this in mind. In some of the preliminary assays I used an Alexa Fluor-conjugated streptavidin to bind to the strep tags on $HN_{ecto\text{-}TS8H}$ and $HN_{head\text{-}TS8H}$ and found that labelling of cells occurred in the secondary only controls indicating that the streptavidin was binding to biotin expressed by the cells. While using the His-tag is potentially a simple fix, an alternative not tried yet is using the same BioLock solution (IBA, cat. # 2-0205-250) used in Strep-tag purifications of proteins to bind up any free biotin. Using this solution as a blocking step may also prevent background binding of the secondary.

Chimeric F and HN proteins to generate pseudoviruses.

While the current panel of rmAbs have been assessed for neutralization, future antibody discovery campaigns still benefit from a BSL-2 neutralization assay. As

discussed in Chapter IV, we suspect the cytoplasmic tails of the SOSV proteins are causing incompatibility with the backbone viruses. To address this, I had generated both chimeric versions of the F and HN protein with PIV5 or VSV cytoplasmic tails. All of these chimeric proteins were confirmed to express using fluorescent microscopy. They have not been tested in either VSV or HIV-1 pseudotyping assays yet. If none of these constructs work, it may be possible to systematically truncate the SOSV cytoplasmic tails similarly to work done for other paramyxoviruses (136).

Screening for stalk-specific anti-HN rmAbs.

As all of the isolated rmAbs in this project bind to the globular head of the HN protein and do not cross-react, a campaign to try and isolate antibodies to the stalk domain may help identify some cross-reactive antibodies. Since current models of paramyxovirus fusion have the HN (or attachment protein) stalk domain interacting with the F protein and triggering fusion. Thus antibodies that bind to the stalk domain are still potentially neutralizing. Additionally, fusion can be induced by expressing just the stalk domain of viruses like PIV5 (70, 161–163). A construct of the SOSV HN stalk (residues 1-125) has already been made, expressed, and shown to induce syncytia in transfected monolayers. Thus a cell-surface display antibody screen using the transmembrane stalk domain could be used to isolate stalk-specific B cells and mAbs.

Syncytia-inhibition assay.

As another alternative to the pseudoviruses, measuring the inhibition of syncytial formation by mAbs could be used to identify neutralizing antibodies. Syncytia formation

can be measured on an xCelligence (Agilent) device that determines the amount of electrical impedance produced by the cell monolayer. During syncytia formation, tight junctions between cells form and the impedance increases, then as the cells die from the cytotoxicity of the SOSV glycoproteins the impedance crashes back down. The result is “Z” shaped curve compared to untransfected cells which logarithmically grow until plateauing. Some of the initial studies for this showed that syncytia could be measured and inhibited. A much higher concentration of antibody is required though due to the high amounts of protein expression. Additionally, none of the anti-HN mAbs appeared to have an effect in the trial runs, which could be due to the amount of receptor abundance in a monolayer and the area of cell-cell interactions compared to virus-cell interactions.

SOSV antibody lineages and public clonotypes.

While there is a single SOSV donor, that donor participated in many of our group’s sequencing studies and so we accrued a large quantity of B cell antibody sequences from this one donor. Using these sequences, searched for ones that shared the anti-SOSV mAb V gene, J gene, and CDR3 amino acid length and 80% amino acid similarity. From doing this, we were able to generate phylogenies of mAb lineages for 9 of the anti-SOSV mAb heavy chains. From these phylogenies we determined the unmutated common ancestor (UCA) and synthesized the putative UCAs using the discovered heavy chain sequence paired with query mAb light chain. Additionally, we also searched sequence databases excluding the SOSV donor to look for potential public clonotypes. Using similar criteria, the antibody sequences were considered

similar to the query mAb sequences if they had the same V and J genes and 80% or more amino acid identity in the CDR3 region. From this search we identified a public clonotype for SOSV-2. Between the UCAs and public clonotype, an additional 44 rSOSV-mAbs were created (rSOSV-86 to rSOSV-129). These antibodies can be screened for cross-reactivity since it is possible the SOSV donor had a mumps recall response during infection and that UCAs may be able to bind mumps and SOSV. Also since there is no other SOSV donor in the world, a public clonotype is likely also a cross-reactive antibody. Since all of the constructs for these additional SOSV antibodies have already been synthesized, all that is needed to be done is express them and screen for cross-reactivity.

Additional future work.

These assays have not been started, however, would be of high interest for continued work on SOSV. Only recently has a potential rodent model for SOSV infection been developed. Syrian hamsters were found to be susceptible to SOSV infection, though the hamsters did not show clinical signs of disease and would not work for severe disease models (164). Interestingly, from the hamster study it was noticed that SOSV has tropism for lymphoid tissue (164). This finding is similar to what has been observed for Menangle virus in pigs (159). As the SOSV antibodies performed well during *in vitro* neutralization assays, it would be interesting to see if any of the mAbs can be used as prophylaxis in a small animal model. While the SOSV receptor is unknown, there are several cell lines that appear to be permissive. Using siRNA knock-out libraries of various cell-surface proteins could potentially be used to identify SOSV

receptor candidates. Since there is an abundance of SOSV donor PBMCs, a more comprehensive screen for cross-reactive antibodies could be done by screening donor B cells immediately for cross-reactivity and not just reactivity to SOSV. Antigen-specific cell-sorting could be potentially used to help separate SOSV-specific B cells much earlier so that future screens could be done on other rubulavirus proteins rather than SOSV. Finally, since there is very little known about the epidemiology of SOSV studies that look into the seroprevalence of SOSV-reactive antibodies of people living in South Sudan and Uganda, especially in areas close to where Egyptian fruit bats are roosting, could be useful for better understanding the endemicity of SOSV and identify other cases of infection or exposure. From a public health standpoint, the seroprevalence results may also be useful informing testing criteria and policies as a high seroprevalence without known incidences of severe disease could indicate SOSV may present more mildly and be mistaken for another virus in endemic regions.

Final remarks

As a novel paramyxovirus there was a lot unknown about SOSV at the start of this project. Now that I have reached the end of my part in this project, there is still a lot unknown about SOSV. I found the entire case study of the SOSV donor becoming infected fascinating, and I am glad I was able to study such an interesting virus. Antibodies obviously have a lot of clinical applications, but an overlooked use is how essential they are to basic research. Antibody staining or binding is utilized in so many

different assays as techniques including microscopy, flow cytometry, western blotting, protein purification, and cell sorting. Working on a project with no reagents developed puts how much antibody reagents are taken for granted. About 20% of the protein content of plasma is composed of antibodies (78) and with having almost nothing besides donor PBMCs at the start of this project, we were only one step above blindly pulling out antibodies to further study. Yet, the use of cell-surface display allowed us to discover 24 human monoclonal antibodies against SOSV. Additionally, many of these antibodies turned out to be quite potent neutralizers with some of the anti-HN rmAbs being ultra-potent. While developing a therapeutic might be the ideal, it is my hope that the antibodies discovered in this project will find themselves useful even without an epidemic/pandemic of SOSV.

REFERENCES

1. Plemper RK, Lamb RA. 2021. Chapter 12 - *Paramyxoviridae*: The Viruses and Their Replication, p. . *In* Peter M. Howley, David M. Knipe, Whelan, S (eds.), Fields Virology: Emerging Viruses. Wolters Kluwer Health, Philadelphia.

2. Rima B, Balkema-Buschmann A, Dundon WG, Duprex P, Easton A, Fouchier R, Kurath G, Lamb R, Lee B, Rota P, Wang L. 2019. ICTV Virus Taxonomy Profile: *Paramyxoviridae*. J Gen Virol 100:1593–1594.

3. Samal SK. 2008. Paramyxoviruses of Animals. Encycl Virol 40–47.

4. Drexler JF, Corman VM, Müller MA, Maganga GD, Vallo P, Binger T, Gloza-Rausch F, Cottontail VM, Rasche A, Yordanov S, Seebens A, Knörnschild M, Oppong S, Sarkodie YA, Pongombo C, Lukashev AN, Schmidt-Chanasit J, Stöcker A, Carneiro AJB, Erbar S, Maisner A, Fronhoffs F, Buettner R, Kalko EKV, Kruppa T, Franke CR, Kallies R, Yandoko ERN, Herrler G, Reusken C, Hassanin A, Krüger DH, Matthee S, Ulrich RG, Leroy EM, Drosten C. 2012. Bats host major mammalian paramyxoviruses. Nat Commun 3:796–796.

5. Payne S. 2017. Chapter 20 - Families *Paramyxoviridae* and *Pneumoviridae*, p. 173–181. *In* Payne, S (ed.), Viruses: From Understanding to Investigation. Academic Press.

6. Jardetzky TS, Lamb RA. 2014. Activation of Paramyxovirus Membrane Fusion and Virus Entry. Curr Opin Virol 5:24–33.

7. Aguilar HC, Henderson BA, Zamora JL, Johnston GP. 2016. Paramyxovirus glycoproteins and the membrane fusion process. Curr Clin Microbiol Rep 3:142–154.

8. Porotto M, Devito I, Palmer SG, Jurgens EM, Yee JL, Yokoyama CC, Pessi A, Moscona A. 2011. Spring-loaded model revisited: paramyxovirus fusion requires engagement of a receptor binding protein beyond initial triggering of the fusion protein. J Virol 85:12867–80.

9. Bose S, Jardetzky TS, Lamb RA. 2015. Timing is everything: fine-tuned molecular machines orchestrate paramyxovirus entry. Virology 479–480:518–531.

10. Bose S, Heath CM, Shah PA, Alayyoubi M, Jardetzky TS, Lamb RA. 2013. Mutations in the Parainfluenza Virus 5 Fusion Protein Reveal Domains Important for Fusion Triggering and Metastability https://doi.org/10.1128/JVI.02123-13.

11. Yin H-S, Paterson RG, Wen X, Lamb RA, Jardetzky TS. 2005. Structure of the uncleaved ectodomain of the paramyxovirus (hPIV3) fusion protein. Proc Natl Acad Sci U S A 102:9288–93.

12. Welch BD, Yuan P, Bose S, Kors CA, Lamb RA, Jardetzky TS. 2013. Structure of the parainfluenza virus 5 (PIV5) hemagglutinin-neuraminidase (HN) ectodomain. 8. PLoS Pathog 9:e1003534.

13. Goldsmith CS, Whistler T, Rollin PE, Ksiazek TG, Rota PA, Bellini WJ, Daszak P, Wong KT, Shieh W-J, Zaki SR. 2003. Elucidation of Nipah virus morphogenesis and replication using ultrastructural and molecular approaches. Virus Res 92:89–98.

14. El Najjar F, Schmitt AP, Dutch RE. 2014. Paramyxovirus glycoprotein incorporation, assembly and budding: a three way dance for infectious particle production. Viruses 6:3019–54.

15. Henrickson KJ. 2003. Parainfluenza Viruses. Clin Microbiol Rev 16:242–64.

16. Ibrahim YM, Zhang W, Werid GM, Zhang H, Pan Y, Zhang L, Xu Y, Li C, Chen H, Wang Y. 2022. Characterization of parainfluenza virus 5 from diarrheic piglet highlights its zoonotic potential. Transbound Emerg Dis 69:e1510–e1525.

17. Albariño CG, Foltzer M, Towner JS, Rowe LA, Campbell S, Jaramillo CM, Bird BH, Reeder DM, Vodzak ME, Rota P, Metcalfe MG, Spiropoulou CF, Knust B, Vincent JP, Frace MA, Nichol ST, Rollin PE, Ströher U. 2014. Novel Paramyxovirus Associated with Severe Acute Febrile Disease, South Sudan and Uganda, 2012. Emerg Infect Dis 20:211–216.

18. Yao Q, Compans RW. 2000. Filamentous particle formation by human parainfluenza virus type 2. J Gen Virol 81:1305–1312.

19. Compans RW, Holmes KV, Dales S, Choppin PW. 1966. An electron microscopic study of moderate and virulent virus-cell interactions of the parainfluenza virus SV5. Virology 30:411–426.

20. Shahriari S, Gordon J, Ghildyal R. 2016. Host Cytoskeleton in Respiratory Syncytial Virus Assembly and Budding. Virol J 13:161.

21. Plemper RK, Lamb RA. 2021. Paramyxoviridae: the viruses and their replication, p. 503–557. *In* Howley, PM, Knipe, DM, Whelan, S (eds.), Fields Virology Volume 1: Emerging Viruses, 7th ed. Wolters Kluwer, Kindle Edition.

22. Philbey AW, Kirkland PD, Ross AD, Davis RJ, Gleeson AB, Love RJ, Daniels PW, Gould AR, Hyatt AD. 1998. An Apparently New Virus (family *paramyxoviridae*) Infectious for Pigs, Humans, and Fruit Bats. Emerg Infect Dis 4:269–71.

23. Amman BR, Albariño CG, Bird BH, Nyakarahuka L, Sealy TK, Balinandi S, Schuh AJ, Campbell SM, Ströher U, Jones MEB, Vodzack ME, Reeder DM, Kaboyo W, Nichol ST, Towner JS. 2015. A recently discovered pathogenic paramyxovirus, Sosuga virus, is present in Rousettus aegyptiacus fruit bats at multiple locations in Uganda. J Wildl Dis 51:774–779.

24. Barr J, Todd S, Crameri G, Foord A, Marsh G, Frazer L, Payne J, Harper J, Baker KS, Cunningham AA, Wood JLN, Middleton D, Wang L-F. 2018. Animal Infection Studies of Two Recently Discovered African Bat Paramyxoviruses, Achimota 1 and Achimota 2. Sci Rep 8:12744–12744.

25. Lau SKP, Woo PCY, Wong BHL, Wong AYP, Tsoi H-W, Wang M, Lee P, Xu H, Poon RWS, Guo R, Li KSM, Chan K-H, Zheng B-J, Yuen K-Y. 2010. Identification and Complete Genome Analysis of Three Novel Paramyxoviruses, Tuhoko Virus 1, 2 and 3, in Fruit Bats from China. Virology 404:106–116.

26. Chua KB, Wang L-F, Lam SK, Eaton BT. 2002. Full Length Genome Sequence of Tioman Virus, a Novel Paramyxovirus in the Genus Rubulavirus Isolated from Fruit Bats in Malaysia. Arch Virol 147:1323–1348.

27. Burroughs AL, Tachedjian M, Crameri G, Durr PA, Marsh GA, Wang L-F. 2015. Complete Genome Sequence of Teviot Paramyxovirus, a Novel Rubulavirus Isolated from Fruit Bats in Australia. Genome Announc 3.

28. Kohl C, Tachedjian M, Todd S, Monaghan P, Boyd V, Marsh GA, Crameri G, Field H, Kurth A, Smith I, Wang L-F. 2018. Hervey Virus: Study on Co-Circulation with Henipaviruses in Pteropid Bats Within Their Distribution Range from Australia to Africa. PLOS ONE 13:e0191933–e0191933.

29. Thibault PA, Watkinson RE, Moreira-Soto A, Drexler JF, Lee B. 2017. Chapter One - Zoonotic Potential of Emerging Paramyxoviruses: Knowns and Unknowns, p. 1–55. *In* Kielian, M, Mettenleiter, TC, Roossinck, MJ (eds.), Advances in Virus Research. Academic Press.

30. 2017. Chapter 17 - *Paramyxoviridae* and *Pneumoviridae*, p. 327–356. *In* MacLachlan, NJ, Dubovi, EJ (eds.), Fenner's Veterinary Virology (Fifth Edition)Fifth Edition. Academic Press, Boston.

31. Hagmaier K, Stock N, Precious B, Childs K, Wang L-F, Goodbourn S, Randall RE. 2007. Mapuera Virus, a Rubulavirus That Inhibits Interferon Signalling in a Wide Variety of Mammalian Cells Without Degrading STATs. J Gen Virol 88:956–966.

32. Bistrian B, Phillips CA, Kaye IS. 1972. Fatal Mumps Meningoencephalitis. JAMA 222:478–478.

33. Aguilar JC, Pérez-Breña MP, García ML, Cruz N, Erdman DD, Echevarría JE. 2000. Detection and identification of human parainfluenza viruses 1, 2, 3, and 4 in clinical samples of pediatric patients by multiplex reverse transcription-PCR. J Clin Microbiol 38:1191–5.

34. Hierweger MM, Werder S, Seuberlich T. 2020. Parainfluenza Virus 5 Infection in Neurological Disease and Encephalitis of Cattle. Int J Mol Sci 21:498.

35. Hause BM, Nelson E, Christopher-Hennings J. 2021. Eptesicus fuscus Orthorubulavirus, a Close Relative of Human Parainfluenza Virus 4, Discovered in a Bat in South Dakota. Microbiol Spectr 9:e00930-21.

36. Tribe GW. 1966. An Investigation of the Incidence, Epidemiology and Control of Simian Virus 5. Br J Exp Pathol 47:472–479.

37. Wilson RL, Fuentes SM, Wang P, Taddeo EC, Klatt A, Henderson AJ, He B. 2006. Function of Small Hydrophobic Proteins of Paramyxovirus. J Virol 80:1700–1709.

38. He B, Leser GP, Paterson RG, Lamb RA. 1998. The Paramyxovirus SV5 Small Hydrophobic (SH) Protein Is Not Essential for Virus Growth in Tissue Culture Cells. Virology 250:30–40.

39. Choi KM. 2010. Reemergence of mumps. Korean J Pediatr 53:623–8.

40. Tsoucalas G, Laios K, Karamanou M, Androutsos G. 2013. The Thasian epidemic of mumps during the 5th century BC. Infez Med 21:149–150.

41. Lewnard JA, Grad YH. 2018. Vaccine waning and mumps re-emergence in the United States. 433. Sci Transl Med 10.

42. Dayan GH, Quinlisk MP, Parker AA, Barskey AE, Harris ML, Schwartz JMH, Hunt K, Finley CG, Leschinsky DP, O'Keefe AL, Clayton J, Kightlinger LK, Dietle EG, Berg J, Kenyon CL, Goldstein ST, Stokley SK, Redd SB, Rota PA, Rota J, Bi D, Roush SW, Bridges CB, Santibanez TA, Parashar U, Bellini WJ, Seward JF. 2008. Recent Resurgence of Mumps in the United States. 15. N Engl J Med 358:1580–1589.

43. Matsubara K, Iwata S, Nakayama T. 2012. Antibodies Against Mumps Virus Component Proteins. J Infect Chemother 18:466–471.

44. Latner DR, Parker Fiebelkorn A, McGrew M, Williams NJ, Coleman LA, McLean HQ, Rubin S, Hickman CJ. 2017. Mumps virus nucleoprotein and hemagglutinin-specific antibody response following a third dose of measles mumps rubella vaccine. Open Forum Infect Dis 4.

45. Latner DR, McGrew M, Williams NJ, Sowers SB, Bellini WJ, Hickman CJ. 2014. Estimates of Mumps Seroprevalence May Be Influenced by Antibody Specificity and Serologic Method. Clin Vaccine Immunol CVI 21:286–97.

46. Hilleman MR, Buynak EB, Weibel RE, Stokes J. 1968. Live, Attenuated Mumps-Virus Vaccine: 1. Vaccine Development. N Engl J Med 278:227–232.

47. Weibel RE, Stokes J, Buynak EB, Whitman JE, Hilleman MR. 1967. Live, Attenuated Mumps-Virus Vaccine: 3. Clinical and Serologic Aspects in a Field Evaluation. N Engl J Med 276:245–251.

48. Hilleman MR, Weibel RE, Buynak EB, Stokes J, Whitman JE. 1967. Live, Attenuated Mumps-Virus Vaccine: 4. Protective Efficacy as Measured in a Field Evaluation. N Engl J Med 276:252–258.

49. Fiebelkorn AP, Coleman LA, Belongia EA, Freeman SK, York D, Bi D, Zhang C, Ngo L, Rubin S. 2014. Mumps Antibody Response in Young Adults After a Third Dose of Measles-Mumps-Rubella Vaccine. Open Forum Infect Dis 1:ofu094–ofu094.

50. Beleni A-I, Borgmann S. 2018. Mumps in the Vaccination Age: Global Epidemiology and the Situation in Germany. Int J Environ Res Public Health 15.

51. Vygen S, Fischer A, Meurice L, Njoya IM, Gregoris M, Ndiaye B, Ghenassia A, Poujol I, Stahl JP, Antona D, Strat YL, Levy-Bruhl D, Rolland P. 2016. Waning immunity against mumps in vaccinated young adults, France 2013. Eurosurveillance 21:30156.

52. Rubin SA, Link MA, Sauder CJ, Zhang C, Ngo L, Rima BK, Duprex WP. 2012. Recent mumps outbreaks in vaccinated populations: no evidence of immune escape. J Virol 86:615–20.

53. Hanna-Wakim R, Yasukawa LL, Sung P, Arvin AM, Gans HA. 2008. Immune responses to mumps vaccine in adults who were vaccinated in childhood. J Infect Dis 197:1669–75.

54. Rasheed MAU, Hickman CJ, McGrew M, Sowers SB, Mercader S, Hopkins A, Grimes V, Yu T, Wrammert J, Mulligan MJ, Bellini WJ, Rota PA, Orenstein WA, Ahmed R, Edupuganti S. 2019. Decreased humoral immunity to mumps in young adults immunized with MMR vaccine in childhood. Proc Natl Acad Sci 116:19071–19076.

55. Latner DR, Hickman CJ. 2015. Remembering Mumps. PLoS Pathog 11:e1004791.

56. Beaty SM, Nachbagauer R, Hirsh A, Vigant F, Duehr J, Azarm K, Stelfox AJ, Bowden TA, Duprex WP, Krammer F, Lee B. 2016. Cross-reactive and cross-neutralizing activity of human mumps antibodies against a novel mumps virus from bats. J Infect Dis 215:jiw534–jiw534.

57. Katoh H, Kubota T, Ihara T, Maeda K, Takeda M, Kidokoro M. 2016. Cross-Neutralization between Human and African Bat Mumps Viruses. Emerg Infect Dis 22:703–706.

58. Krüger N, Sauder C, Hoffmann M, Örvell C, Drexler JF, Rubin S, Herrler G. 2016. Recombinant mumps viruses expressing the batMuV fusion glycoprotein are highly fusion active and neurovirulent. J Gen Virol 97:2837–2848.

59. Genus: Orthorubulavirus | ICTV. https://ictv.global/report/chapter/paramyxoviridae/paramyxoviridae/orthorubulavirus. Retrieved 21 January 2023.

60. Williamson LE, Gilliland T, Yadav P, Binshtein E, Bombardi R, Kose N, Nargi RS, Sutton RE, Durie CL, Armstrong E, Carnahan RH, Walker LM, Kim AS, Fox JM, Diamond MS, Ohi MD,

Klimstra WB, Crowe JE. 2020. Human Antibodies Protect Against Aerosolized Eastern Equine Encephalitis Virus Infection. Cell 183:1884-1900.e23.

61. Alvarado G, Ettayebi K, Atmar RL, Bombardi RG, Kose N, Estes MK, Crowe JE. 2018. Human Monoclonal Antibodies That Neutralize Pandemic GII.4 Noroviruses. Gastroenterology 155:1898–1907.

62. Vogt MR, Fu J, Kose N, Williamson LE, Bombardi R, Setliff I, Georgiev IS, Klose T, Rossmann MG, Bochkov YA, Gern JE, Kuhn RJ, Crowe JE. 2020. Human Antibodies Neutralize Enterovirus D68 and Protect Against Infection and Paralytic Disease. Sci Immunol 5:eaba4902.

63. Chapman NS, Zhao H, Kose N, Westover JB, Kalveram B, Bombardi R, Rodriguez J, Sutton R, Genualdi J, LaBeaud AD, Mutuku FM, Pittman PR, Freiberg AN, Gowen BB, Fremont DH, Crowe JE. 2021. Potent Neutralization of Rift Valley Fever Virus by Human Monoclonal Antibodies Through Fusion Inhibition. Proc Natl Acad Sci 118:e2025642118.

64. Gaebler C, Gruell H, Velinzon K, Scheid JF, Nussenzweig MC, Klein F. 2013. Isolation of HIV-1-Reactive Antibodies Using Cell Surface-Expressed gp160ΔcBal. J Immunol Methods 397:47–54.

65. Welch SR, Chakrabarti AK, Wiggleton Guerrero L, Jenks HM, Lo MK, Nichol ST, Spiropoulou CF, Albariño CG. 2018. Development of a Reverse Genetics System for Sosuga Virus Allows Rapid Screening of Antiviral Compounds. PLoS Negl Trop Dis 12:e0006326.

66. Li M, Schmitt PT, Li Z, McCrory TS, He B, Schmitt AP. 2009. Mumps virus matrix, fusion, and nucleocapsid proteins cooperate for efficient production of virus-like particles. J Virol 83:7261–72.

67. Fields VS, Safi H, Waters C, Dillaha J, Capelle L, Riklon S, Wheeler JG, Haselow DT. 2019. Mumps in a highly vaccinated Marshallese community in Arkansas, USA: an outbreak report. Lancet Infect Dis 19:185–192.

68. Boye C, Arpag S, Francis M, DeClemente S, West A, Heller R, Bulysheva A. 2022. Reduction of Plasmid Vector Backbone Length Enhances Reporter Gene Expression. Bioelectrochemistry 144:107981.

69. Chong ZX, Yeap SK, Ho WY. 2021. Transfection Types, Methods and Strategies: A Technical Review. PeerJ 9:e11165.

70. Bose S, Zokarkar A, Welch BD, Leser GP, Jardetzky TS, Lamb RA. 2012. Fusion activation by a headless parainfluenza virus 5 hemagglutinin-neuraminidase stalk suggests a modular mechanism for triggering. Proc Natl Acad Sci U S A 109:E2625–E2634.

71. Connolly SA, Leser GP, Jardetzky TS, Lamb RA. 2009. Bimolecular complementation of paramyxovirus fusion and hemagglutinin-neuraminidase proteins enhances fusion: implications for the mechanism of fusion triggering. J Virol 83:10857–68.

72. Krarup A, Truan D, Furmanova-Hollenstein P, Bogaert L, Bouchier P, Bisschop IJM, Widjojoatmodjo MN, Zahn R, Schuitemaker H, McLellan JS, Langedijk JPM. 2015. A Highly

Stable Prefusion Rsv F Vaccine Derived from Structural Analysis of the Fusion Mechanism. Nat Commun 6:8143.

73. McLellan JS, Chen M, Leung S, Graepel KW, Du X, Yang Y, Zhou T, Baxa U, Yasuda E, Beaumont T, Kumar A, Modjarrad K, Zheng Z, Zhao M, Xia N, Kwong PD, Graham BS. 2013. Structure of RSV fusion glycoprotein trimer bound to a prefusion-specific neutralizing antibody. Science 340:1113–7.

74. Zhu Q, McLellan JS, Kallewaard NL, Ulbrandt ND, Palaszynski S, Zhang J, Moldt B, Khan A, Svabek C, McAuliffe JM, Wrapp D, Patel NK, Cook KE, Richter BWM, Ryan PC, Yuan AQ, Suzich JA. 2017. A highly potent extended half-life antibody as a potential RSV vaccine surrogate for all infants. Sci Transl Med 9:eaaj1928–eaaj1928.

75. Xiao X, Tang A, Cox KS, Wen Z, Callahan C, Sullivan NL, Nahas DD, Cosmi S, Galli JD, Minnier M, Verma D, Babaoglu K, Su H, Bett AJ, Vora KA, Chen Z, Zhang L. 2019. Characterization of Potent RSV Neutralizing Antibodies Isolated from Human Memory B Cells and Identification of Diverse RSV/hMPV Cross-Neutralizing Epitopes. mAbs 11:1415–1427.

76. Schuh AJ, Amman BR, Sealy TK, Kainulainen MH, Chakrabarti AK, Guerrero LW, Nichol ST, Albarino CG, Towner JS. 2019. Antibody-Mediated Virus Neutralization Is Not a Universal Mechanism of Marburg, Ebola, or Sosuga Virus Clearance in Egyptian Rousette Bats. J Infect Dis 219:1716–1721.

77. Owen JA, Punt J, Stranford SA, Jones PP. 2013. Kuby Immunology. W. H. Freeman and Company, New York.

78. Alberts B, Johnson A, Lewis J, Raff M, Roberts K, Walter P. 2002. B Cells and Antibodies. Mol Biol Cell 4th Ed.

79. Gotoh B, Komatsu T, Takeuchi K, Yokoo J. 2001. Paramyxovirus Accessory Proteins as Interferon Antagonists. Microbiol Immunol 45:787–800.

80. Dochow M, Krumm SA, Crowe JE, Moore ML, Plemper RK. 2012. Independent Structural Domains in Paramyxovirus Polymerase Protein. J Biol Chem 287:6878–6891.

81. Rima B, Collins P, Easton A, Fouchier R, Kurath G, Lamb RA, Lee B, Maisner A, Rota P, Wang L, ICTV Report ConsortiumYR 2017. ICTV Virus Taxonomy Profile: Pneumoviridae. J Gen Virol 98:2912–2913.

82. McLaughlin JM, Khan F, Schmitt H-J, Agosti Y, Jodar L, Simões EAF, Swerdlow DL. 2022. Respiratory Syncytial Virus–Associated Hospitalization Rates among US Infants: A Systematic Review and Meta-Analysis. J Infect Dis 225:1100–1111.

83. Boyoglu-Barnum S, Chirkova T, Anderson LJ. 2019. Biology of Infection and Disease Pathogenesis to Guide RSV Vaccine Development. Front Immunol 10:1675.

84. Schindelin J, Arganda-Carreras I, Frise E, Kaynig V, Longair M, Pietzsch T, Preibisch S, Rueden C, Saalfeld S, Schmid B, Tinevez J-Y, White DJ, Hartenstein V, Eliceiri K, Tomancak

P, Cardona A. 2012. Fiji: an open-source platform for biological-image analysis. 7. Nat Methods 9:676–682.

85. Lan K, Verma SC, Murakami M, Bajaj B, Robertson ES. 2007. Epstein-Barr Virus (EBV): infection, propagation, quantitation, and storage. Curr Protoc Microbiol 6:14E.2.1-14E.2.21.

86. Hartmann G, Krieg AM. 2000. Mechanism and Function of a Newly Identified CpG DNA Motif in Human Primary B Cells1. J Immunol 164:944–953.

87. Yu X, McGraw PA, House FS, Crowe JE. 2008. An Optimized Electrofusion-Based Protocol for Generating Virus-Specific Human Monoclonal Antibodies. J Immunol Methods 336:142–151.

88. Davis JM, Pennington JE, Kubler A-M, Conscience J-F. 1982. A Simple, Single-Step Technique for Selecting and Cloning Hybridomas for the Production of Monoclonal Antibodies. J Immunol Methods 50:161–171.

89. Szybalski W. 1992. Roots. Use of the HPRTGene and the Hat Selection Technique in Dna-Mediated Transformation of Mammalian Cells: First Steps Toward Developing Hybridoma Techniques and Gene Therapy. BioEssays 14:495–500.

90. Jantscheff P, Winkler L, Karawajew L, Kaiser G, Böttger V, Micheel B. 1993. Hybrid hybridomas producing bispecific antibodies to CEA and peroxidase isolated by a combination of HAT medium selection and fluorescence activated cell sorting. J Immunol Methods 163:91–97.

91. Zost SJ, Gilchuk P, Case JB, Binshtein E, Chen RE, Nkolola JP, Schäfer A, Reidy JX, Trivette A, Nargi RS, Sutton RE, Suryadevara N, Martinez DR, Williamson LE, Chen EC, Jones T, Day S, Myers L, Hassan AO, Kafai NM, Winkler ES, Fox JM, Shrihari S, Mueller BK, Meiler J, Chandrashekar A, Mercado NB, Steinhardt JJ, Ren K, Loo Y-M, Kallewaard NL, McCune BT, Keeler SP, Holtzman MJ, Barouch DH, Gralinski LE, Baric RS, Thackray LB, Diamond MS, Carnahan RH, Crowe JE. 2020. Potently Neutralizing and Protective Human Antibodies Against SARS-CoV-2. 7821. Nature 584:443–449.

92. Zost SJ, Gilchuk P, Chen RE, Case JB, Reidy JX, Trivette A, Nargi RS, Sutton RE, Suryadevara N, Chen EC, Binshtein E, Shrihari S, Ostrowski M, Chu HY, Didier JE, MacRenaris KW, Jones T, Day S, Myers L, Eun-Hyung Lee F, Nguyen DC, Sanz I, Martinez DR, Rothlauf PW, Bloyet L-M, Whelan SPJ, Baric RS, Thackray LB, Diamond MS, Carnahan RH, Crowe JE. 2020. Rapid isolation and profiling of a diverse panel of human monoclonal antibodies targeting the SARS-CoV-2 spike protein. 9. Nat Med 26:1422–1427.

93. Gilchuk P, Bombardi RG, Erasmus JH, Tan Q, Nargi R, Soto C, Abbink P, Suscovich TJ, Durnell LA, Khandhar A, Archer J, Liang J, Fouch ME, Davidson E, Doranz BJ, Jones T, Larson E, Ertel S, Granger B, Fuerte-Stone J, Roy V, Broge T, Linnekin TC, Linde CH, Gorman MJ, Nkolola J, Alter G, Reed SG, Barouch DH, Diamond MS, Crowe JE, Van Hoeven N, Thackray LB, Carnahan RH. 2020. Integrated Pipeline for the Accelerated Discovery of Antiviral Antibody Therapeutics. 11. Nat Biomed Eng 4:1030–1043.

94. Stelfox AJ, Bowden TA. 2019. A Structure-Based Rationale for Sialic Acid Independent Host-Cell Entry of Sosuga Virus. Proc Natl Acad Sci U S A 116:21514–21520.

95. Stewart-Jones GBE, Chuang G-Y, Xu K, Zhou T, Acharya P, Tsybovsky Y, Ou L, Zhang B, Fernandez-Rodriguez B, Gilardi V, Silacci-Fregni C, Beltramello M, Baxa U, Druz A, Kong W-P, Thomas PV, Yang Y, Foulds KE, Todd J-P, Wei H, Salazar AM, Scorpio DG, Carragher B, Potter CS, Corti D, Mascola JR, Lanzavecchia A, Kwong PD. 2018. Structure-Based Design of a Quadrivalent Fusion Glycoprotein Vaccine for Human Parainfluenza Virus Types 1–4. Proc Natl Acad Sci U S A 115:12265–12270.

96. Gilchuk P, Kuzmina N, Ilinykh PA, Huang K, Gunn BM, Bryan A, Davidson E, Doranz BJ, Turner HL, Fusco ML, Bramble MS, Hoff NA, Binshtein E, Kose N, Flyak AI, Flinko R, Orlandi C, Carnahan R, Parrish EH, Sevy AM, Bombardi RG, Singh PK, Mukadi P, Muyembe-Tamfum JJ, Ohi MD, Saphire EO, Lewis GK, Alter G, Ward AB, Rimoin AW, Bukreyev A, Crowe JE, Jr. 2018. Multifunctional Pan-ebolavirus Antibody Recognizes a Site of Broad Vulnerability on the Ebolavirus Glycoprotein. Immunity 49:363-374.e10.

97. Williamson LE, Reeder KM, Bailey K, Tran MH, Roy V, Fouch ME, Kose N, Trivette A, Nargi RS, Winkler ES, Kim AS, Gainza C, Rodriguez J, Armstrong E, Sutton RE, Reidy J, Carnahan RH, McDonald WH, Schoeder CT, Klimstra WB, Davidson E, Doranz BJ, Alter G, Meiler J, Schey KL, Julander JG, Diamond MS, Crowe JE. 2021. Therapeutic Alphavirus Cross-Reactive E1 Human Antibodies Inhibit Viral Egress. Cell 184:4430-4446.e22.

98. Mousa JJ, Binshtein E, Human S, Fong RH, Alvarado G, Doranz BJ, Moore ML, Ohi MD, Crowe JE. 2018. Human Antibody Recognition of Antigenic Site IV on Pneumovirus Fusion Proteins. PLOS Pathog 14:e1006837–e1006837.

99. Bar-Peled Y, Diaz D, Pena-Briseno A, Murray J, Huang J, Tripp RA, Mousa JJ. 2019. A Potent Neutralizing Site III-Specific Human Antibody Neutralizes Human Metapneumovirus In Vivo. J Virol 93:e00342-19.

100. Wen X, Mousa JJ, Bates JT, Lamb RA, Crowe JE, Jardetzky TS. 2017. Structural Basis for Antibody Cross-Neutralization of Respiratory Syncytial Virus and Human Metapneumovirus. 4. Nat Microbiol 2:1–7.

101. Baker KS, Todd S, Marsh G, Fernandez-Loras A, Suu-Ire R, Wood JLN, Wang LF, Murcia PR, Cunningham AA. 2012. Co-circulation of diverse paramyxoviruses in an urban African fruit bat population. J Gen Virol 93:850–6.

102. Schmidt TGM, Batz L, Bonet L, Carl U, Holzapfel G, Kiem K, Matulewicz K, Niermeier D, Schuchardt I, Stanar K. 2013. Development of the Twin-Strep-Tag and Its Application for Purification of Recombinant Proteins from Cell Culture Supernatants. Protein Expr Purif 92:54–61.

103. Harbury PB, Zhang T, Kim PS, Alber T. 1993. A switch between two-, three-, and four-stranded coiled coils in GCN4 leucine zipper mutants. Science 262:1401–1407.

104. Schmidt TG, Skerra A. 2007. The Strep-Tag System for One-Step Purification and High-Affinity Detection or Capturing of Proteins. 6. Nat Protoc 2:1528–1535.

105. Bose S, Song AS, Jardetzky TS, Lamb RA. 2014. Fusion activation through attachment protein stalk domains indicates a conserved core mechanism of paramyxovirus entry into cells. 8. J Virol 88:3925–41.

106. Komada H, Klippmark E, Orvell C, Randall RE, Ito Y, Norrby E. 1991. Immunological Relationships Between Parainfluenza Virus Type 4 and Other Paramyxoviruses Studied by Use of Monoclonal Antibodies. Arch Virol 116:277–283.

107. van Wyke Coelingh K, Tierney EL. 1989. Antigenic and Functional Organization of Human Parainfluenza Virus Type 3 Fusion Glycoprotein. J Virol 63:375–82.

108. Poor TA, Song AS, Welch BD, Kors CA, Jardetzky TS, Lamb RA. 2015. On the stability of parainfluenza virus 5 F proteins. J Virol 89:3438–41.

109. McLellan JS, Chen M, Leung S, Graepel KW, Du X, Yang Y, Zhou T, Baxa U, Yasuda E, Beaumont T, Kumar A, Modjarrad K, Zheng Z, Zhao M, Xia N, Kwong PD, Graham BS. 2013. Structure of RSV fusion glycoprotein trimer bound to a prefusion-specific neutralizing antibody. 6136. Science 340:1113–7.

110. Barr JA, Smith C, Marsh GA, Field H, Wang L-F. 2012. Evidence of Bat Origin for Menangle Virus, a Zoonotic Paramyxovirus First Isolated from Diseased Pigs. J Gen Virol 93:2590–2594.

111. Ohi M, Li Y, Cheng Y, Walz T. 2004. Negative Staining and Image Classification – Powerful Tools in Modern Electron Microscopy. Biol Proced Online 6:23–34.

112. Mastronarde DN. 2005. Automated Electron Microscope Tomography Using Robust Prediction of Specimen Movements. J Struct Biol 152:36–51.

113. Punjani A, Rubinstein JL, Fleet DJ, Brubaker MA. 2017. CryoSPARC: Algorithms for Rapid Unsupervised Cryo-EM Structure Determination. 3. Nat Methods 14:290–296.

114. Rohou A, Grigorieff N. 2015. CTFFIND4: Fast and Accurate Defocus Estimation from Electron Micrographs. J Struct Biol 192:216–221.

115. Xiang Q, Li L, Wu J, Tian M, Fu Y. 2022. Application of Pseudovirus System in the Development of Vaccine, Antiviral-Drugs, and Neutralizing Antibodies. Microbiol Res 258:126993.

116. Li Q, Liu Q, Huang W, Li X, Wang Y. 2018. Current Status on the Development of Pseudoviruses for Enveloped Viruses. Rev Med Virol 28:e1963.

117. Liu G, Cao W, Salawudeen A, Zhu W, Emeterio K, Safronetz D, Banadyga L. 2021. Vesicular Stomatitis Virus: From Agricultural Pathogen to Vaccine Vector. Pathogens 10:1092.

118. Whitt MA. 2010. Generation of VSV Pseudotypes Using Recombinant ΔG-VSV for Studies on Virus Entry, Identification of Entry Inhibitors, and Immune Responses to Vaccines. J Virol Methods 169:365–74.

119. Sakata M, Tani H, Anraku M, Kataoka M, Nagata N, Seki F, Tahara M, Otsuki N, Okamoto K, Takeda M, Mori Y. 2017. Analysis of VSV Pseudotype Virus Infection Mediated by Rubella Virus Envelope Proteins. Sci Rep 7:11607.

120. Lee B-H, Yoshimatsu K, Araki K, Okumura M, Nakamura I, Arikawa J. 2006. A Pseudotype Vesicular Stomatitis Virus Containing Hantaan Virus Envelope Glycoproteins G1 and G2 as an Alternative to Hantavirus Vaccine in Mice. Vaccine 24:2928–2934.

121. Matsuura Y, Tani H, Suzuki K, Kimura-Someya T, Suzuki R, Aizaki H, Ishii K, Moriishi K, Robison CS, Whitt MA, Miyamura T. 2001. Characterization of Pseudotype VSV Possessing HCV Envelope Proteins. Virology 286:263–275.

122. Johnson MC, Lyddon TD, Suarez R, Salcedo B, LePique M, Graham M, Ricana C, Robinson C, Ritter DG. 2020. Optimized Pseudotyping Conditions for the SARS-COV-2 Spike Glycoprotein. J Virol 94:e01062-20.

123. Moeschler S, Locher S, Conzelmann K-K, Krämer B, Zimmer G. 2016. Quantification of Lyssavirus-Neutralizing Antibodies Using Vesicular Stomatitis Virus Pseudotype Particles. 9. Viruses 8:254.

124. van den Pol AN, Mao G, Chattopadhyay A, Rose JK, Davis JN. 2017. Chikungunya, Influenza, Nipah, and Semliki Forest Chimeric Viruses with Vesicular Stomatitis Virus: Actions in the Brain. J Virol 91:e02154-16.

125. Ma J, Chen R, Huang W, Nie J, Liu Q, Wang Y, Yang X. 2019. In Vitro and in Vivo Efficacy of a Rift Valley Fever Virus Vaccine Based on Pseudovirus. Hum Vaccines Immunother 15:2286–2294.

126. Logan N, McMonagle E, Drew AA, Takahashi E, McDonald M, Baron MD, Gilbert M, Cleaveland S, Haydon DT, Hosie MJ, Willett BJ. 2016. Efficient Generation of Vesicular

Stomatitis Virus (VSV)-Pseudotypes Bearing Morbilliviral Glycoproteins and Their Use in Quantifying Virus Neutralising Antibodies. Vaccine 34:814–822.

127. Ayala-Breton C, Barber GN, Russell SJ, Peng K-W. 2012. Retargeting Vesicular Stomatitis Virus Using Measles Virus Envelope Glycoproteins. Hum Gene Ther 23:484–491.

128. Negrete OA, Levroney EL, Aguilar HC, Bertolotti-Ciarlet A, Nazarian R, Tajyar S, Lee B. 2005. EphrinB2 Is the Entry Receptor for Nipah Virus, an Emergent Deadly Paramyxovirus. 7049. Nature 436:401–405.

129. Kowolik CM, Yee J-K. 2002. Preferential Transduction of Human Hepatocytes with Lentiviral Vectors Pseudotyped by Sendai Virus F Protein. Mol Ther 5:762–769.

130. Jung C, Grzybowski BN, Tong S, Cheng L, Compans RW, Doux JML. 2004. Lentiviral Vectors Pseudotyped with Envelope Glycoproteins Derived from Human Parainfluenza Virus Type 3. Biotechnol Prog 20:1810–1816.

131. Cronin J, Zhang X-Y, Reiser J. 2005. Altering the Tropism of Lentiviral Vectors through Pseudotyping. Curr Gene Ther 5:387–398.

132. Crawford KHD, Eguia R, Dingens AS, Loes AN, Malone KD, Wolf CR, Chu HY, Tortorici MA, Veesler D, Murphy M, Pettie D, King NP, Balazs AB, Bloom JD. 2020. Protocol and Reagents for Pseudotyping Lentiviral Particles with SARS-CoV-2 Spike Protein for Neutralization Assays. Viruses 12:513.

133. Duvergé A, Negroni M. 2020. Pseudotyping Lentiviral Vectors: When the Clothes Make the Virus. Viruses 12:1311.

134. Hofmann H, Hattermann K, Marzi A, Gramberg T, Geier M, Krumbiegel M, Kuate S, Überla K, Niedrig M, Pöhlmann S. 2004. S Protein of Severe Acute Respiratory Syndrome-Associated Coronavirus Mediates Entry into Hepatoma Cell Lines and Is Targeted by Neutralizing Antibodies in Infected Patients. J Virol 78:6134–6142.

135. Witting SR, Vallanda P, Gamble AL. 2013. Characterization of a 3rd Generation Lentiviral Vector Pseudotyped With Nipah Virus Envelope Proteins For Endothelial Cell Transduction. Gene Ther 20:997–1005.

136. Palomares K, Vigant F, Van Handel B, Pernet O, Chikere K, Hong P, Sherman SP, Patterson M, An DS, Lowry WE, Mikkola HKA, Morizono K, Pyle AD, Lee B. 2013. Nipah Virus Envelope-Pseudotyped Lentiviruses Efficiently Target ephrinB2-Positive Stem Cell Populations In Vitro and Bypass the Liver Sink When Administered In Vivo. J Virol 87:2094–2108.

137. Finkelshtein D, Werman A, Novick D, Barak S, Rubinstein M. 2013. LDL Receptor and Its Family Members Serve as the Cellular Receptors for Vesicular Stomatitis Virus. Proc Natl Acad Sci U S A 110:7306–7311.

138. Susan Payne. 2017. Chapter 36 - Family *Retroviridae*, p. 287–301. *In* Viruses: From Understanding to Investigation. Academic Press.

139. Seitz R. 2016. Human Immunodeficiency Virus (HIV). Transfus Med Hemotherapy 43:203–222.

140. Susan Payne. 2017. Chapter 37 - Replication and Pathogenesis of Human Immunodeficiency Virus, p. 303–320. *In* Viruses : From Understanding to Investigation. Academic Press.

141. McGregor A, Choi KY, Schachtele S, Lokensgard J. 2013. Chapter 37 - Human Herpesviruses and Animal Models: Recombinant Viruses and Reporter Genes, p. 910–916. *In* Conn, PM (ed.), Animal Models for the Study of Human Disease. Academic Press, Boston.

142. Karron RA. 2018. 51 - Respiratory Syncytial Virus Vaccines, p. 943-949.e4. *In* Plotkin, SA, Orenstein, WA, Offit, PA, Edwards, KM (eds.), Plotkin's Vaccines (Seventh Edition). Elsevier.

143. Lawson ND, Stillman EA, Whitt MA, Rose JK. 1995. Recombinant Vesicular Stomatitis Viruses from DNA. Proc Natl Acad Sci U S A 92:4477–4481.

144. Robinson LR, Whelan SPJ. 2016. Infectious Entry Pathway Mediated by the Human Endogenous Retrovirus K Envelope Protein. J Virol 90:3640–3649.

145. Suder E, Furuyama W, Feldmann H, Marzi A, de Wit E. 2018. The Vesicular Stomatitis Virus-Based Ebola Virus Vaccine: From Concept to Clinical Trials. Hum Vaccines Immunother 14:2107–2113.

146. Roberts A, Kretzschmar E, Perkins AS, Forman J, Price R, Buonocore L, Kawaoka Y, Rose JK. 1998. Vaccination with a Recombinant Vesicular Stomatitis Virus Expressing an Influenza Virus Hemagglutinin Provides Complete Protection from Influenza Virus Challenge. J Virol 72:4704–4711.

147. Foster SL, Woolsey C, Borisevich V, Agans KN, Prasad AN, Deer DJ, Geisbert JB, Dobias NS, Fenton KA, Cross RW, Geisbert TW. 2022. A Recombinant VSV-Vectored Vaccine Rapidly Protects Nonhuman Primates Against Lethal Nipah Virus Disease. Proc Natl Acad Sci U S A 119:e2200065119.

148. Schuh AJ, Amman BR, Sealy TK, Kainulainen MH, Chakrabarti AK, Guerrero LW, Nichol ST, Albarino CG, Towner JS. 2018. Antibody-Mediated Virus Neutralization Is Not a Universal Mechanism of Marburg, Ebola, or Sosuga Virus Clearance in Egyptian Rousette Bats. J Infect Dis https://doi.org/10.1093/infdis/jiy733.

149. Donnelly MLL, Hughes LE, Luke G, Mendoza H, ten Dam E, Gani D, Ryan MDY 2001. The 'Cleavage' Activities of Foot-and-Mouth Disease Virus 2A Site-Directed Mutants and Naturally Occurring '2A-Like' Sequences. J Gen Virol 82:1027–1041.

150. Latner DR, Parker Fiebelkorn A, McGrew M, Williams NJ, Coleman LA, McLean HQ, Rubin S, Hickman CJ. 2017. Mumps virus nucleoprotein and hemagglutinin-specific antibody response following a third dose of measles mumps rubella vaccine. 4. Open Forum Infect Dis 4.

151. McLellan JS, Chen M, Chang J-S, Yang Y, Kim A, Graham BS, Kwong PD. 2010. Structure of a Major Antigenic Site on the Respiratory Syncytial Virus Fusion Glycoprotein in Complex with Neutralizing Antibody 101F. J Virol 84:12236–12244.

152. Syed AM, Taha TY, Tabata T, Chen IP, Ciling A, Khalid MM, Sreekumar B, Chen P-Y, Hayashi JM, Soczek KM, Ott M, Doudna JA. 2021. Rapid Assessment of SARS-CoV-2–Evolved Variants Using Virus-Like Particles. Science 374:1626–1632.

153. Orvell C. 1984. The reactions of monoclonal antibodies with structural proteins of mumps virus. J Immunol 132:2622–2629.

154. Lewnard JA, Grad YH. 2018. Vaccine waning and mumps re-emergence in the United States. Sci Transl Med 10.

155. Smith SA, Silva LA, Fox JM, Flyak AI, Kose N, Sapparapu G, Khomandiak S, Ashbrook AW, Kahle KM, Fong RH, Swayne S, Doranz BJ, McGee CE, Heise MT, Pal P, Brien JD, Austin SK, Diamond MS, Dermody TS, Crowe JE. 2015. Isolation and Characterization of Broad and Ultrapotent Human Monoclonal Antibodies with Therapeutic Activity against Chikungunya Virus. Cell Host Microbe 18:86–95.

156. Heydarchi B, Fong DS, Gao H, Salazar-Quiroz NA, Edwards JM, Gonelli CA, Grimley S, Aktepe TE, Mackenzie C, Wales WJ, van Gils MJ, Cupo A, Rouiller I, Gooley PR, Moore JP, Sanders RW, Montefiori D, Sethi A, Purcell DFJ. 2022. Broad and Ultra-Potent Cross-Clade Neutralization of HIV-1 by a Vaccine-Induced CD4 Binding Site Bovine Antibody. Cell Rep Med 3:100635.

157. Johnson RI, Tachedjian M, Clayton BA, Layton R, Bergfeld J, Wang L-F, Marsh GA. 2019. Characterization of Teviot virus, an Australian bat-borne paramyxovirus. J Gen Virol 100:403–413.

158. Yaiw KC, Crameri G, Wang L, Chong HT, Chua KB, Tan CT, Goh KJ, Shamala D, Wong KT. 2007. Serological evidence of possible human infection with Tioman virus, a newly described paramyxovirus of bat origin. J Infect Dis 196:884–886.

159. Bowden TR, Bingham J, Harper JA, Boyle DB. 2012. Menangle virus, a pteropid bat paramyxovirus infectious for pigs and humans, exhibits tropism for secondary lymphoid organs and intestinal epithelium in weaned pigs. J Gen Virol 93:1007–1016.

160. Yaiw KC, Bingham J, Crameri G, Mungall B, Hyatt A, Yu M, Eaton B, Shamala D, Wang L-F, Thong Wong K. 2008. Tioman virus, a paramyxovirus of bat origin, causes mild disease in pigs and has a predilection for lymphoid tissues. J Virol 82:565–8.

161. Bose S, Song AS, Jardetzky TS, Lamb RA. 2014. Fusion activation through attachment protein stalk domains indicates a conserved core mechanism of paramyxovirus entry into cells. J Virol 88:3925–41.

162. Tsurudome M, Ito M, Ohtsuka J, Hara K, Komada H, Nishio M, Nosaka T. 2015. The Fusion Protein Specificity of the Parainfluenza Virus Hemagglutinin-Neuraminidase Protein Is Not Solely Defined by the Primary Structure of Its Stalk Domain https://doi.org/10.1128/JVI.01448-15.

163. Tsurudome M, Ohtsuka J, Ito M, Nishio M, Nosaka T. 2018. The Hemagglutinin-Neuraminidase (HN) Head Domain and the Fusion (F) Protein Stalk Domain of the Parainfluenza Viruses Affect the Specificity of the HN-F Interaction. Front Microbiol 9:391.

164. Welch SR, Ritter JM, Schuh AJ, Genzer SC, Sorvillo TE, Harmon JR, Coleman-McCray JD, Jain S, Shrivastava-Ranjan P, Seixas JN, Estetter LB, Fair PS, Towner JS, Montgomery JM, Albariño CG, Spiropoulou CF, Spengler JR. 2023. Tissue Replication and Mucosal Swab Detection of Sosuga Virus in Syrian Hamsters in the Absence of Overt Tissue Pathology and Clinical Disease. Antiviral Res 209:105490.